

# **AGGREGATE PACKING CHARACTERISTICS OF ASPHALT MIXTURES**

by

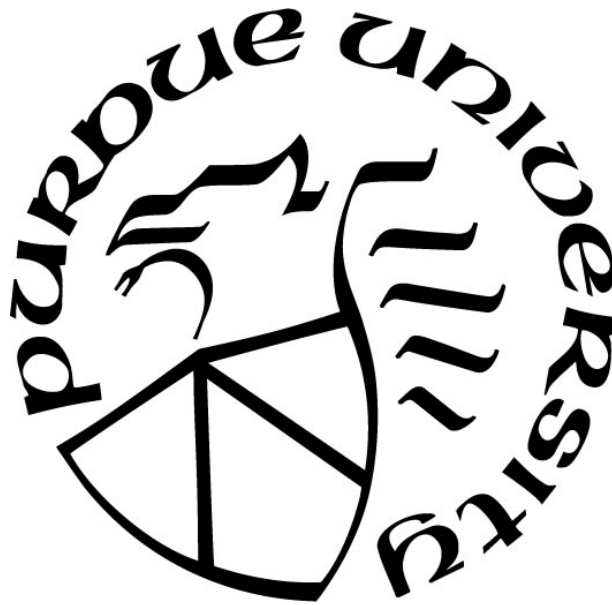
**Mohammadreza Pouranian**

**A Dissertation**

*Submitted to the Faculty of Purdue University*

*In Partial Fulfillment of the Requirements for the degree of*

**Doctor of Philosophy**



Lyles School of Civil Engineering

West Lafayette, Indiana

December 2019

**THE PURDUE UNIVERSITY GRADUATE SCHOOL**  
**STATEMENT OF COMMITTEE APPROVAL**

Dr. John E. Haddock, Chair

Lyles School of Civil Engineering

Dr. Jan Olek

Lyles School of Civil Engineering

Dr. Pablo D. Zavattieri

Lyles School of Civil Engineering

Dr. Marcial Gonzalez

School of Mechanical Engineering

**Approved by:**

Dr. Dulcy M. Abraham

Head of the Graduate Program

*To my parents*  
*Morteza and Zahra*

## **ACKNOWLEDGMENTS**

I would like to express my sincere gratitude to my advisor Professor John Haddock for his constant guidance, invaluable support, advice, guidance, and friendship throughout my doctorate program at Purdue University. He has been a source of immense motivation for me throughout the course of the project.

I would also like to thank the members of my advisory and examination committee, Prof. Jan Olek, Prof. Pablo Zavattieri and Prof. Marcial Gonzalez for serving on my advisory and defense committee and for contributing towards my research through their valuable suggestions. I would like to express my deep gratitude to Dr. Reyhaneh Rahbar-Rastegar for her support and help throughout my research.

Finally, I would like to thank my family for their patience and help throughout my studies. This dissertation would not have been written without them and I cannot thank them enough for their understanding and unconditional support throughout my life. They have been always been my motivation in life.



# TABLE OF CONTENTS

LIST OF TABLES .....	8
LIST OF FIGURES .....	10
ABSTRACT .....	14
CHAPTER 1. INTRODUCTION .....	16
1.1 Introduction.....	16
1.2 Objectives .....	18
1.3 Methodology .....	19
1.4 Organization of Dissertation .....	20
CHAPTER 2. LINEAR-MIXTURE PACKING MODEL.....	21
2.1 Introduction.....	21
2.2 Model Framework.....	24
2.2.1 Background .....	24
2.2.2 Linear-Mixture Model.....	26
2.2.3 Model Implementation for Asphalt Mixtures .....	28
2.3 Model Evaluation.....	36
2.3.1 Experimental Data .....	36
2.3.2 VMA Estimation .....	39
2.3.3 Aggregate Skeleton Determination.....	41
2.4 Summary .....	46
CHAPTER 3. A FRAMEWORK FOR UNDERSTANDING AGGREGATE STRUCTURE IN ASPHALT MIXTURES .....	47
3.1 Introduction.....	47
3.2 Analytical Model .....	50
3.3 Numerical Verification .....	56
3.3.1 Packing Density .....	60
3.3.2 Coordination Number .....	61
3.3.3 Radial Distribution Function.....	65
3.4 Proposed Aggregate Structure Definition.....	66
3.5 Application of Analytical Model to Multi-Sized Aggregate Stockpiles.....	68

3.6 Summary .....	70
CHAPTER 4. EFFECT OF AGGREGATE STRUCTURE ON ASPHALT MIXTURE	
COMPACTION PARAMETERS.....	71
4.1 Introduction.....	71
4.2 Materials .....	73
4.2.1 Aggregate Gradations .....	74
4.3 Specimen Preparation .....	76
4.3.1 Mixture Design Approach.....	77
4.3.2 Mixture Design Results.....	80
4.4 Gradation and Compactability .....	84
4.4.1 Compaction Parameters .....	84
4.4.2 Gradation Parameters .....	85
4.4.3 Mixtures without Filler .....	88
4.4.4 Mixtures with Fillers.....	92
4.5 Evaluation of Compactability Models .....	96
4.5.1 Laboratory Data .....	96
4.5.2 Field Data.....	99
4.6 Summary .....	102
CHAPTER 5. IMPACT OF THE COARSE AGGREGATE SHAPE PARAMETERS ON	
COMPACTION CHARACTERISTICS.....	104
5.1 Introduction.....	104
5.2 Shape Parameters .....	106
5.3 Generation of 3D Particles.....	111
5.3.1 Computational Modeling .....	111
5.3.2 Sample Preparation .....	115
5.4 Discrete Element Method Simulation.....	117
5.5 Results and Discussion .....	122
5.1 Compaction Parameters .....	122
5.2 Microscopic Packing Properties .....	129
5.6 Summary .....	134
CHAPTER 6. SUMMARY AND CONCLUSIONS .....	135

REFERENCES .....	138
------------------	-----

## LIST OF TABLES

Table 2.1 Aggregate Gradations and Properties (after Vavrik, 2000). .....	37
Table 2.2 Asphalt Mixture Data (after Vavrik, 2000). .....	37
Table 2.3 Input Parameters for Aggregate Size Distribution Function. ....	39
Table 2.4 Estimated and Laboratory-measured Voids in the Mineral Aggregate. ....	40
Table 2.5 Statistical Analysis of Model-estimated and Laboratory-measured Voids in the Mineral Aggregate. ....	41
Table 2.6 Three Aggregate Size Ranges of Mixtures. ....	42
Table 2.7 Statistical Analysis Results of Controlling Particle Size and Chosen Unit Weight. ....	43
Table 2.8 Disruptive Factors and Coordination Numbers of the Asphalt Mixtures. ....	44
Table 2.9 Results of Statistical Analysis between Accumulated Strain at 5000 Cycles and Disruptive Factors and Coordination Numbers. ....	44
Table 2.10 Results of Statistical Analysis between Compaction Slope Values and Controlling Particle Size. ....	46
Table 3.1 Material Simulation Parameters. ....	58
Table 3.2 Calculated Values of the Mass of the Fine Fraction. ....	61
Table 3.3 Radial Distribution Function Probabilities. ....	66
Table 3.4 Coarse and Fine Stockpile Size Distributions. ....	69
Table 4.1 Aggregate Stockpile Properties. ....	73
Table 4.2 Gradation information. ....	76
Table 4.3 Initial Volumetric Data (without filler). ....	81
Table 4.4 Initial Results of Required Filler and Binder Contents. ....	82
Table 4.5 Volumetric Results of First Trial. ....	83
Table 4.6 Final Mixture Design Results. ....	83
Table 4.7 Half Sieve and Control Sieve Sizes based on the Bailey Method (Pine, 2016). ....	85

Table 4.8 Gradation Parameters.....	87
Table 4.9 Compaction Parameters for Mixtures without Filler. ....	88
Table 4.10 ANOVA Results for Normalized Initial Density and Compaction Slope Models (without filler).....	90
Table 4.11 Classification Analysis using the Self Organizing Map Method.....	91
Table 4.12 Compaction Parameters for Mixtures Containing Filler.....	92
Table 4.13 ANOVA Results for the Normalized Initial Density and Compaction Slope Models (with filler).....	94
Table 4.14 Aggregate Gradations and Properties (after Vavrik, 2000). ....	96
Table 4.15 Gradation and Compaction Parameters (after Vavrik, 2000). ....	97
Table 4.16 Laboratory and Field Compaction Parameters. ....	101
Table 5.1 Particle Classification Based on Form Parameters (after Blott and Pye, 2008). ....	108
Table 5.2 Particle Roundness Classification.....	109
Table 5.3 Sphericity Classification (Riley, 1941).....	110
Table 5.4 Contact Model's Parameters.....	119
Table 5.5 Regression Equations and Corresponding Statistical Parameters for Initial Density. ....	124
Table 5.6 Regression Equation and Corresponding ANOVA for Compaction Slope.....	128
Table 5.7 Fitting Parameters of PDF Distribution for some Mixtures. ....	133

## LIST OF FIGURES

Figure 2.1 Schematic Illustration of Filling and Occupation Mechanisms. ....	25
Figure 2.2 Two-dimensional Analysis of Particle Combinations with Different Faces. ....	30
Figure 2.3 Graphical Definition of Three-particle Size Ranges. ....	31
Figure 2.4 Voids in the Mineral Aggregate Variation as a Function of Controlling Particle Size. .....	32
Figure 2.5 Real and Estimated Gradations for Block 1 mixtures. ....	38
Figure 2.6 Laboratory-measured and Model-estimated Voids in the Mineral Aggregate. ....	41
Figure 2.7 Controlling Particle Size and Main Particle Size Range of Mixtures. ....	43
Figure 2.8 Accumulated Strain at 5000 Cycles as a Function of the Disruptive Factor. ....	45
Figure 2.9 Accumulated Strain at 5000 Cycles as a Function of the Main Particle Size Range Coordination Number. ....	45
Figure 3.1 Three binary mixture conditions. ....	50
Figure 3.2 Air Volume between Coarse Particles. ....	52
Figure 3.3 SRF Function Equations for Various Particle Face Configurations: (a) All Round Faces; (b) Two Flat Faces, One Round Face; (c) Two Round Faces, One Flat Face; (d) All Flat Faces. ....	53
Figure 3.4 Linear Regression Equations of SRF Functions. ....	54
Figure 3.5 Hypothetical Particles (a) $k=1$ and (b) $k=2$ . ....	55
Figure 3.6 Superpave Gyratory Compactor Schematic. ....	58
Figure 3.7 Simulation Process: (a) Cloud Condition; (b) Applying Gravity Force; (c) Settlement in the Container; (d) Applying Vertical Load; and (e) Final binary mixture after compaction. ....	59
Figure 3.8 Variation of Original Gradation after Three Gyration Levels. ....	60
Figure 3.9 Packing Density Values for Different Size Ratios and Corresponding Mass of the Fine Fraction at (a) CDT, (b) DFT ( $k=1$ ), and (c) DFT ( $k=2$ ). ....	63
Figure 3.10 Analytical Model $CN_c$ Values for all Size Ratios and Corresponding Mass of Fines Fraction at (a) CDT and (b) DFT. ....	64

Figure 3.11 Radial Distribution Function for (a) Coarse Particles (size = 2 mm) and (b) Fine Particles (size = 1 mm).....	65
Figure 3.12 Proposed Aggregate Structure Definition Illustration. ....	67
Figure 3.13 Variation of $CN_c$ and Packing Density for Coarse and Fine Stockpile Mixtures.....	70
Figure 4.1 Selected Aggregate Blend Gradations (without filler). ....	75
Figure 4.2 Schematic of Coarse Pack, Coarse Dense Pack, Fine Dense Pack, and Fine Pack. ....	75
Figure 4.3 Flowchart of Mixture Design Approach.....	78
Figure 4.4 Definition of (a): Compaction Slope and; (b): Compaction Energy Index. ....	84
Figure 4.5 Illustration of RDPI and Bailey Control Sieves. ....	87
Figure 4.6 Normalized Compaction Parameters for Various Gradation Types (without filler). ..	89
Figure 4.7 Comparison of Compaction Parameters for Mixtures with and without Filler: (a) Initial Density; (b) Compaction Slope; (c) Locking Point and; (d) Compaction Energy Index. ....	93
Figure 4.8 Predicted and Laboratory Normalized Initial Density and Compaction Slope Values for Mixtures Containing Filler. ....	94
Figure 4.9 Recommended Gradation based on Initial Density and Compaction Slope.....	95
Figure 4.10 Comparison of Laboratory Initial Density and Corresponding Predicted Normalized Values for: (a) Block 1; (b) Block 2; (c) Block 3; (d) Block 4; (e) Block 5. ....	98
Figure 4.11 Comparison of Laboratory Compaction Slope and Corresponding Predicted Normalized Values for: (a) Block 1; (b) Block 2; (c) Block 3; (d) Block 4; (e) Block 5. ....	99
Figure 4.12 Compaction on US 40 Field Project. ....	100
Figure 4.13 Gradation of US 40 Mixtures. ....	101
Figure 4.14 Comparison of Laboratory Compaction and Corresponding Normalized Estimated Parameters for: (a) Initial Density; and (b) Compaction Slope.....	102
Figure 5.1 Form Parameter Definitions. ....	107
Figure 5.2 Spherical Particle Classification based on Flatness and Elongation. ....	108
Figure 5.3 Roundness Classes (Blott and Pye 2008). ....	109
Figure 5.4 Sphericity Classification for Round Particles.....	110

Figure 5.5 Spherical Coordinate System. ....	111
Figure 5.6 Effect of Change in $D_2$ , $D_3$ , and $D_8$ on: (a) Flatness, (b) Elongation, (c) Roundness, (d) Sphericity, and (e) Regularity of a Particle. ....	114
Figure 5.7 Illustrative Example of Change in Three Selected Spectrum Mode Descriptors ( $D_2$ , $D_3$ and $D_8$ ) on Shape Parameters (Flatness (F); Elongation (E); Roundness (R); Sphericity (S); and Regularity (R)). ....	115
Figure 5.8 (a) Convex Polyhedral Cells; (b) Corresponding 2000 Generated 3D Particles; (c) Normal Distribution (Covariance = 0.80) at 10% Error.....	116
Figure 5.9 Selected Gradation (Size Distribution) Simulated. ....	118
Figure 5.10 Applying the Overlapping Discrete Element Cluster Algorithm to Import a 3D Irregular Particle into the Discrete Element Model Package. ....	118
Figure 5.11 (a) Burger’s Contact Model; (b) Normal and (c) Shear Aggregate Contact Models. ....	120
Figure 5.12 Asphalt Mastic Mixture $ E^* $ Master Curve. ....	120
Figure 5.13 Compaction Simulation Process: (a) Cloud Condition; (b) Applying Gravity Force; (c) Settlement in the Mold; (d) Applying Vertical Load; and (e) Final Compaction Condition. ....	121
Figure 5.14 Example Compaction Curve.....	122
Figure 5.15 Correlation between Flatness and Elongation and Sphericity. ....	123
Figure 5.16 Predicted vs. Actual Initial Density Values: (a) Flatness, Elongation as Explanatory Variables, and (b) Roundness, Sphericity, and Regularity as Explanatory Variables. ....	125
Figure 5.17 Changes in Initial Density due to Changes in Flatness and Elongation. ....	126
Figure 5.18 Changes in Initial Density due to Changes in Roundness and Sphericity.....	127
Figure 5.19 Effect of Flat and Elongated Particle Percentage on Initial Mixture Density. ....	129
Figure 5.20 Changes in Average Coordination Number due to Changes in Flatness and Elongation. ....	130
Figure 5.21 Changes in Average Coordination Number due to Changes in sphericity. ....	131
Figure 5.22 Coordination Number Distributions for Three Mixtures with Different Shape Parameters. ....	131



Figure 5.23 Probability Density Function of Normalized Contact Force for Mixtures with Different Shape Parameters.....	133
---	-----

## ABSTRACT

Voids in the mineral aggregate (VMA), as a main volumetric design parameter in the Superpave mixture design method, is an important factor to ensure asphalt mixture durability and rutting performance. Moreover, an asphalt mixture's aggregate skeleton, related to VMA, is another important factor that affects critical asphalt mixture properties such as durability, workability, permeability, rutting, and cracking resistance. The objective of this study is to evaluate the effects of aggregate size distribution and shape parameters on aggregate packing characteristics (volumetric and compaction properties) of asphalt mixtures. Three tasks were undertaken to reach this goal.

The first task was to propose an analytical approach for estimating changes in voids in the mineral aggregate (VMA) due to gradation variation and determining the relevant aggregate skeleton characteristics of asphalt mixtures using the linear-mixture packing model, an analytical packing model that considers the mechanisms of particle packing, filling and occupation. Application of the linear-mixture packing model to estimate the VMA of asphalt mixtures showed there is a high correlation between laboratory measured and model estimated values. Additionally, the model defined a new variable, the central particle size of asphalt mixtures that characterized an asphalt mixture's aggregate skeleton. Finally, the proposed analytical model showed a significant potential to be used in the early stages of asphalt mixture design to determine the effect of aggregate gradation changes on VMA and to predict mixture rutting performance.

As the second task, a framework to define and understand the aggregate structure of asphalt mixtures was proposed. To develop this framework, an analytical model for binary mixtures was proposed. The model considers the effect of size ratio and air volume between the particles on the aggregate structure and packing density of binary mixtures. Based on this model, four aggregate structures, namely coarse pack (CP), coarse-dense pack (CDP), fine-dense pack (FDP) and fine pack (FP), were defined. The model was validated using a series of 3D discrete element simulation. Furthermore, the simulation of multi-sized aggregate blends using two representative sizes for fine and coarse stockpiles was carried out to apply the proposed analytical model to actual aggregate blends. The numerical simulations verified the proposed analytical model could satisfactorily determine the particle structure of binary and multi-sized asphalt mixture gradations and could, therefore, be used to better design asphalt mixtures for improved performance.

The third task virtually investigated the effect of shape characteristics of coarse aggregates on the compactability of asphalt mixtures using a discrete element method (DEM). The 3D particles were constructed using a method based on discrete random fields' theory and spherical harmonic and their size distribution in the container was controlled by applying a constrained Voronoi tessellation (CVT) method. The effect of fine aggregates and asphalt binder was considered by constitutive Burger's interaction model between coarse particles. Five aggregate shape descriptors including flatness, elongation, roundness, sphericity and regularity and, two Superpave gyratory compactor (SGC) parameters (initial density at  $N_{ini}$  and compaction slope) were selected for investigation and statistical analyses. Results revealed that there is a statistically significant correlation between flatness, elongation, roundness, and sphericity as shape descriptors and initial density as compaction parameter. Also, the results showed that the maximum percentage of change in initial density is 5% and 18% for crushed and natural sands, respectively. The results of analysis discovered that among all particle shape descriptors, only roundness and regularity had a statistically significant relation with compaction slope, and as the amount of roundness and regularity increase (low angularity), the compaction slope decreases. Additionally, the effect of flat and elongated (F&E) particles percentage in a mixture using a set of simulations with five types of F&E particles (dimensional ratios 1:2, 1:3, 1:4 and 1:5) and ten different percentage (0, 5, 10, 15, 20, 30, 40, 50, 80 and 100) with respect to a reference mixture containing particles with flatness and elongation equal to 0.88 was conducted. Results indicated that increase of F&E particles in a mixture (more than 15%) results in a significant reduction in the initial density of the mixture especially for lower dimensional ratio (1:4 and 1:5).

# CHAPTER 1. INTRODUCTION

## 1.1 Introduction

The necessity of building additional roadway infrastructure has greatly increased over the past decades in most parts of the world due to increased economic growth and the resulting growth in the number of heavily loaded vehicles traveling the roads. To build a high-performance roadway infrastructure for a given set of traffic and environmental conditions, it is necessary to have a comprehensive and practical design methodology, including a methodology for designing asphalt mixtures. Over the years, numerous research projects have been conducted to find an efficient and cost-effective asphalt mixture design method that will produce asphalt mixtures able to meet desired field performance (Benson, 1970; Prowell et al., 2005; Muras, 2010; Pouranian and Shishehbor, 2019). Although current asphalt mixture design methods are mostly empirically based, research on more mechanistic based design methods has been increasing. Developing a mechanistic asphalt mixture design and characterization method to help mixture designers better understand the expected engineering performance of mixtures, over all stages of an asphalt mixture's life, would greatly assist the industry in producing better-performing asphalt mixtures.

On a mass basis, asphalt mixture is a combination of approximately 95% aggregates (coarse and fine) bound together by asphalt binder. The goal of asphalt mixture design is to determine the optimum combination of mixture constituents (coarse aggregate, fine aggregate and asphalt binder) that can provide appropriate field performance for anticipated traffic loads and environmental conditions. This is most often accomplished by evaluating the volumetric properties of the mixture. However, the mechanical behavior of various asphalt mixtures, even those with similar volumetric properties, can differ significantly due to a wide range in the properties of the material constituents and the many possible variations in combining the materials.

Under typical environmental conditions, the aggregate matrix within an asphalt mixture is responsible for carrying the loads imposed by traffic. The aggregate size distribution, or aggregate gradation of an asphalt mixture is a key factor that affects important properties of the asphalt mixture, such as durability, workability, permeability, and rutting and cracking resistance. Much research has been focused on the relationship between aggregate gradation and asphalt mixture performance, but this relationship remains poorly understood (Benson, 1970; Gaudette and Welke,

1977; Dukatz, 1989; Button et.al, 1990; Haddock et al., 1999; Bahuguna et al., 2006; Pouranian et al., 2018).

Many researchers have shown that aggregate inter-particle contact and interlocking are critical to the mechanical strength and stability of asphalt mixtures (Brown et al., 1997; Brown et al., 2009; Huang, 2012). Inter-particle contacts and interlocking allow applied loads to be transferred through, and thus carried by the aggregate matrix of an asphalt mixture. Appropriately packing aggregates in an asphalt mixture gradation can greatly enhance the degree of aggregate inter-particle contact and interlocking, and consequently, improve important asphalt mixture engineering properties such as strength, thereby increasing asphalt mixture field performance.

Only a few researchers have evaluated aggregate packing and the correlation between the aggregate structure of asphalt mixtures and their volumetric properties and performance (Benson, 1970; Birgisson and Ruth, 2001; Vavrik et al., 2002). Development of an analytical, systematic method to establish asphalt mixture gradations that create strong aggregate skeletons resulting in mixtures with desired performance would be a great leap forward. This can be done by quantifying the packing characteristics of aggregate particles and the role of aggregate packing plays in achieving asphalt mixtures in-service performance. Determination of how aggregate gradation affects aggregate packing, compatibility and volumetric properties of asphalt mixtures can then be used to predict the performance of the asphalt mixtures.

Today there are various aggregate gradation design approaches, such as the Superpave design method and the Bailey method that are widely used in asphalt mixture design. Introduced in 1993 as one of the principal outcomes of the Strategic Highway Research Program (SHRP), the current version of the Superpave mixture design method lacks sufficient guidance on the selection of a proper aggregate gradation in that it does not provide a correlation between the selected aggregate gradation and the expected volumetric and compatibility properties (Christensen, 2009). The Bailey method of aggregate gradation design was originally developed by Robert Bailey as a proposed strategy to develop within the asphalt mixture an aggregate skeleton capable of resisting rutting, having an acceptable level of durability, and containing adequate voids in the mineral aggregate (VMA) (Vavrik et al., 2002). In the Bailey method, a certain degree of aggregate interlock is defined by selecting an appropriate aggregate unit weight, suggested to be between 95 and 105% of the loose unit weight (Vavrik et al., 2002). Although both these methods try to

systematically describe the aggregate skeleton and inter-particle interlock, neither provides a direct and quantitative identification of aggregate interlock.

In general, four factors have the greatest effect on the development of the aggregate structure in asphalt mixtures (Vavrik et al., 2002; Olard and Perraton, 2010):

- Aggregate morphological properties (shape and surface macro-texture);
- Particle size distribution;
- Method and amount of compaction; and
- Asphalt mixture lift thickness.

The impact of aggregate morphological features such as shape and macro-texture on packing characteristics and compactability of aggregate is important but has not been widely evaluated. Most work in this area is based on laboratory experiments using local materials, costly equipment, and time consuming methods (Garboczi, 2002; Pan et al., 2006; Pan and Tutumluer, 2006 ; Masad et.al, 2007). Alternatively, numerical analysis can be an excellent substitutional approach, although the challenge of precisely characterizing aggregate shape properties and determining their effects on aggregate packing characteristics in a quantifiable and controllable manner remains. To this end, development of a comprehensive numerical framework able to generate three-dimensional (3D) aggregate particles with realistic, controllable shape parameters is desirable. Such a framework can be used to determine the effect of different shape properties on packing and compaction characteristics of aggregate particles, thus assisting asphalt mixture designers in selecting the best aggregate type and gradation in terms of design requirements and costs.

## **1.2 Objectives**

Given the importance of aggregate morphological properties and particle size distribution to the performance of asphalt mixtures, as well as the lack of quantitative research of the two factors, the objective of this research is to use particle packing theories and discrete element methods (DEM) to better define the impact of aggregate morphological properties and particle size distribution on asphalt mixture aggregate structure and thereby asphalt mixture volumetric and compaction properties. The work thus has three main tasks:

- 1) Propose a theoretical approach for evaluating the impact of aggregate gradation on asphalt mixture volumetric properties, compactability and deformation resistance;
- 2) Develop an analytical model, based on the basic concepts of particle packing, to blend coarse and fine aggregate particles in a manner that will enhance the understanding of aggregate structure in asphalt mixtures; and
- 3) Numerically evaluate the effect of aggregate morphological properties on the volumetric characteristics and compactability of aggregate particles.

### **1.3 Methodology**

The first research task is to propose and develop an analytical framework for estimating VMA and determining the aggregate skeleton characteristics of asphalt mixtures using a linear-mixture packing model. The proposed model uses aggregate gradation as input and relates the aggregate skeleton characteristics to asphalt mixture rutting performance. While many factors can affect asphalt mixture VMA and rutting characteristics (aggregate physical and chemical properties, binder content, compaction effort, etc.), the model attempts to remove these variables from the experiment in order to determine the sole effects due to changes in aggregate gradation.

The second study task develops a theoretical framework to better define asphalt mixture aggregate structures based on particle size distribution. Such a model could better optimize asphalt mixture aggregate gradations. The model is first developed based on binary mixtures and then modified to be applicable for mixtures containing multi-sized aggregates. Finally, the framework proposed by the model is evaluated using the discrete element method (DEM) to simulate asphalt mixtures packing and compaction parameters when compacted by the Superpave gyratory compactor (SGC).

Due to importance of aggregate shape features on asphalt mixture performance, the third study task evaluates the effect of changes in aggregate shape parameters on the compaction parameters of asphalt mixtures using DEM simulation. For this purpose, the spherical harmonics (SH) approach with discrete random fields theory is used to generate 3D particle shapes with prescribed shape features. The Voronoi tessellation (VT) method is applied to create mixtures of generated particles having the same size distribution. Asphalt mixture laboratory compaction is simulated with DEM and the correlation between five particle shape parameters (flatness,

elongation, roundness, sphericity, and regularity) and two laboratory compaction parameters, compaction slope and initial density investigated.

#### **1.4 Organization of Dissertation**

This dissertation contains 6 chapters:

- Chapter 1: Introduction
- Chapter 2: Linear-Mixture Packing Model
- Chapter 3: A Framework for Understanding Aggregate Structure in Asphalt Mixture
- Chapter 4: Effect of Aggregate Structure on Asphalt Mixture Compaction Parameters
- Chapter 5: Impact of the Coarse Aggregate Shape Parameters on Compaction Characteristics of Asphalt Mixtures
- Chapter 6: Summary and Conclusions



## CHAPTER 2. LINEAR-MIXTURE PACKING MODEL

*This chapter was published in Construction and Building Materials Journal  
Pouranian, M. R., & Haddock, J. E. (2018). Determination of voids in the mineral aggregate and  
aggregate skeleton characteristics of asphalt mixtures using a linear-mixture packing  
model. Construction and Building Materials, 188, 292-  
304. <https://doi.org/10.1016/j.conbuildmat.2018.08.101>*

### 2.1 Introduction

Asphalt mixtures are typically thought to be heterogeneous materials consisting of aggregates, asphalt binder, and air voids. Most of a dense-graded asphalt mixture is the aggregates (approximately 85% by volume) and as such, the load bearing capacity of an asphalt mixture is strongly related to its aggregate skeleton. Besides the physical and mechanical properties of the asphalt binder, the aggregate related parameters such as shape, texture, chemical properties, and gradation affect the volumetric properties and subsequently, the performance of asphalt mixtures. At high pavement temperatures, the role of the aggregate skeleton on rutting performance can be even more prominent, since at such temperatures the asphalt binder becomes less viscous. Therefore, designing asphalt mixtures with effective aggregate skeletons is especially crucial to rutting performance at high mixture temperatures.

Over the years, much research has been conducted on the effect of aggregate skeleton on asphalt mixture performance (Benson, 1970; Gaudette and Welke, 1977; Button et al, 1990; Bahuguna et al., 2006). In 1956, Lottman and Goetz showed the significant role of aggregate in an asphalt mixture, pointing out that aggregate structure and aggregate characteristics, such as gradation, shape, and coarse aggregate surface texture are main factors influencing the development of the aggregate skeleton. Dukatz (1989) concluded that asphalt mixture rutting resistance is highly dependent on aggregate gradation and that mixtures produced with the best possible materials can show poor rutting resistance without an appropriate aggregate gradation. The effect of aggregate gradation on the asphalt mixture properties was also evaluated by Elliott et al. (1991) who concluded that changing the gradation curve shape has a substantial effect on the mechanical and volumetric properties of asphalt mixtures.

Haddock et al. (1999) also evaluated the impact of aggregate gradation on asphalt mixture performance. They used two mixture types having nominal maximum aggregate sizes (NMAS) of 9.5 and 19.0 mm to evaluate the sensitivity of asphalt mixture performance to gradation changes. For each mixture type, three aggregate gradations (above, through, and below the Superpave restricted zone) were designed. Triaxial tests, accelerated pavement tests, and laboratory wheel tracking tests were used to gauge mixture response. Results of the study indicated that mixtures with gradations above the restricted zone (fine-graded) had the best rutting resistance in both the accelerated pavement tests and the laboratory wheel tests. Additionally, the fine-graded mixtures displayed higher strength, based on the triaxial compression testing results.

In addition to experimental approaches, the effect of particle size distribution on the packing behavior of mixtures has been studied by two other approaches, numerical and analytical analyses (Brouwers, 2006; He, 2010). Discrete element modeling (DEM) is perhaps the best-known numerical approach (He, 2010; Shen and Yu, 2011; Mostofinejad and Reisi, 2012; Minh and Cheng, 2013). However, this method has some limitations. First, the full range of particles cannot be considered, especially when there is a large difference between the maximum and minimum particle sizes (Chen, 2011). Secondly, DEM requires large amounts of computational time, and the time requirement increases with increasing number of particle sizes. Alternatively, the analytical approaches are able to cover the full range of particle sizes with negligible computational time, though they are usually based on basic packing concepts and need to be calibrated by experimental works. Due to the ability to cover the full particle size distribution and the need for less computer time, the analytical approach was chosen for this study.

A conceptual and analytical approach to the effects of asphalt mixture gradation on asphalt mixture performance has also been studied by Roque et al. (2006) who proposed an analytical model to evaluate the coarse aggregate structure of asphalt mixtures based on the basic principles of particle packing. Their work determined the main aggregate size range of the aggregate structure in an asphalt mixture and related the quality of this structure to asphalt mixture performance. The researchers named the main aggregate size range the dominant aggregate size range (DASR) and suggested that to keep the DASR particles in contact with each other, the DASR porosity should not exceed 48 percent. Evaluation of their proposed model using an extensive range of asphalt

mixtures indicated the model could identify asphalt mixture gradations that resulted in asphalt mixtures with poor rutting performance.

Guarin et al. (2013) used the concept of DASR to evaluate the effects of binder content changes, aggregate smaller than the DASR, and air voids content on asphalt mixture performance, both (rutting and cracking). In the study, aggregates smaller than the DASR were referred to as the interstitial component (IC) and a new parameter, the disruption factor, was introduced to measure the disruptive effect of the IC particles on the DASR particle structure. Additionally, Lira et al. (2013) presented a framework to recognize the range of aggregate sizes which form the load carrying structure in asphalt mixtures and determine its quality. The porosity and coordination number were considered as two parameters to evaluate the quality of the load carrying structure and relate it to mixture rutting resistance. In this framework, the gradations were considered as discrete particle sizes having a size ratio of 2 to 1 between contiguous sieve sizes. Results of this study were fairly consistent with experimental rutting performance data.

Voids in mineral aggregate (VMA) is an important volumetric parameter in asphalt mixture design that, when used properly, can reduce the risk of designing poorly-performing mixtures. A great deal of research has shown that asphalt mixture gradation and properties such as the NMAS, aggregate surface texture, and aggregate shape are factors that significantly influence asphalt mixture VMA (McLeod, 1959; Coree and Hislop, 2000; Asphalt Institute, 2001; Prowell et al., 2005; Christensen, 2009). Like many asphalt mixture design methods, the Superpave mixture design methods recommends a minimum VMA requirement dependent on the size of the aggregate particles used in the mixture. The importance of VMA to asphalt mixture performance means that asphalt mixture designers expend a great deal of time and effort to select the best aggregate gradation that meets the target mixture VMA. Currently, the common approach to do so is a trial and error procedure, sometimes based on empirical predictive equations, but almost always requiring a good deal of experimental testing. Although some experimental methods, such as the Bailey method, can reduce the experimental testing necessary to determine the proper aggregate gradation for an asphalt mixture, development of an analytical procedure to predict asphalt mixture VMA based on the mixture gradation would allow asphalt mixture designers to more quickly and accurately design mixtures that meet their respective VMA requirements.

## 2.2 Model Framework

### 2.2.1 Background

The packing of solid particles has been of interest to most applied sciences for centuries (Yu and Standish, 1991). Generally, most particle packing studies can be classified into two groups, those that consider an assessment of how the variables, such as particle characteristics, container, packing methods, etc. govern the packing of a particle bed, and those that observe the particle bed structure to explain the particle packing behavior, with specific attention to particle arrangement, or pore spaces in the structure. In both groups, the behavior of particle packing is usually characterized by porosity, or its related concepts, packing fraction and specific volume. Much research has shown a high correlation between porosity and particle packing structure and packed particle properties such as particle mass, density, and size distribution (Furnas, 1931; Westman, 1936; Lee, 1970, Standish and Borger, 1979; Standish and Yu, 1987). Among these properties, the particle size distribution strongly affects the packed bed porosity (Fuller and Thompson, 1907). Therefore, it has been of historical importance to theoretically determine the relationship between the porosity and particle size distribution of materials.

In 1936, Westman proposed a mathematical approach to predict the porosity of multi-component mixtures of spherical particles using the results of binary mixtures. This approach has been studied by other researchers and has led to useful results (Lee, 1970; Standish and Borger, 1979; Standish and Yu, 1987). These studies have shown there are two main packing mechanisms, namely a filling mechanism and an occupation mechanism that describe the behavior of packing systems. For the filling mechanism, the introduction of a new particle component to an existing packing system does not change the skeleton or connection of the existing components, but instead simply fills the voids between existing components. This mechanism is valid if the size ratio between the new component and existing components is infinitely small. The linear packing model is the most popular model developed based on this mechanism. The occupation mechanism is different in that the introduction of a new component does change the skeleton of an existing packing system; the size of the new component is too large to fill the voids in the existing packing structure. The mixture packing model is an example of a packing model using this mechanism (see Figure 2.1).

The linear packing model is a theoretical model that has been used by many researchers to describe the random packing of particles (Westman, 1936; Furnas, 1931; Stovall et al., 1986; De Larrard, 1999). The theory of this model is based on the filling mechanism and was first proposed by Westman (1936) for binary mixtures of spherical particles.

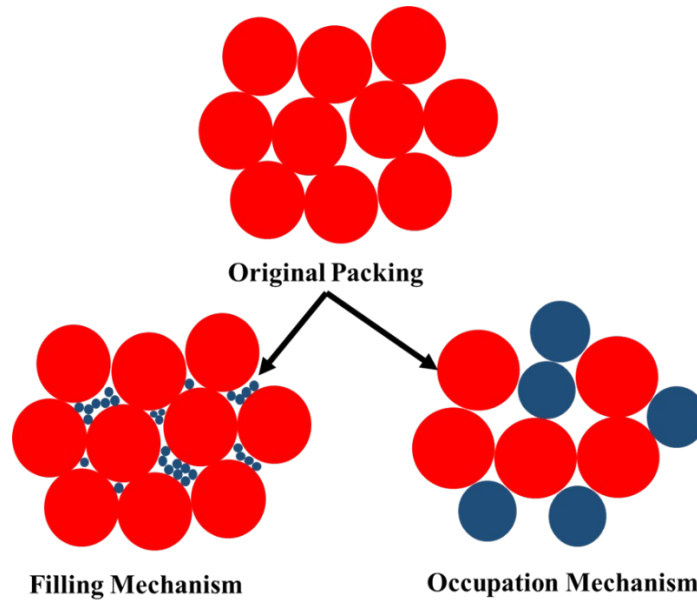


Figure 2.1 Schematic Illustration of Filling and Occupation Mechanisms.

It was subsequently extended to multicomponent mixtures by other researchers (Stovall et al., 1986; De Larrard, 1999). In the model, the overall specific volume of a multi-component mixture is controlled by one specific component and considered to vary linearly with the fractional solid volumes of the other components. Therefore, the co-interactions between components of the mixture are not considered. However, Standish and Yu (1987) demonstrated that this model is only able to describe a packing system structure composed of small particle size ratios.

The mixture packing model is an analytical-experimental packing model that describes packing system structure based on theoretical experiments with mixtures such as Scheffe's simplex-centroid design and D-optimal design (Yu and Standish, 1991). It provides an alternate, explicit scheme to the linear packing model in order to estimate the porosity of multi-component mixtures. The mixture packing model uses the occupation mechanism and assumes the overall packing structure of a mixture is controlled by two or more components. Some studies have compared experimental results with the predicted results of the mixture packing model to show that it could

satisfactorily estimate the porosity of multi-component mixtures (Standish and Borger, 1979; Leitzement et al., 1985; Standish and Yu, 1987). Comparisons between the filling and occupational mechanisms and their corresponding packing models reveal that the size ratio between mixture components is the critical parameter for selecting the appropriate packing model to use in modeling any given packing system. For spherical particles, Yu and Standish (1991) proposed the critical size ratio between small and large components is 0.154. Thus, the linear packing model is applicable if the particle size ratio is less than 0.154; otherwise, the mixture packing model should be used to describe the packing structure of a multi-component mixture.

### 2.2.2 Linear-Mixture Model

The linear-mixture model is a combination of the linear and mixture packing models and was first introduced by Yu and Standish (1991). In this model, the mixture is assumed to be a system composed of a specific number,  $n$ , of equal-density, spherical and non-deformable particles. Each particle size has an effective diameter,  $d$ , and initial porosity,  $\epsilon$ . Packing density ( $r$ ) is defined as one minus porosity, while specific volume ( $V$ ) is defined as the apparent volume occupied by a unit solid volume of particles (reciprocal of packing density). The order of particle diameter is considered to be decreasing ( $d_1 \geq d_2 \geq d_3 \geq \dots \geq d_n$ ) and the fraction volume of particles,  $X$ , should satisfy the constraint in Equation 2.1.

$$X_1 + X_2 + X_3 + X_4 + \dots + X_n = 1 \quad (2.1)$$

As previously mentioned, the linear packing model assumes that overall specific volume varies linearly with the fractional volumes of each component. Thus, if component  $i$  is considered as the main component ( $1 \leq i \leq n$ ), the overall specific volume,  $V^T$ , can be determined as shown in Equation 2.2.

$$V^T = \sum_{j=1}^{i-1} [V_i - (V_i - 1)A(i,j)]X_j + V_i X_i + \sum_{j=i+1}^n V_i [1 - B(i,j)]X_j \quad (2.2)$$

In this equation,  $A(i, j)$  and  $B(i, j)$  are the interaction functions to describe the interface between components  $i$  and  $j$  and are defined as (Yu and Standish, 1993):

$$A(i,j) = (1 - (d_i/d_j))^{2.0} + 0.4(d_i/d_j)(1 - (d_i/d_j))^{3.7} \quad (2.3a)$$

$$B(i,j) = (1 - (d_i/d_j))^{3.3} + 2.8(d_i/d_j)(1 - (d_i/d_j))^{2.7} \quad (2.3b)$$

Finally, the overall specific volume of a mixture,  $V$ , based on the linear packing model, can be represented by:

$$V = \max \{V_1^T, V_2^T, V_3^T, V_4^T, \dots, V_n^T\} \quad (2.4)$$

Conversely, a mixture model can also estimate the overall specific volume of a mixture using the equation:

$$V = \sum_{i=1}^n C_{ij} X_i + \sum_{i=1}^{n-1} \sum_{j=i+1}^n C_{ij} X_i X_j + \sum_{i=1}^{n-1} \sum_{j=i+1}^n D_{ij} X_i X_j (X_i - X_j) \quad (2.5)$$

where  $C_{ij}$  and  $D_{ij}$  are interaction coefficients for components  $i$  and  $j$  and can be determined from the results of binary mixture experiments. Yu and Standish (1991) proposed two functions to determine these coefficients based on the size ratio,  $r_{ij}$ , of each particle pair and corresponding to the average initial packing density,  $\rho_0$ , as shown in Equations 2.6a and 2.6b.

$$C_{ij} = \begin{cases} 0 & r_{ij} \geq 0.741 \\ 10.288 \times 10^{-1.4566\rho_0} (-1.0002 + 0.1126r_{ij} + 5.8455r_{ij}^2 - 7.9488r_{ij}^3 + 3.1222r_{ij}^4) & r_{ij} < 0.741 \end{cases} \quad (2.6a)$$

$$D_{ij} = \begin{cases} 0 & r_{ij} \geq 0.741 \\ (-1.309 + 15.04\rho_0 - 37.453\rho_0^2 + 40.869\rho_0^3 - 17.11\rho_0^4) \times (-1.003 + 0.359r_{ij} + 1097r_{ij}^2 - 22.197r_{ij}^3 + 12.434r_{ij}^4) & r_{ij} < 0.741 \end{cases} \quad (2.6b)$$

To estimate the overall porosity of a mixture, the upper and lower mixture zone limit for each component must first be determined using Equation 2.7.

$$d_i^{\min} = 0.154d_i \quad \text{and} \quad d_i^{\max} = d_i / 0.154 \quad (2.7)$$

Next, the mixture model (Equation 2.5) is used to calculate the partial specific volume ( $V1_i^T$ ) for particles within the range of  $d_i^{\min}$  and  $d_i^{\max}$ . The linear model (Equation 2.2) is then used to calculate the overall specific volume ( $V2_i^T$ ) for particles out of the range of  $d_i^{\min}$  to  $d_i^{\max}$ . Finally, the overall specific volume of the corresponding mixture component  $i$  is calculated using Equation 2.8.

$$V_i^T = V1_i^T + V2_i^T \quad (2.8)$$

All the above steps are repeated for all mixture components and the overall specific volume of the mixture can be determined as:

$$V = \max \{V_1^T, V_2^T, V_3^T, V_4^T, \dots, V_n^T\} \quad (2.9)$$

In the case of asphalt mixtures, the overall porosity of a mixture is VMA and can be estimated by Equation 2.10.

$$\varepsilon = \frac{(V^T - 1)}{V^T} \quad (2.10)$$

### 2.2.3 Model Implementation for Asphalt Mixtures

To estimate the VMA and determine the characteristic of the main aggregate skeleton of an asphalt mixture, it is necessary to first define the initial packing density using the different aggregate sizes as input data. This initial packing density is determined using the unit weight of aggregates (American Association of State Highway and Transportation Officials (AASHTO) T19, “Standard Method of Test for Bulk Density (Unit Weight) and Voids in Aggregate”). For dense-graded asphalt mixtures, the initial packing density of aggregates can be determined for coarse and fine aggregates based on corresponding loose unit weight (LUW) and rodded unit weight (RUW) respectively (Equations 2.11a and 2.11b).

$$\text{Coarse Packing Density (CPD)} = \frac{\text{Loose Unit Weight of Coarse Stockpile}}{G_{sb \text{ coarse}} \times \gamma_w} \quad (2.11a)$$

$$\text{Fine Packing Density (FPD)} = \frac{\text{Roddod Unit Weight of Fine Stockpile}}{G_{sb \text{ fine}} \times \gamma_w} \quad (2.11b)$$



where,  $G_{sb}$  is aggregate bulk specific gravity and  $\gamma_w$  is unit weight of water.

The definition of coarse and fine aggregate is based on the coarse and fine aggregate definitions used by the Bailey method. In the Bailey method, coarse and fine aggregates are defined by a sieve size known as the primary control sieve (PCS) (Vavrik et al., 2001). The PCS is a function of the NMAS of the aggregate blend and is calculated as:

$$PCS = NMPS \times 0.22 \quad (2.12)$$

If component  $i$  is considered the controlling particle size (CPS) ( $1 \leq i \leq n$ ), the main particle size range (MPSR) where the interaction between particles is defined by the mixture packing model, can be defined by two parameters,  $M$  and  $N$  as:

$$M \text{ (upper limit)} = CPS/0.22 \quad \text{and} \quad N \text{ (lower limit)} = CPS \times 0.22 \quad (2.13)$$

The coefficient of 0.22 is selected because two-dimensional (2-D) packing analyses of different shaped particles show that particle diameter ratios range from 0.155 (all round particles) to 0.289 (all flat particles) with an average value of 0.22 (Vavrik, 2000) (see Figure 2.2).

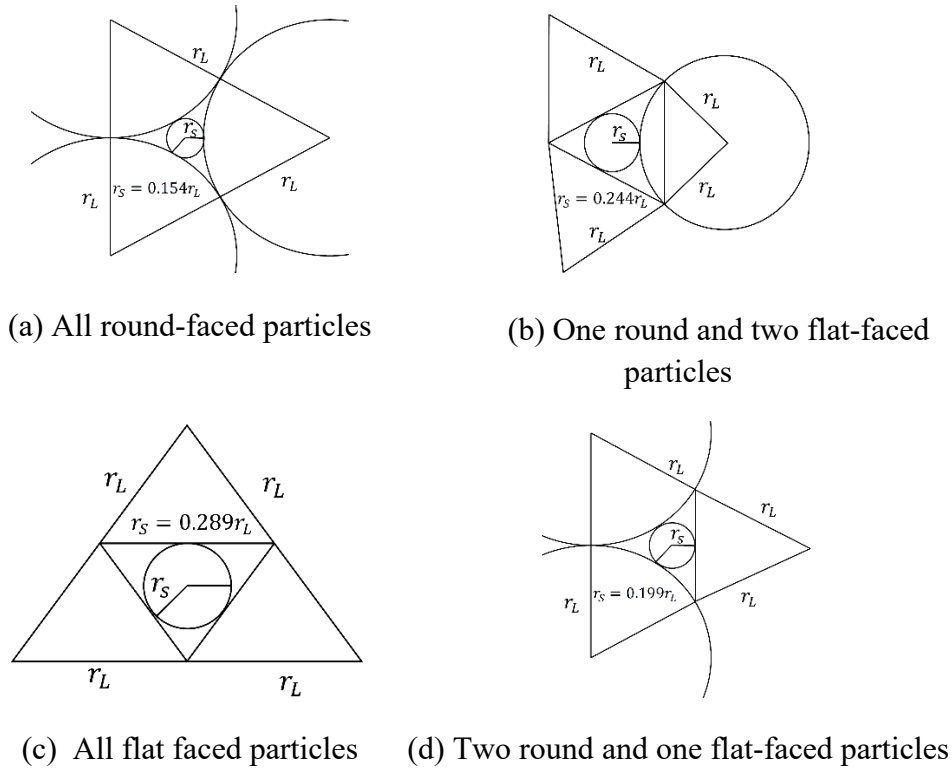


Figure 2.2 Two-dimensional Analysis of Particle Combinations with Different Faces.

The MPSR defines the size range of particles that creates the main skeleton of the mixture (Particles #1, #2 and #3 in Figure 2.3). The group of particle sizes smaller than  $N$  is defined as the small un-mixing range (SUMR) and fill the voids between the MPSR and contribute to the stability of the main particle skeleton of the mixture (Particles # 4 in Figure 2.3). The particle sizes larger than  $M$  are defined as being the large un-mixing range (LUMR) particles. These particles essentially float in the MPSR particle matrix and do not contribute to the stability of the mixture (Particle #5 in Figure 2.3).

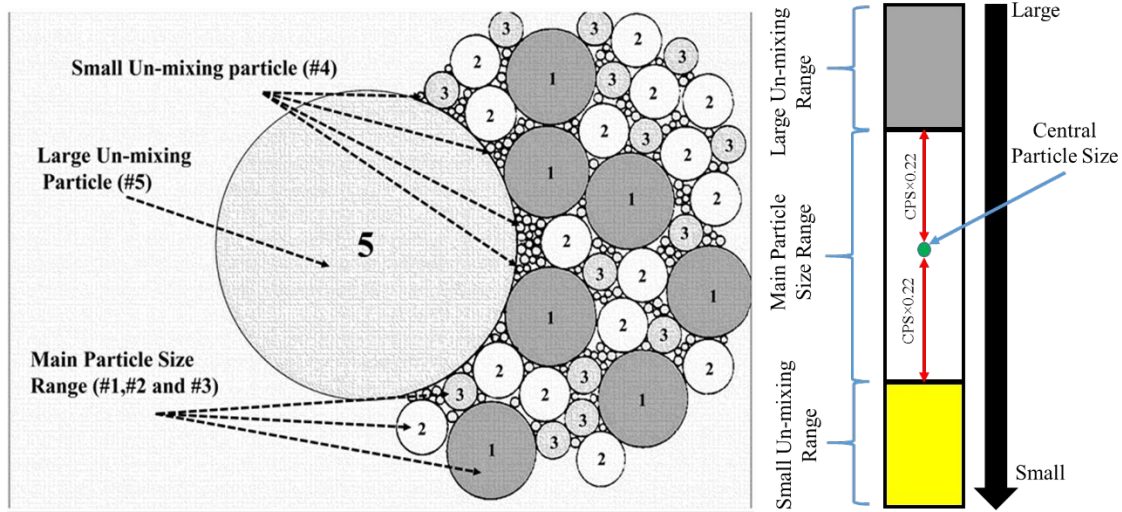


Figure 2.3 Graphical Definition of Three-particle Size Ranges.

The CPS is defined as the main particle size that creates the closest overall porosity to the actual VMA of an asphalt mixture. The change in VMA as a function of controlling particle sizes for an asphalt mixture sample is shown in Figure 2.4. The figure shows two CPS that result in porosity closest to the actual VMA of the asphalt mixture. The larger CPS is called coarse controlling particle size (CCPS) and the smaller, fine controlling particle size (FCPS). Selection of which CPS is the main CPS of a given asphalt mixture is based on the type of mixture gradation. If the asphalt mixture gradation is coarse-graded, stone matrix asphalt (SMA) or open-graded friction course, the CCPS will be the main CPS of the mixture; otherwise, FCPS will be the main CPS.

Since this study defined asphalt mixture gradation type (coarse- or fine-graded) based on the Bailey method designation, a coarse-graded mixture is one having a coarse aggregate skeleton and fine-graded mixtures as those which do not have enough coarse aggregate particles to form a skeleton. The dividing line between fine- and coarse-graded mixtures is the chosen unit weight (CUW), defined as some percentage of LUW. If the CUW is selected to be less than 90% of the LUW, the mixture is categorized as fine-graded; otherwise it is a coarse-graded mixture.

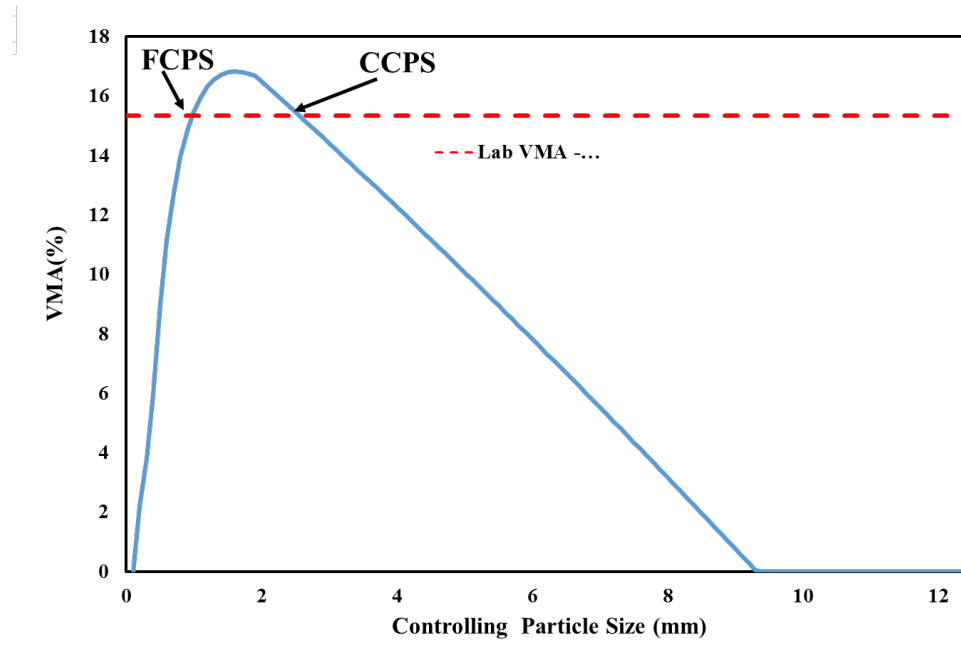


Figure 2.4 Voids in the Mineral Aggregate Variation as a Function of Controlling Particle Size.

For mixtures with a continuous size distribution function,  $f(d)$ , the overall specific volume of the mixture,  $V$ , can be determined by Equations 2.14a and 2.14b,

$$V = \text{Max}(V_{d_i}^T(d) \quad d_{\min} \leq d_i \leq d_{\max}) \quad (2.14a)$$

$$V_{d_i}^T(d) = V_{d_i}^{\text{MPSR}}(d) \int_N^M f(x) dx + V_{d_i}^{\text{SUMR}}(d) + V_{d_i}^{\text{LUMR}}(d) \quad (2.14b)$$

where,  $V_{d_i}^{\text{MPSR}}$ ,  $V_{d_i}^{\text{SUMR}}(d)$  and  $V_{d_i}^{\text{LUMR}}(d)$  are the overall specific volumes of the MPSR, SUMR and LUMR ranges of particles respectively. These are defined by:

$$\begin{aligned}
V_{d_i}^{\text{MPSR}}(d) &= V_0 + \frac{\int_N^M \int_N^M C\left(\frac{y}{x}, \rho_0\right) f(x) f(y) dx dy}{\left(\int_N^M f(x) dx\right)^2} \\
V_0 &= \int_N^M f(x) V_x dx \\
C\left(\frac{y}{x}, \rho_0\right) &= \begin{cases} 0 & \frac{y}{x} \geq 0.741 \\ 10.288 \times 10^{-1.456 \rho_0} (-1.0002 + 0.112 \frac{y}{x} + 5.845 (\frac{y}{x})^2 - 7.948 (\frac{y}{x})^3 + 3.12 (\frac{y}{x})^4) & \frac{y}{x} < 0.741 \end{cases} \\
V_d^{\text{SUMR}}(d) &= \int_{d_{\min}}^N [(V_d - (V_d - 1)A(x, d))] f(x) dx \\
V_d^{\text{LUMR}}(d) &= \int_M^{d_{\max}} [(V_d (1 - B(x, d)))] f(x) dx
\end{aligned} \tag{2.15}$$

where  $d_{\min}$  and  $d_{\max}$  are the minimum and maximum sizes in the volume frequency distribution respectively (mm),  $V_0$  is the overall initial specific volume of MPSR (dimensionless),  $\rho_0$  is the overall initial packing density of MPSR, equal to  $1/V_0$  (dimensionless),  $C(y/x, \rho_0)$  is the interaction function based on the mixture packing model, and  $A$  and  $B$  are interaction functions of a of pair particle sizes based on the linear packing model (Equations 2.3a and 2.3b).

Goltermann et.al (1997) showed that many crushed aggregates have size distribution curves represented by the Rosin-Raimmer-Sperling-Bennett (RRSB) distribution. Therefore, in this study, the RRSB function is used as the aggregate size distribution function to determine the CPS, as shown in Equation 2.16.

$$f(d) = \left(\frac{n}{d}\right) \left(\frac{d}{d_m}\right)^n e^{-\left(\frac{d}{d_m}\right)^n} \tag{2.16}$$

where  $f(d)$  is the percentage retained of size  $d$  (mm),  $d_m$  is the mean particle size (mm), and  $n$  is a measure of the spread in particle sizes.

Additionally, two parameters, the disruptive factor (DF) and the coordination number (CN) are introduced to evaluate the quality of the described model in defining the asphalt mixture aggregate structures. These parameters are used to show the relationship between the MPSR structure and rutting performance of asphalt mixtures, which is related to the mixture's capacity to resist shear. The DF is defined as the effect of SUMR and LUMR on the stability of MPSR and is related to asphalt mixture rutting performance.

$$DF = \frac{\text{Volume of potentially disruptive particles}}{\text{Volume of MPSR void}} = \frac{V_{dp}}{V_v^{MPSR}} \quad (2.17)$$

The volume of disruptive aggregate particles ( $V_{dp}$ ) is the sum of the LUMR volume and the partial volume of the SUMR ( $0.22 \times N$ ), the particles that are too large to fill the average voids between MPSR aggregate particles. The volume of MPSR voids ( $V_v^{MPSR}$ ) can be estimated by the mixture packing model, as shown in Equation 2.18.

$$V_v^{MPSR} = \sum_{i=1}^n C_{ij} X_i + \sum_{i=1}^{n-1} \sum_{j=i+1}^n C_{ij} X_i X_j + \sum_{i=1}^{n-1} \sum_{j=i+1}^n D_{ij} X_i X_j (X_i - X_j) \quad (2.18a)$$

$$V_v^{MPSR} = \frac{1}{1 - V^{MPSR}} \quad (2.18b)$$

CN is another parameter that can be used to evaluate the structural capacity of asphalt mixtures. CN is defined as the total number of contact points between a central particle and its neighboring particles. Based on theoretical analysis and experimental results, Zhao et al. (2012) concluded that increasing the number of contact points between aggregate particles results in a decrease of stress between the contact points and consequently increases the strength of the aggregate skeleton. So, the CN parameter can be used to describe the stability of the MPSR structure in asphalt mixtures. The model derived by Suzuki and Oshima (1983) is proposed for use in determining the CN of a given MPSR structure. This model estimates the CN of spherical particles in multi-component mixtures. For a mixture, with particle 'i' as the central particle,  $CN_i$  can be defined by:

$$CN_i = \sum_{k=1}^m S_{a(k)} \cdot N_{i,k} \quad (2.19)$$

where,  $S_{a(k)}$  is the fractional area of particle  $k$  that is calculated from the fractional volume. In this study, the CPS of a mixture is considered at the central particle to determine the overall mixture CN.  $S_{a(k)}$  is calculated using  $S_{v(k)}$ , volume fraction of particle  $k$ , and  $D_{(k)}$ , the diameter of particle  $k$ , as shown in Equation 2.20.

$$S_{a(k)} = \frac{\frac{S_{v(k)}}{D_{(k)}}}{\sum_{j=1}^m \frac{S_{v(j)}}{D_{(j)}}} \quad (2.20)$$

Also,  $N_{i,k}$  is the CN of particle  $i$ , which is in direct contact with particle  $k$  and is determined by:

$$N_{i,k} = \frac{2\alpha_i \left( \frac{D_{(i)}}{D_{(k)}} + 1 \right)}{1 + \frac{D_{(i)}}{D_{(k)}} - \left[ \frac{D_{(i)}}{D_{(k)}} \left( \frac{D_{(i)}}{D_{(k)}} + 2 \right) \right]^{0.5}} \quad (2.21)$$

where the constant  $\alpha_i$  can be defined using the CN of a mixture consisting of only  $i$  particles,  $\widehat{N}_{ci}$ , as follows:

$$\alpha_i = \frac{(2-\sqrt{3})\widehat{N}_{ic}}{4} \approx 0.067\widehat{N}_{ic} \quad (2.22)$$

The equation to calculate  $\widehat{N}_{ci}$  is shown in Equation 2.23.

$$\widehat{N}_{ci} = \frac{2.812(1-\varepsilon_i)^{-1/3}}{\left( \frac{G}{D_{(i)}} \right)^2 \left[ 1 + \left( \frac{G}{D_{(i)}} \right)^2 \right]} \quad (2.23)$$

where  $\varepsilon_i$  is the porosity of a mixture consisting of only  $i$  particles and the constant  $G$  can be estimated using Equation 2.24.

$$\frac{G}{D_{(i)}} = 7.318 \times 10^{-2} + 2.193 \epsilon_i - 3.357 \epsilon_i^2 + 3.194 \epsilon_i^3 \quad (2.24)$$

## 2.3 Model Evaluation

### 2.3.1 Experimental Data

The experimental data used to evaluate the proposed analytical model were extracted from work done by Vavrik (2000). These data were selected because they include the initial aggregate unit weights needed as input for the model. In his experiment, Vavrik divided the coarse and fine stockpiles into 3 levels, coarse, medium and fine. Table 2.1 shows the gradations for each of the three levels for both the coarse and fine stockpiles, along with the corresponding properties such as unit weights (loose and rodded) and bulk specific gravities. Based on the different stockpile combinations and five coarse aggregate CUW levels, 90, 95, 100, 105 and 110 percent, twenty-five, 12.5-mm asphalt mixtures were designed and specimens produced. All mixtures contained 5.5% asphalt binder (PG 64-22) by total mixture mass. Specimens were compacted using 100 gyrations of the Superpave gyratory compactor (SGC). Therefore, this experimental work is an appropriate for evaluating the proposed analytical model since binder type, binder content, aggregate physical (shape and texture) and chemical properties, as well as compaction effort and type, have been removed from the experiment. While these variables do affect asphalt mixture VMA and rutting performance, their effects have been eliminated or minimized in this experiment in order to more clearly determine the effects of changes in aggregate gradation. The repeated shear constant height (RSCH) test was used to evaluate the rutting performance of each of the 25 mixtures (Vavrik, 2000). In the test, a constant shear stress was applied to mixture specimens for 5,000 cycles and the accumulated deformation recorded and used to rank the mixtures for rutting potential. The results are shown in Table 2.2, along with the mixture VMAs and compaction slope data obtained during compaction in the SGC.



Table 2.1 Aggregate Gradations and Properties (after Vavrik, 2000).

Coarse Stockpile				Fine Stockpile		
Sieve (mm)	Coarse	Medium	Fine	Coarse	Medium	Fine
12.50	100.0	100.0	100.0	100.0	100.0	100.0
9.50	94.0	97.0	100.0	100.0	100.0	100.0
4.75	15.0	30.0	45.0	94.0	97.0	100.0
2.38	7.0	16.0	25.0	81.0	82.5	84.0
1.18	–	2.0	4.0	62.0	65.0	68.0
0.60	–	1.0	1.0	30.0	45.0	60.0
0.30	–	–	–	3.0	16.0	29.0
0.15	–	–	–	1.9	1.9	1.9
0.08	–	–	–	0.20	0.20	0.20
LUW (kg/m <sup>3</sup> )	1401.6	1420.8	1416	–	–	–
RUW (kg/m <sup>3</sup> )	1611.4	1611.4	1616.3	1616.3	1806.9	1819.7
G <sub>sb</sub>	2.692	2.692	2.692	2.572	2.572	2.572

Table 2.2 Asphalt Mixture Data (after Vavrik, 2000).

Mixture Name	Coarse Stockpile	Fine Stockpile	VMA (%)	Accumulated Strain	Compaction Slope
Block 1-10	Med	Med	15.33	----	7.7
Block 1-5	Med	Med	16.60	2.8	7.4
Block 1-LUW	Med	Med	16.58	2.7	7.9
Block 1+5	Med	Med	17.17	2.3	8.3
Block 1+10	Med	Med	17.64	1.4	8.7
Block 2-10	Coarse	Med	14.82	1.4	6.6
Block 2-5	Coarse	Med	14.67	2.6	7.0
Block 2-LUW	Coarse	Med	14.30	2.4	7.8
Block 2+5	Coarse	Med	14.07	2.2	8.2
Block 2+10	Coarse	Med	14.78	2.9	9.0
Block 3-10	Fine	Med	17.73	1.4	8.0
Block 3-5	Fine	Med	17.53	2.6	8.1
Block 3-LUW	Fine	Med	16.84	2.4	8.8
Block 3+5	Fine	Med	18.20	2.2	8.7
Block 3+10	Fine	Med	18.82	2.9	8.9
Block 4-10	Med	Coarse	15.66	1.8	7.8
Block 4-5	Med	Coarse	16.14	2.2	8.1
Block 4-LUW	Med	Coarse	16.44	2.1	8.3
Block 4+5	Med	Coarse	17.21	1.7	8.5
Block 4+10	Med	Coarse	18.36	3.7	8.7
Block 5-10	Med	Fine	12.48	1.7	7.4
Block 5-5	Med	Fine	12.72	1.7	8.3
Block 5-LUW	Med	Fine	13.07	1.6	8.9
Block 5+5	Med	Fine	13.48	2.0	9.5
Block 5+10	Med	Fine	14.67	2.1	9.6

The compaction slope is a parameter thought to yield information about the development of aggregate structure in asphalt mixtures. It is defined as the slope of the percent of maximum density (%Gmm) versus the log number of gyrations from gyration 10 to the end of compaction (Vavrik, 2000). When asphalt mixture specimens are compacted in the SGC, the larger the compaction slope, the stronger the aggregate structure. Conversely, a smaller compaction slope is thought to be indicative of an asphalt mixture that can be more easily densified and is more likely to have a weak aggregate structure, making it less resistant to deformation under traffic loading.

The data in Table 2.3 show the input values required to determine the MPSR, SUMR, and LUMR aggregate size ranges of the asphalt mixtures. Additionally, the initial packing densities for coarse and fine aggregates is shown in Table 2.3. The exponent parameter for the aggregate size distribution function,  $n$ , (see Equation 2.16) was determined using the MATLAB fitting curve toolbox. Comparisons between real and estimated gradations using the RRSB size distribution function of the mixtures shows the modified power law method can be satisfactorily used as an aggregate size distribution function (see Figure 2.5). Because the mixtures are 12.5-mm mixtures, the 2.36-mm sieve is the PCS, as dictated by the Bailey method.

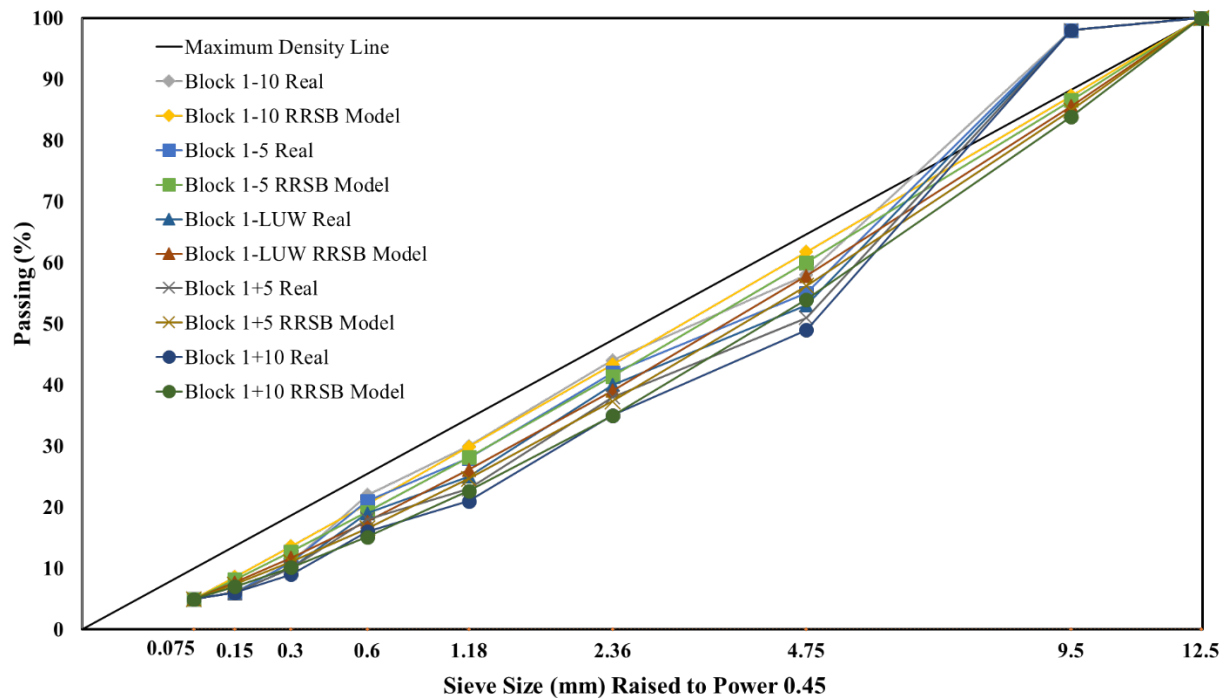


Figure 2.5 Real and Estimated Gradations for Block 1 mixtures.

Table 2.3 Input Parameters for Aggregate Size Distribution Function.

Mixture Name	Dm (mm)	n	Coarse Packing Density	Fine Packing Density
Block 1-10	3.9900	0.9031	0.475	0.703
Block 1-5	4.2285	0.9306	0.517	0.703
Block1-LUW	4.4641	0.9926	0.528	0.703
Block 1+5	4.6625	1.0392	0.554	0.703
Block 1+10	4.9124	1.1258	0.581	0.703
Block 2-10	4.1262	0.8577	0.469	0.703
Block 2-5	4.3629	0.8848	0.495	0.703
Block2-LUW	4.6566	0.9279	0.520	0.703
Block 2+5	4.8984	0.9812	0.547	0.703
Block 2+10	5.1158	1.0460	0.573	0.703
Block 3-10	3.1793	0.9593	0.470	0.703
Block 3-5	3.9114	0.9955	0.500	0.703
Block3-LUW	4.1520	1.0530	0.526	0.703
Block 3+5	4.3138	1.0980	0.550	0.703
Block 3+10	4.4639	1.1579	0.580	0.703
Block 4-10	4.1793	0.9701	0.480	0.680
Block 4-5	4.4242	1.0227	0.500	0.680
Block4-LUW	4.6240	1.0743	0.528	0.680
Block 4+5	4.8200	1.1287	0.554	0.680
Block 4+10	4.9991	1.1795	0.580	0.680
Block 5-10	3.8723	0.8296	0.480	0.708
Block 5-5	4.1092	0.8751	0.500	0.708
Block5-LUW	4.3267	0.9220	0.528	0.708
Block 5+5	4.5856	0.9779	0.550	0.708
Block 5+10	4.8412	1.0581	0.580	0.708

### 2.3.2 VMA Estimation

After determination of model input parameters, the porosity, or VMA of each asphalt mixture was estimated using the previously described linear-mixture model; the data are shown in Table 2.4. Figure 2.6 is a plot of the model-estimated and laboratory-measured VMA values. The values are clustered about the line-of-equality, confirming the proposed model reasonably predicts asphalt mixture VMA and could, therefore, be used as an analytical tool to predict the VMA of asphalt mixtures prior to compaction. These two VMA groups were statistically analyzed to determine if they are significantly different; the results are shown in Table 2.5. Although the average model-

estimated VMA is slightly higher than the average laboratory-measured VMA, there is a high correlation (90%) between the two and the relationship is statistically significant (95% confidence level).

Table 2.4 Estimated and Laboratory-measured Voids in the Mineral Aggregate.

Mixture Name	Lab VMA (%)	Estimated VMA (%)
Block 1-10	15.33	15.83
Block 1-5	16.60	15.26
Block 1-LUW	16.58	16.14
Block 1+5	17.17	16.06
Block 1+10	17.65	17.06
Block 2-10	14.82	13.67
Block 2-5	14.67	13.14
Block 2-LUW	14.30	13.23
Block 2+5	14.07	13.62
Block 2+10	14.78	14.22
Block 3-10	17.73	18.17
Block 3-5	17.53	18.58
Block 3-LUW	16.84	19.07
Block 3+5	18.20	18.87
Block 3+10	18.82	18.94
Block 4-10	15.66	15.46
Block 4-5	16.14	16.03
Block 4-LUW	16.44	17.18
Block 4+5	17.21	17.78
Block 4+10	18.36	17.99
Block 5-10	12.48	13.59
Block 5-5	12.72	12.40
Block 5-LUW	13.07	13.76
Block 5+5	13.48	14.08
Block 5+10	14.67	14.98

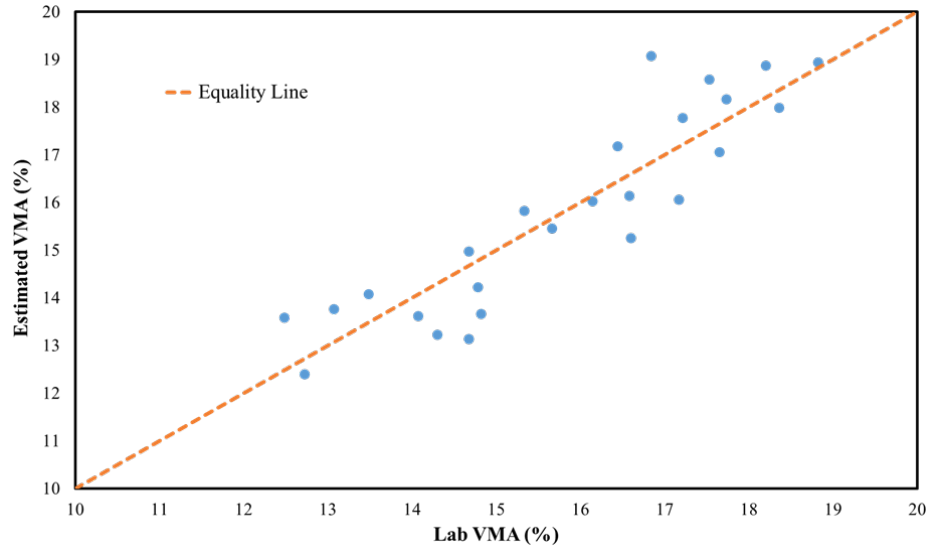


Figure 2.6 Laboratory-measured and Model-estimated Voids in the Mineral Aggregate.

Table 2.5 Statistical Analysis of Model-estimated and Laboratory-measured Voids in the Mineral Aggregate.

Variable	Mean	Std. Dev	Sum	Minimum	Maximum
Lab VMA (%)	15.8	1.84	395.32	12.48	18.82
Estimated VMA (%)	17.3	1.81	432.65	13.31	20.22
				R-Square	0.91
Variable	DF	Parameter	Standard Error	Pr >  t	Significant
Intercept	1	-0.87	1.13	0.44	No
Estimated VMA (%)	1	0.96	0.06	<.0001	Yes

### 2.3.3 Aggregate Skeleton Determination

Table 2.6 and Figure 2.7 show the main controlling particle sizes for the 25 mixtures. Because all mixtures are categorized as coarse-graded (CUW of all samples are greater than 90% of LUW), the CCPS values were selected as the main CPS for all mixtures. Figure 2.7 also shows that for each block, increasing the CUW results in higher CPS and consequently a more coarsely graded main aggregate structure. This result is in good agreement with the Bailey method assumption which states that increasing the CUW of an asphalt mixture gradation results in a coarser gradation, and consequently increased coarse aggregate particle interlock. Statistical analysis between values of CPS and corresponding CUW of the mixtures indicates there is a statistically significant relationship between CPS and CUW (Table 2.7).

After determination of mixture CPS values, the DF and CN for each mixture can be determined using Equations 17 and 23 respectively (Table 2.8). These two parameters are used to assess the quality of the MPSR and relate it to mixture rutting performance. Statistical analysis between these two parameters (DF and CN) and the RSCH accumulated strain of the mixtures indicates a significant relationship between them (Table 2.9).

Table 2.6 Three Aggregate Size Ranges of Mixtures.

Mixture Name	Control Particle Size (mm)	Main Particle Size Range (mm)	Small Un-mixing Range (mm)	Large Un-mixing Range (mm)
BLOCK 1-10	2.5	12.5-0.38	0-0.38	N/A
BLOCK 1-5	2.5	12.5-0.38	0-0.38	N/A
BLOCK 1-LW	4.1	12.5-0.63	0-0.63	N/A
BLOCK 1+5	5.1	12.5-0.78	0-0.78	N/A
BLOCK 1+10	8.3	12.5-1.28	0-1.28	N/A
BLOCK 2-10	2.0	12.5-0.3	0-0.30	N/A
BLOCK 2-5	2.6	12.5-0.4	0-0.40	N/A
BLOCK 2-LW	3.8	12.5-0.58	0-0.58	N/A
BLOCK 2+5	5.7	12.5-0.88	0-0.88	N/A
BLOCK 2+10	7.5	12.5-1.15	0-1.15	N/A
BLOCK3-10	2.6	12.5-0.4	0-0.40	N/A
BLOCK 3-5	3.8	12.5-0.58	0-0.58	N/A
BLOCK3-LW	5.8	12.5-0.9	0-0.90	N/A
BLOCK 3+5	6.3	12.5-0.97	0-0.97	N/A
BLOCK 3+10	7.6	12.5-1.17	0-1.17	N/A
BLOCK4-10	4.9	12.5-0.75	0-0.75	N/A
BLOCK 4-5	5.5	12.5-0.84	0-0.84	N/A
BLOCK4-LW	6.9	12.5-1.10	0-1.10	N/A
BLOCK 4+5	8.2	12.5-1.26	0-1.26	N/A
BLOCK 4+10	9.0	12.5-1.38	0-1.38	N/A
BLOCK5-10	2.1	12.5-0.32	0-0.32	N/A
BLOCK 5-5	3.0	12.5-0.46	0-0.46	N/A
BLOCK5-LW	4.0	12.5-0.61	0-0.61	N/A
BLOCK 5+5	5.4	12.5-0.83	0-0.83	N/A
BLOCK 5+10	7.4	12.5-1.40	0-1.40	N/A

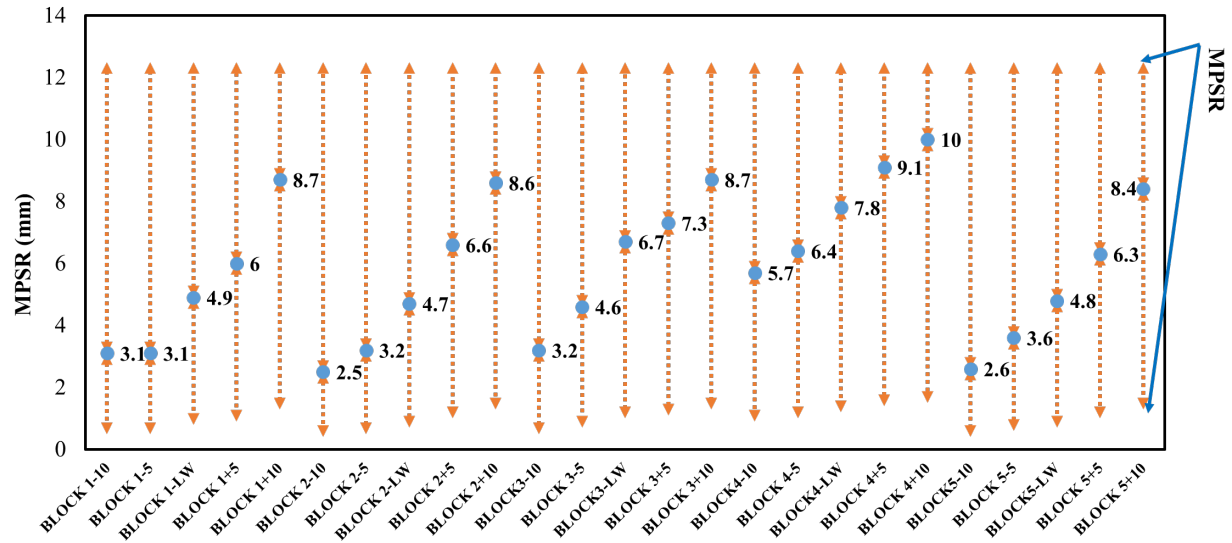


Figure 2.7 Controlling Particle Size and Main Particle Size Range of Mixtures.

Table 2.7 Statistical Analysis Results of Controlling Particle Size and Chosen Unit Weight.

Relation	R-Square	F Value	Pr >  t	Significant
$CPS = -21.32 + 50.108 \times CUW$	0.84	67.27	< 0.0001	Yes

The relationship suggests that increasing the disruptive factor in asphalt mixtures results in higher accumulated strain under loading; a higher mixture rutting potential (Figure 2.8). Thus, the volume of disruptive aggregate and the volume of MPSR voids can be considered as two structural attributes in asphalt mixture aggregate gradations that have a significant relationship to asphalt mixture rutting resistance. The results in Table 2.9 also indicate a statistically significant relationship between CN and the RSCH accumulated strain. Such a relationship suggests that increasing the number of contact points between aggregates (CN) will result in decreased stress between the contact points, and a subsequent increase in aggregate skeleton strength, improving resistance to deformation (Figure 2.9).

The statistical analysis of the CPS and compaction slope relationship shows there is a significant relation between the two (Table 2.10). This relationship indicates that mixtures with higher CPS have stronger aggregate structures, and as a result should be more difficult to densify, yet another validation of the Bailey method suggestion for improving aggregate interlock in asphalt mixtures.

Table 2.8 Disruptive Factors and Coordination Numbers of the Asphalt Mixtures.

Mixture Name	$V_v^{MPSR}$	$V_{dp}$	Disruptive Factor	Coordination Number
Block 1-10	0.09	0.19	2.01	7.81
Block 1-5	0.09	0.16	1.81	6.79
Block1-LUW	0.06	0.12	1.91	7.28
Block 1+5	0.06	0.09	1.53	6.29
Block 1+10	0.09	0.07	0.75	7.12
Block 2-10	0.26	0.17	0.65	7.78
Block 2-5	0.11	0.18	1.69	7.25
Block2-LUW	0.09	0.16	1.74	6.73
Block 2+5	0.18	0.11	0.61	6.80
Block 2+10	0.13	0.19	1.46	6.94
Block 3-10	0.19	0.14	0.74	7.58
Block 3-5	0.10	0.19	1.83	6.63
Block3-LUW	0.07	0.11	1.58	8.08
Block 3+5	0.07	0.11	1.47	6.70
Block 3+10	0.09	0.18	1.95	7.94
Block 4-10	0.16	0.15	0.96	7.86
Block 4-5	0.09	0.14	1.51	7.35
Block4-LUW	0.07	0.09	1.28	6.85
Block 4+5	0.13	0.08	0.62	6.40
Block 4+10	0.06	0.17	2.62	5.91
Block 5-10	0.20	0.24	1.21	6.81
Block 5-5	0.17	0.20	1.15	7.32
Block5-LUW	0.19	0.17	0.91	7.04
Block 5+5	0.08	0.11	1.40	6.95
Block 5+10	0.13	0.19	1.47	6.81

Table 2.9 Results of Statistical Analysis between Accumulated Strain at 5000 Cycles and Disruptive Factors and Coordination Numbers.

Source	DF	Sum of Squares	Mean Square	F Value	Pr > F
Model	2	6.56394	3.28197	51.34	<.0001
				R-Square	0.62
Variable	DF	Parameter	Standard Error	Pr >  t	Significant
Intercept	1	2.74968	1.23596	0.0367	Yes
DF	1	0.81162	0.16266	<.0001	Yes
CN	1	-0.23325	0.14802	0.01293	Yes



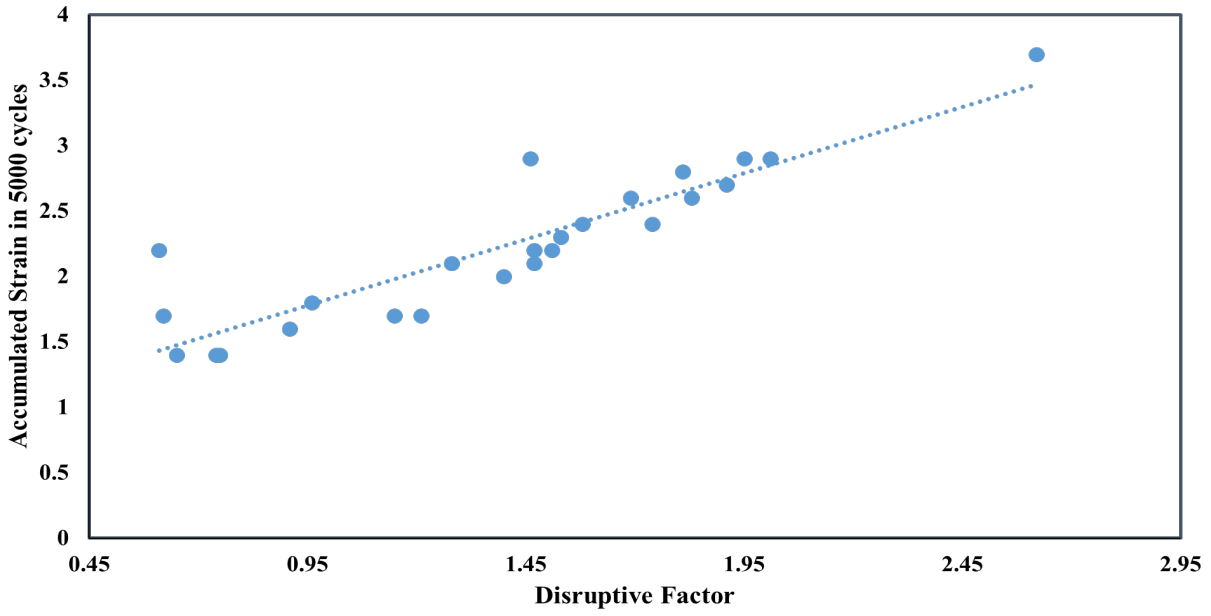


Figure 2.8 Accumulated Strain at 5000 Cycles as a Function of the Disruptive Factor.

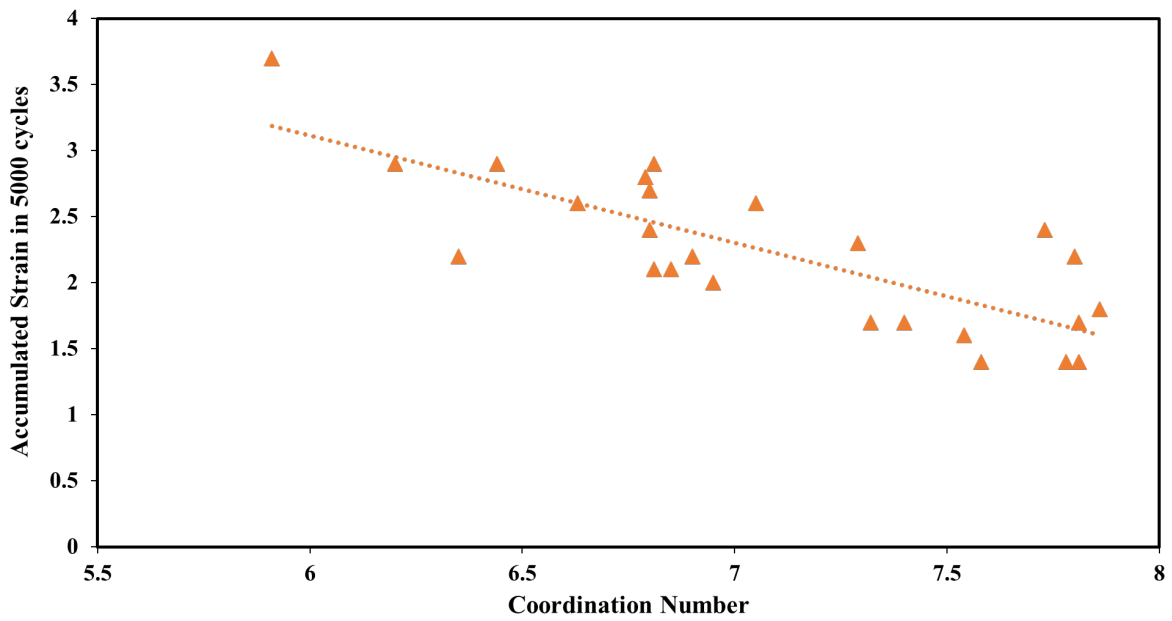


Figure 2.9 Accumulated Strain at 5000 Cycles as a Function of the Main Particle Size Range Coordination Number.

Table 2.10 Results of Statistical Analysis between Compaction Slope Values and Controlling Particle Size.

Source	DF	Sum of Squares	Mean Square	F Value	Pr > F
Model	1	44.65995	44.65995	35.06	<.0001
				R-Square	0.7938
Variable		Parameter	Standard Error	Pr >  t	Significant
Intercept	1	-12.17028	2.64888	0.0001	No
Compaction Slope	1	1.89455	0.31999	<.0001	Yes

## 2.4 Summary

In this chapter, the linear-mixture packing model, a combination of linear and mixture packing models, is described in detail. The model simultaneously considers mechanisms of random particle packing, filling, and occupation to predict the porosity of multi-component mixtures. Application of the linear-mixture packing model to estimate voids in the mineral aggregate of asphalt mixtures indicates there is a high correlation between laboratory-measured and model-estimated values. Therefore, the model has a significant potential to be used as an analytical tool to predict and evaluate the effect of aggregate gradation changes on the VMA of asphalt mixtures.

In addition, based on the linear-mixture model, a systematic approach was used to determine the main particle size of asphalt mixtures and proposed as a variable that defines the aggregate skeleton of an asphalt mixture. In the proposed approach, the aggregate structure of an asphalt mixtures is divided into three ranges: (1) the main particle size range (MPSR), which is the main skeleton of the mixture and is responsible for carrying the traffic load, (2) the small un-mixing range (SUMR), consisting of the aggregates that fill the voids between MPSR and thereby contribute to main aggregate skeleton stability in a mixture, and (3) the large un-mixing range (LUMR), the aggregate particles that essentially float in the matrix of MPSR aggregates and do not contribute to asphalt mixture stability.

Rutting in asphalt mixtures is highly correlated to a mixture's aggregate structure. Two parameters, the disruptive factor, and coordination number were defined based on the proposed three aggregate ranges and used to relate them to rutting performance. Based on the experimental data used in this study, there is a statistically significant relation between the main aggregate skeleton of asphalt mixtures and rutting performance. Thus, the proposed approach can model aggregate packing within an asphalt mixture and predict a mixture's capacity to resist rutting.

## CHAPTER 3. A FRAMEWORK FOR UNDERSTANDING AGGREGATE STRUCTURE IN ASPHALT MIXTURES

*This chapter was published in the International Journal of Pavement Engineering Pouranian, M. R., & Haddock, J. E. (2019). A new framework for understanding aggregate structure in asphalt mixtures. International Journal of Pavement Engineering, 1-17. <https://doi.org/10.1080/10298436.2019.1660340>*

### 3.1 Introduction

The development of a strong aggregate skeleton with adequate mechanical properties is often believed to be an accomplishment of the mixture design procedure used to design the asphalt mixture. However, three widely known asphalt mixture design methods, Hveem, Marshall, and Superpave, focus on determining optimum asphalt binder content based on an aggregate gradation that falls within predefined upper and lower gradation limits (Vavrik, 2000; Roberts et al., 2002; Brown et al., 2009), but otherwise may not give adequate thought to the aggregate structure. While various approaches to improving the mechanical properties of asphalt mixtures have been used in the past, modification of the asphalt mixture design methods has perhaps attracted less attention as compared to asphalt binder modification. However, an efficient and cost-effective asphalt mixture design method can help ensure asphalt mixtures with optimal field performance.

Previous studies have shown that aggregate structure in asphalt mixtures is influenced by factors such as aggregate size distribution, aggregate morphological properties (shape and surface macro-texture), method of compaction, compaction effort, and asphalt mixture lift thickness (Vavrik, 2000; Olard and Perraton, 2010; Pine, 2016). Asphalt mixture durability, workability, permeability, rutting characteristics, and cracking resistance are all significantly affected by aggregate size distribution (aggregate gradation) (Huang, 2012). Thus, careful attention to the aggregate gradation of an asphalt mixture can help to ensure the mixture's successful in-service performance.

The earliest work on designing aggregate gradations for concrete and asphalt mixtures aimed to achieve mixture gradations corresponding to the densest possible packing. To this end, the maximum density line (MDL) was widely used for concrete mixture design prior to the 1940s (Fuller and Thompson, 1907; Andreasen and Anderson, 1929). Nijboer (1948) first studied the

effect of aggregate size distribution and shape on asphalt mixtures. He observed the densest packing was represented by a 45-degree straight line on a semi-log plot of the percent passing as a function of the sieve size, these being plotted on a logarithmic scale. In 1965 Goode and Lufsey reported the maximum packing of aggregate solids occurred when the gradation was represented by a 45-degree straight line on a plot of the percent passing as a function of the sieve size, when the sieve sizes in millimeters are raised to the 0.45 power. When aggregate gradations are plotted on such a graph, it is visually easy to determine when the gradation is becoming less dense; as the gradation moves away from the MDL, either above or below, the packing becomes less dense.

Changing the aggregate gradation changes the voids content of the asphalt mixture aggregate structure, and consequently results in a different load distribution within the aggregates structure. Additionally, the densest aggregate packing in an asphalt mixture is the aggregate gradation having the least void space for asphalt binder and air, both of which are important to asphalt mixture performance. While minimizing asphalt binder content is financially desirable, a sufficient amount of binder is necessary to ensure mixture durability. An adequate air voids content is necessary to ensure mixture stability, as low air voids content can increase the chances of bleeding, rutting, or both.

The Superpave mixture design method proposed aggregate gradation control bands based upon the nominal maximum aggregate size (NMAS) of the mixture. The minimum voids-in-the-mineral-aggregate (VMA) was also defined according to NMAS (Kennedy et al., 1994; McGennis et al., 1995). However, as there is no specific guidance in how to select the best-performing aggregate gradation, any aggregate blend that falls within the control bands and can satisfy the mixture volumetric properties can be chosen as the optimal gradation. When attempting to find a workable aggregate gradation it is often necessary to trial several different aggregate gradations, a process that can be time-consuming, costly, and may still not result in the best gradation to carry the anticipated traffic loads.

In an effort to determine which gradations would likely perform best in asphalt mixtures the Bailey method was introduced (Vavrik et al., 2002; Pine, 2016). Based on packing theory, the Bailey method was originally developed in the early 1980s as a method to control the volumetric properties, workability, segregation, and compactability of asphalt mixtures. This method employs aggregate packing theory and defines coarse and fine aggregate fractions to establish a relationship

between aggregate gradation and volumetric properties of asphalt mixtures. Although the Bailey method suggests a systematic approach for gradation determination of dense-graded asphalt mixtures, it does not directly link the resulting aggregate structure to asphalt mixture performance. Additionally, the effects of the differences in the various aggregate sizes are not considered during the blending of coarse and fine stockpiles to determine the final gradation.

Olard and Perraton (2010) presented a new method to designing of high-performance asphalt mixtures using the basic concepts of granular blending and aggregate packing. They utilized the aggregate packing model first proposed by Baron and Sauterey (1995) to design high-performance Portland cement concrete. The model considers two types of inter-particle interaction, the wall effect and the interference effect, that can influence the voids content of a binary mixture, such a mixture being defined as one with only two particle sizes, one coarse aggregate and one fine aggregate. In this model, when a small number of coarse particles is added to a mixture containing only fine particles, the air voids content decreases, but at the interface of coarse and fine particles, the coarse particles disrupt the arrangement of fine particles and results in increasing local voids. This local void increase is defined as the wall effect. On the other hand, when fine particles are added gradually into a mixture containing only coarse particles, the fine particles begin to push apart the coarse particles thereby destroying the stone-on-stone contact of the larger particles. This behavior is defined as the interference effect. The proposed method involves a graphical approach to determine the optimum amount of fine aggregate by compacting aggregates in a gyratory compactor (20 gyrations) to measure air voids content of coarse and fine aggregates separately.

Given the lack of an objective method to optimize the aggregate gradation of asphalt mixtures, the main objective of this chapter is to develop a theoretical model to better define asphalt mixture aggregate structures based on particle size distribution. Such a model could better optimize asphalt mixture aggregate gradations. As reported herein, the model is first developed based on binary mixtures and then modified to be applicable for mixtures containing multi-sized aggregates. Finally, the framework proposed by the model is evaluated using the discrete element method (DEM) packing simulation.

### 3.2 Analytical Model

The particle structure of binary aggregate mixtures can be divided into three conditions, coarse-pack (CP), dense-pack (DP), and fine-pack (FP). In the CP condition, the coarse particles are in contact with each other (stone-on-stone contact) creating the main skeleton of the mixture with the fine particles filling the voids between them. For the DP, the mixture structure is controlled by both the coarse and fine particles. Finally, FP indicates a condition in which the fine particles constitute the main aggregate skeleton in the mixture and the coarse particles float in the fine particles. The three conditions are represented schematically in Figure 3.1.

As shown in Figure 3.1, these three conditions can be distinguished using two boundary thresholds, the coarse-dense threshold (CDT) and the dense-fine threshold (DFT). The former is the boundary between CP and DP and can be defined as the maximum mass of fine particles that can be added into a mixture of coarse particles without disrupting the coarse particle structure. The latter is the boundary between DP and FP conditions and is defined as the minimum mass of fine particles that can dominate the main aggregate structure of a mixture in the presence of coarse particles. Determination of these two thresholds results in the clear definition of three aggregate structure conditions for binary mixtures. Thus, the objective is the development of a mathematical model to define the CDT and DFT boundaries, while considering the effect of size ratio and shape of both coarse and fine particles.

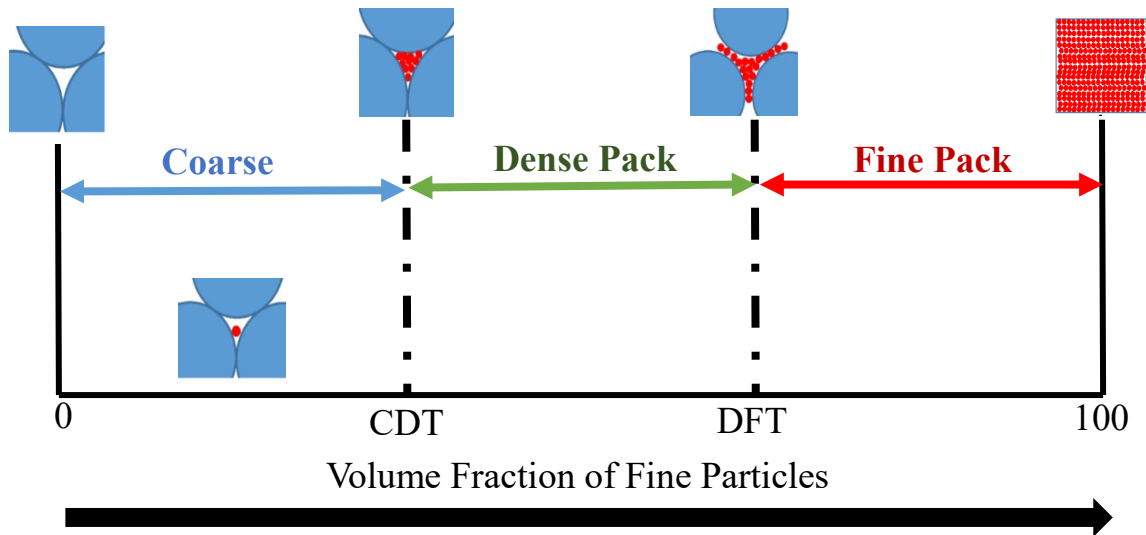


Figure 3.1 Three binary mixture conditions.

If it is assumed that an aggregate mixture consists of only coarse particles, the packing void ratio (ratio of the volume of voids to the volume of solid particles) can be defined as:

$$e_c = \frac{V_{\text{void}}^c}{V_{\text{solid}}^c} \quad (3.1)$$

where  $V_{\text{void}}^c$  and  $V_{\text{solid}}^c$  are the volumes of the voids and the coarse particle solids. By adding fine particles into the coarse particles, the  $V_{\text{void}}^c$  can be computed by:

$$V_{\text{void}}^c = V_{\text{void}}^f + V_{\text{solid}}^f + V_{\text{air}} \quad (3.2)$$

where,  $V_{\text{void}}^f$  and  $V_{\text{solid}}^f$  are the volumes of voids and solids in the fine particles, respectively.  $V_{\text{air}}$  is the volume between the coarse particles that cannot be filled by fine particles (see Figure 3.2). If the void ratios of coarse and fine particles are defined by  $e_c = \frac{V_{\text{void}}^c}{V_{\text{solid}}^c}$  and  $e_f = \frac{V_{\text{void}}^f}{V_{\text{solid}}^f}$ , respectively, Equation 3.2 can be rewritten as:

$$e_c \times V_{\text{solid}}^c = V_{\text{solid}}^f \times (1 + e_f) + V_{\text{air}} \quad (3.3)$$

Additionally,  $V_{\text{air}}$  can be considered as a function of  $V_{\text{solid}}^c$  as shown in Equation 3.4.

$$V_{\text{air}} = V_{\text{solid}}^c \times \text{SRF}(\text{sr}) \quad (3.4)$$

where SRF (sr) is a function of particle size ratio (ratio of fine particle size to coarse particle size,  $\text{sr} = \frac{D_f}{D_c}$ ) and is mathematically defined as the ratio of air volume to the volume of the coarse particles ( $\frac{V_{\text{air}}}{V_{\text{solid}}^c}$ ). Therefore, the volume fraction of fine particles (VFF) at the CDT boundary can be obtained from Equation 3.5.

$$\text{VFF@CMT} = \frac{V_{\text{solid}}^f}{(V_{\text{solid}}^f + V_{\text{solid}}^c)} = 100 \times \left\{ \frac{(e_c - \text{SRF}(\text{sr}))}{(1 + e_c + e_f - \text{SRF}(\text{sr}))} \right\} \quad (3.5)$$

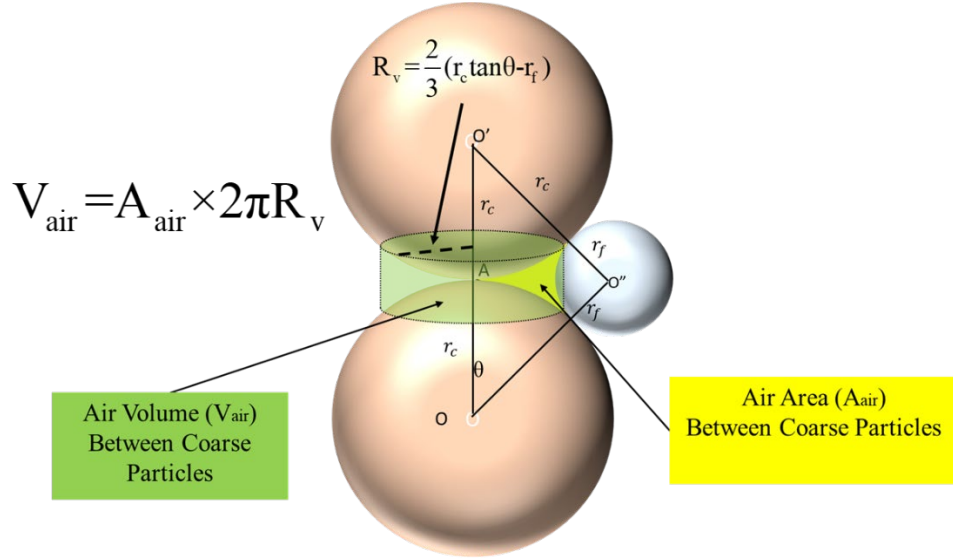


Figure 3.2 Air Volume between Coarse Particles.

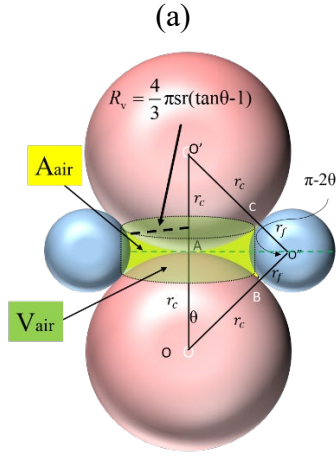
In Equation 3.5, the only unknown variable is SRF(sr). Figure 3.3 gives the mathematical and geometrical formulation to determine this value for four different configurations of particle faces including all-round faces, two flat faces and one round face, two round faces and one flat face, and all flat faces.

In Figure 3.3,  $CN_c$  is defined as the coordination number of coarse particles. In granular material science, the coordination number is the number of contacts a particle has with its adjacent particles. It is a popular geometric parameter to define the structure of particle packing and can be determined using Equation 6, as proposed by Ueda et al. (2011).

$$CN_c = 15.75 - 10.74e_c \quad (3.6)$$

For the four possible particle face combinations illustrated in Figure 3.3, the ratio of SRF to  $CN_c$  was found to have a linear relationship with size ratio (Figure 3.4). Thus, instead of using the lengthy and complex equations of Figure 3.3 to determine SRF, the simple linear equations of Figure 3.4 can be used. Notice in Figure 3.4 there is an “average” equation representing the average SRF of the four faces combinations, since an actual aggregate mixture will potentially contain all the four combinations of the two faces.

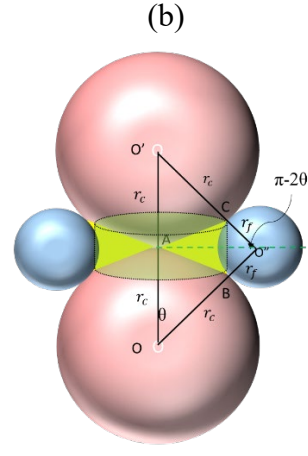




$$R_v = \frac{4}{3} \pi sr (\tan \theta - 1)$$

$$A_{\text{air}} = r_c^2 (\tan \theta - \theta - sr^2 (\frac{\pi}{2} - \theta))$$

$$V_{\text{air}} = A_{\text{air}} \times R_v = \frac{4}{3} \pi sr (\tan \theta - 1)$$

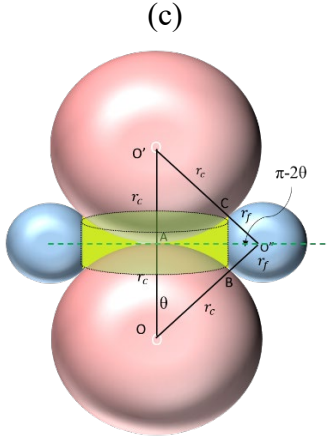


$$SRF_2(sr) = (\frac{V_{\text{air}} + 2V_{\text{AB}}}{\frac{4}{3} \pi r_c^3}) CN_c$$

$$P = \frac{(OA + OB + AB)}{2} = r_c (1 + \sin \frac{\theta}{2})$$

$$A_{\text{OAB}} = (p - r_c) \sqrt{p(p - 2r_c)} \sin \frac{\theta}{2}$$

$$V_{\text{AB}} = (\frac{2}{3}) \left\{ (\frac{r_c^2 \theta}{2}) - A_{\text{OAB}} \right\} \times \{sr(\tan \theta - 1)\}$$

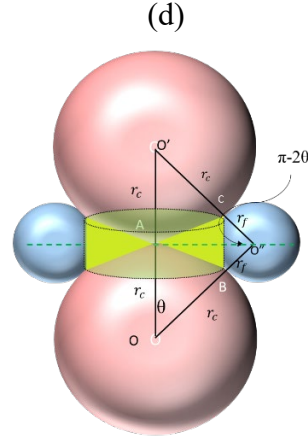


$$SRF_3(sr) = (\frac{V_{\text{air}} + V_{\text{BC}}}{\frac{4}{3} \pi r_c^3}) CN_c$$

$$P = \frac{(O''C + O''B + BC)}{2} = r_c (1 + \sin \frac{\theta}{2})$$

$$A_{\text{O''BC}} = (p - r_c) \sqrt{p(p - 2r_c)} \sin \frac{\theta}{2}$$

$$V_{\text{BC}} = (\frac{2}{3}) \left\{ (\frac{r_c^2 \theta}{2}) - A_{\text{O''BC}} \right\} \times \{sr(\tan \theta - 1)\}$$



$$SRF_4(sr) = (\frac{V_{\text{air}} + 2V_{\text{AB}} + V_{\text{BC}}}{\frac{4}{3} \pi r_c^3}) CN_c$$

$$V_{\text{AB}} = (\frac{2}{3}) \left\{ (\frac{r_c^2 \theta}{2}) - A_{\text{OAB}} \right\} \times \{sr(\tan \theta - 1)\}$$

$$V_{\text{BC}} = (\frac{2}{3}) \left\{ (\frac{r_c^2 \theta}{2}) - A_{\text{O''BC}} \right\} \times \{sr(\tan \theta - 1)\}$$

Figure 3.3 SRF Function Equations for Various Particle Face Configurations: (a) All Round Faces; (b) Two Flat Faces, One Round Face; (c) Two Round Faces, One Flat Face; (d) All Flat Faces.

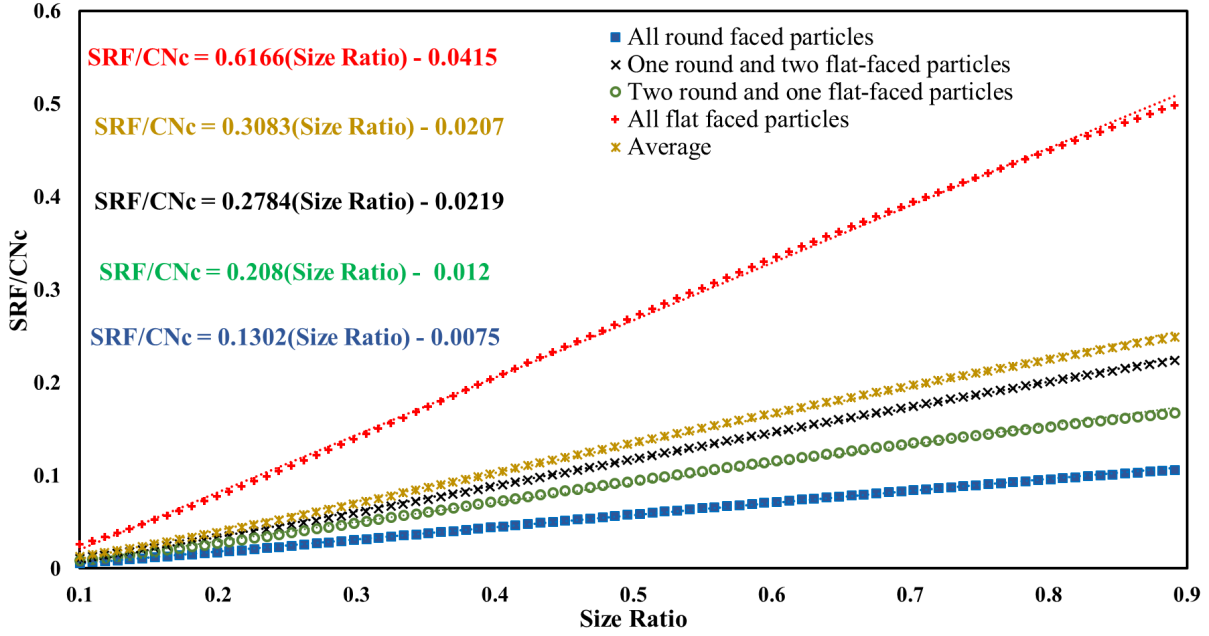
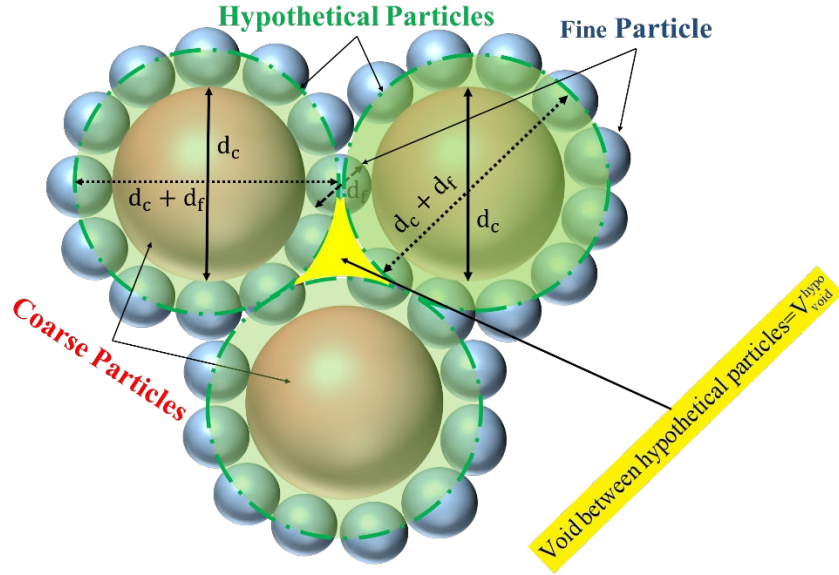


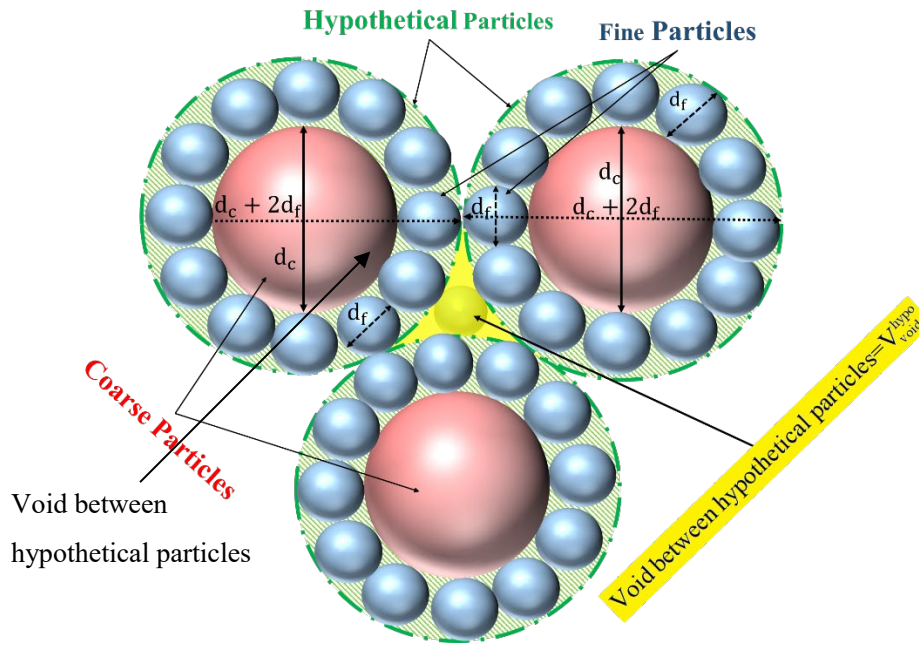
Figure 3.4 Linear Regression Equations of SRF Functions.

The volume fraction of fine particles at DFT can also be determined using a hypothetical particle whose radius is a summation of coarse and fine radii. In this study, two hypothetical particles are considered: 1) a hypothetical particle with a radius equal to the summation of the coarse and fine radii (Figure 3.5a), and 2) a hypothetical particle with a radius equal to the summation of the coarse and two fine radii (Figure 3.5b). It is assumed that these hypothetical particles are in contact with each other. Therefore, the void ratio of a mixture with the hypothetical particles can be defined as:

$$e_{\text{hypo}} = \frac{V_{\text{void}}^{\text{hypo}}}{V_{\text{solid}}^{\text{hypo}}} = \frac{(V_{\text{solid}}^c (1+sr)^3) e_c}{(V_{\text{solid}}^c (1+sr)^3)} = e_c \quad (3.7)$$



(a)



(b)

Figure 3.5 Hypothetical Particles (a)  $k=1$  and (b)  $k=2$ .

The difference between the volume of hypothetical particle voids and volume of coarse particles is  $V_d$  and can be obtained from Equation 3.8:

$$V_d = \frac{4}{3} \pi (r_{\text{hypo}}^3 - r_c^3) \quad , \quad r_{\text{hypo}} = r_c + k r_f \quad k=1,2 \quad (3.8)$$

where  $k$  is the number of fine particles placed between two coarse particles. The volume of coarse particle voids can then be calculated using Equations 3.9a and 3.9b.

$$V_{\text{void}}^c = V_{\text{void}}^{\text{hypo}} + V_{\text{solid}}^c \left( \frac{V_d}{V_c} \right), \quad V_c = \frac{4}{3} \pi r_c^3 \quad (3.9a)$$

$$V_{\text{void}}^c = V_{\text{solid}}^c (1 + sr^3) + V_{\text{solid}}^c ((1 + sr)^3 - 1) \quad (3.9b)$$

As a result, VFF at the DFT boundary can be determined by Equation 3.10.

$$\text{VFF@DFT} = \frac{V_{\text{solid}}^f}{(V_{\text{solid}}^f + V_{\text{solid}}^c)} = 100 \times \left\{ \frac{((1 + e_c) \times (1 + k \times sr)^3 - 1)}{((1 + e_c) \times (1 + k \times sr)^3 + e_f)} \right\}, k=1,2 \quad (3.10)$$

The volume of fine particles at the CDT and DFT boundaries can be determined using Equations 3.5 and 3.10, respectively. The inputs for both equations are the void ratio of coarse and fine particles as well as size ratio. For asphalt mixtures, the aggregates are blended proportionally based on mass. The mass of the fine particle fraction (MFF) is derived using Equations 3.11a and 3.11b, in accordance with what was obtained from Equations 3.5 and 3.10.

$$\text{MFF@CDT} = 100 \times \left\{ \frac{G_{\text{sbf}}(e_c - \text{SRF}(sr))}{G_{\text{sbc}}(1 + e_f) + G_{\text{sbf}}(e_c - \text{SRF}(sr))} \right\} \quad (3.11a)$$

$$\text{MFF@DFT} = 100 \times \left\{ \frac{G_{\text{sbf}}[(1 + e_c)(1 + k \times sr)^3 - 1]}{G_{\text{sbc}}(1 + e_f) + G_{\text{sbf}}[(1 + e_c)(1 + k \times sr)^3 - 1]} \right\} k=1,2 \quad (3.11b)$$

where,  $G_{\text{sbc}}$  and  $G_{\text{sbf}}$  are bulk specific gravities of the coarse and fine particles, respectively.

### 3.3 Numerical Verification

An asphalt mixture is a complex heterogeneous material with irregular geometry and nonlinear boundary conditions (Meegoda and Chang, 1995). It is usually considered as a discontinuous field because of discontinuities in material properties at the interfaces between aggregates and asphalt matrix, and asphalt matrix and air voids. The mechanical properties of an asphalt mixture depend on the structure formed during compaction due to aggregate particle movement. Such characteristics lend themselves to behavioral descriptions using numerical solutions as an alternative to costly, time-consuming laboratory experiments.

Five common numerical methods used in materials engineering are the finite element method (FEM), discrete element method (DEM), finite difference method (FDM), boundary element method (BEM), and element-free method (EFM) (Jiang et al., 2005; Zhu et al., 2007; Alavi et al., 2014; Shishehbor et al., 2018; Shishehbor and Zavattieri, 2019). Although continuum models, like FEM, are able to model discontinuities in asphalt mixtures using additional assumptions, they are not able to model and track the change in microstructure (Meegoda and Chang, 1995). Conversely, DEM is able to simultaneously model the discontinuities of microstructure and aggregate particle movement in asphalt mixtures. Therefore, DEM is the best numerical method for analysis of asphalt mixture microstructure.

DEM is widely used as an effective numerical method to solve many engineering problems in granular materials as well as in solids with discontinuities (Thornton et al., 1996; Herrmann and Luding, 1998; Krut and Rothenburg, 2006; Alonso-Marroquín et al., 2008; Ketterhagen et al., 2009). In DEM, a solid material is represented by a collection of discrete particles. This method is capable of modeling the macro-mechanical response of a material through its motions and interactions (Cundall and Strack, 1979). This method utilizes constitutive models to describe the material behavior at the local scale, which subsequently determines macro behavior.

In this study, an open source 3D DEM code (Kozicki and Donzé, 2009) was employed to assess the validity of the proposed analytical model using the packing characteristics of binary and multi-size mixtures. The final position of aggregate particles in a compacted asphalt mixture can be determined after the compaction process, a process usually done in the laboratory using the Superpave Gyratory Compactor (SGC). The SGC compaction process is controlled by three parameters: vertical pressure, the angle of gyration, and the number of gyrations. The typical values for the angle and applied vertical compressive pressure are 1.16 degrees (internal) and 600 kPa, respectively (Asphalt Institute, 2015). In order to simulate the SGC compaction process a C++ subroutine was developed and used to numerically create the SGC constant pressure ram plate and harmonic rotational movement. The SGC schematic is shown in Figure 3.6.

A series of simulations with 7 different aggregate particle size ratios and 11 different fine particle mass fractions (0 to 100% of the total aggregate mass in 10% increments) were conducted to evaluate the particle structure of binary mixtures. The number of particles varied from 12,000 to 50,000, depending on the size ratio and fine particle mass fraction.

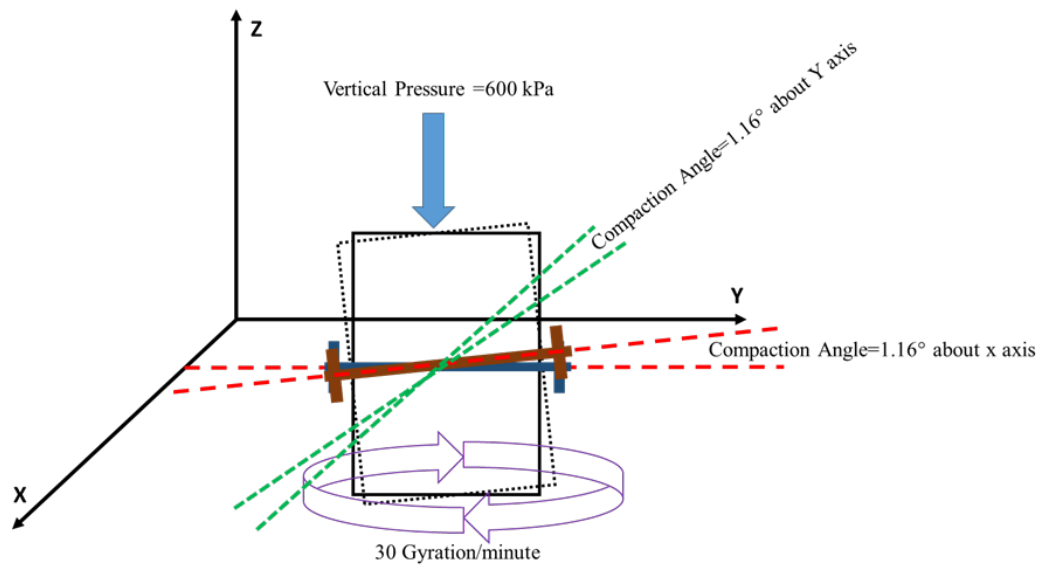


Figure 3.6 Superpave Gyratory Compactor Schematic.

The numerical simulation was conducted using a soft-particle approach. In this approach, all particles were allowed to deform and overlap. Also, the dynamic behavior of all particles was considered using a Lagrangian force-displacement approach to determine the position, velocity, and acceleration of each particle. The values of forces between particles (normal and tangential) were computed using a linear-friction model. The Young modulus, particle density, Poisson ratio, and friction angle are the main parameters influencing particle interaction. Friction angle considers the effect of particle roughness. More details about the interaction model can be found in Widulinski et al. (2009). Material properties and simulation parameters of the present study are listed in Table 3.1.

Table 3.1 Material Simulation Parameters.

Parameter	Value
Size ratio	0.10, 0.166, 0.20, 0.25, 0.33, 0.50, 0.66
Mass fraction of fine particles (%)	0, 10, 20, 30, 40, 50, 60, 70, 80, 90, 100
Container size (mm <sup>3</sup> )	Cylinder with r= 75 mm and Height = 500 mm
Particle density (kg/m <sup>3</sup> )	2600
Young modulus (N/m <sup>2</sup> )	$5 \times 10^7$
Poisson ratio	0.30
Friction angle (°)	35

The approach to numerically simulate the SGC compaction mechanism for each binary mixture is summarized as follows:

1. In a confined volume (bin), create a cloud of random particles with no contact between the particles (Figure 3.7a);
2. Apply a gravity force to the particles, completely settling them in the mold beneath the bin (Figure 3.8b and 3.7c);
3. Apply a 600 kPa vertical pressure on the particles in the mold, then a 1.16-degree internal mold angle, and while holding the constant pressure simultaneously rotate the mold up to 25 gyrations (Figures 3.7d to 3.7f). For better visualization, a rectangular box was used, however, the results of the cylindrical and rectangular box are approximately the same.
- 4.

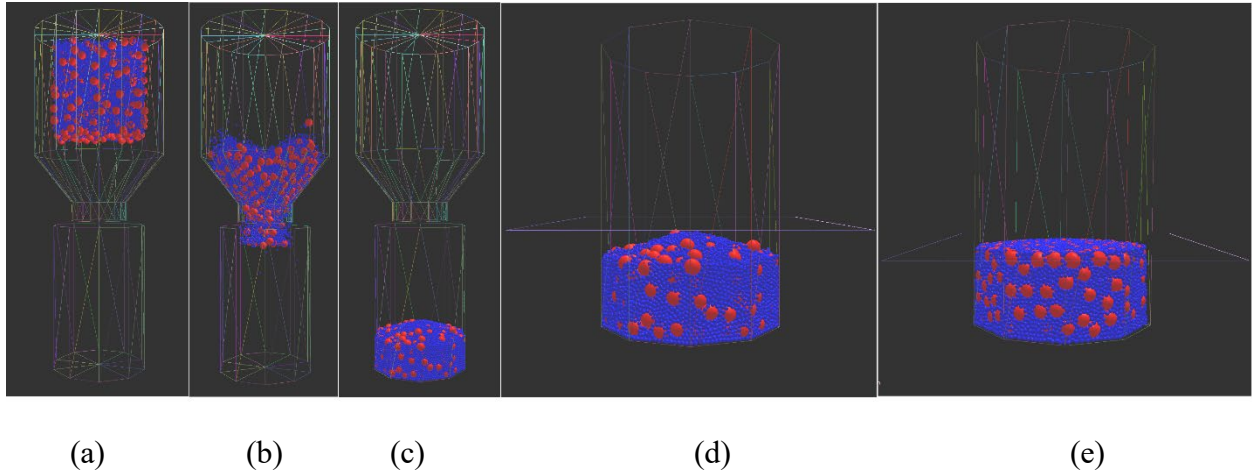


Figure 3.7 Simulation Process: (a) Cloud Condition; (b) Applying Gravity Force; (c) Settlement in the Container; (d) Applying Vertical Load; and (e) Final binary mixture after compaction.

Compaction at three gyration levels, 20, 25 and 30, was performed in the laboratory using actual aggregates containing no binder to determine the maximum number of gyrations at which there is no variation in the final gradation (after compaction) from the initial gradation due to aggregate breakdown. Results of the experiment indicate that 25 gyrations are the maximum number of gyrations at which the mixture of aggregates can be compacted without significantly changing the initial gradation (Figure 3.8). Therefore, all numerical simulations were performed using 25 gyrations or less.

In order to assess the structure of the particles at the CDT and DFT boundaries for  $k=1$  and 2, three structural parameters are used, packing density, average coordination number, and radial distribution function of coarse and fine particles.

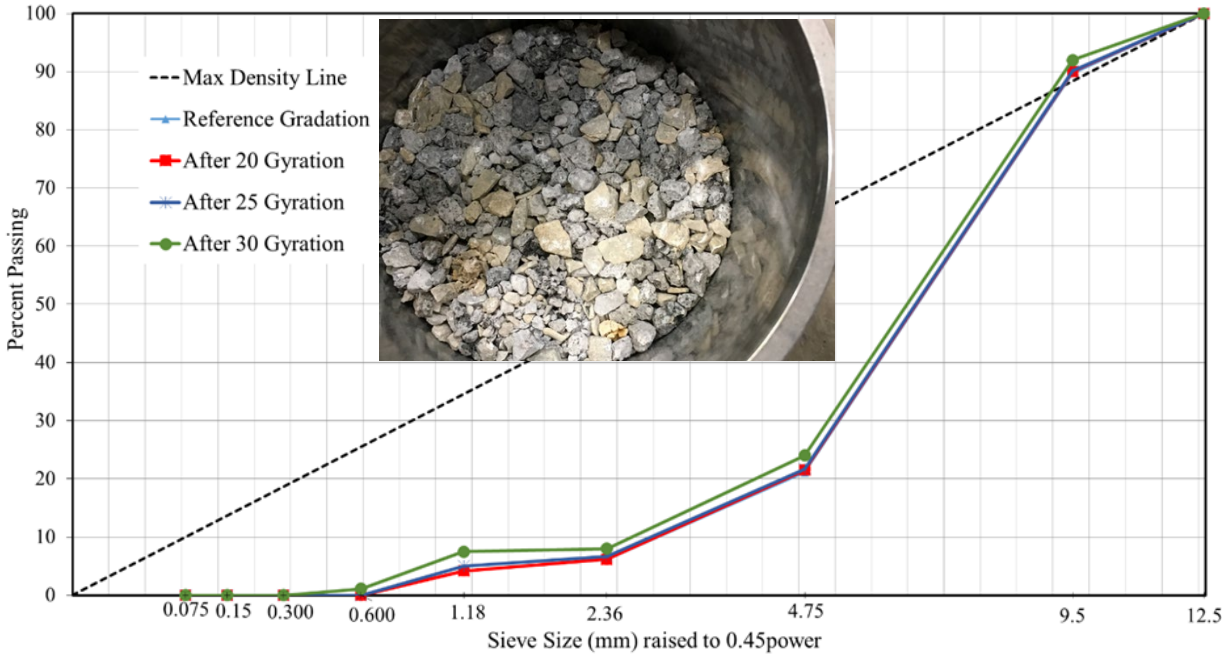


Figure 3.8 Variation of Original Gradation after Three Gyration Levels.

### 3.3.1 Packing Density

Particle packing is a process whereby a system of interconnected particles is put into contact. One of the most important indices to describe the state of particle packing is packing density, defined as the fraction of the total volume the packed aggregates fill. The mass fraction of fine particles at three main thresholds was calculated using the proposed analytical model; the results of the simulation are given in Table 3.2.



Table 3.2 Calculated Values of the Mass of the Fine Fraction.

SR	Mass of fine particle fraction (%)		
	CDT	DFT (k=1)	DFT (k=2)
0.666	18.8	80.1	89.5
0.500	23.0	73.8	81.2
0.333	26.8	64.7	73.7
0.250	29.6	59.4	70.3
0.200	31.3	55.7	67.3
0.166	32.4	53.0	64.6
0.100	35.1	47.9	55.9

The packing density curves for different size ratios and their corresponding values of packing density at the three thresholds of CDT, DFT (k=1), and DFT (k=2) are depicted in Figure 3.9. The results show that increasing the size ratio leads to decreases in the packing density variation with changes in MFF percentage. This means that for higher size ratios (especially greater than 0.333), the packing density curve tends to be flatter with less packing density variation. Also, the figure shows that mixture packing density at the DFT (k=1) threshold is very close to the maximum packing density values, especially for size ratios less than 0.25. The values of packing density at CDT and DFT (k=2) are not close to the maximum packing density values for all size ratios. They can therefore be used as a separator to define the coarse, fine, and dense pack areas.

### 3.3.2 Coordination Number

In this study, the coordination numbers of only coarse particles were used to evaluate the particle structure of all mixtures. This parameter can be calculated by the equation:

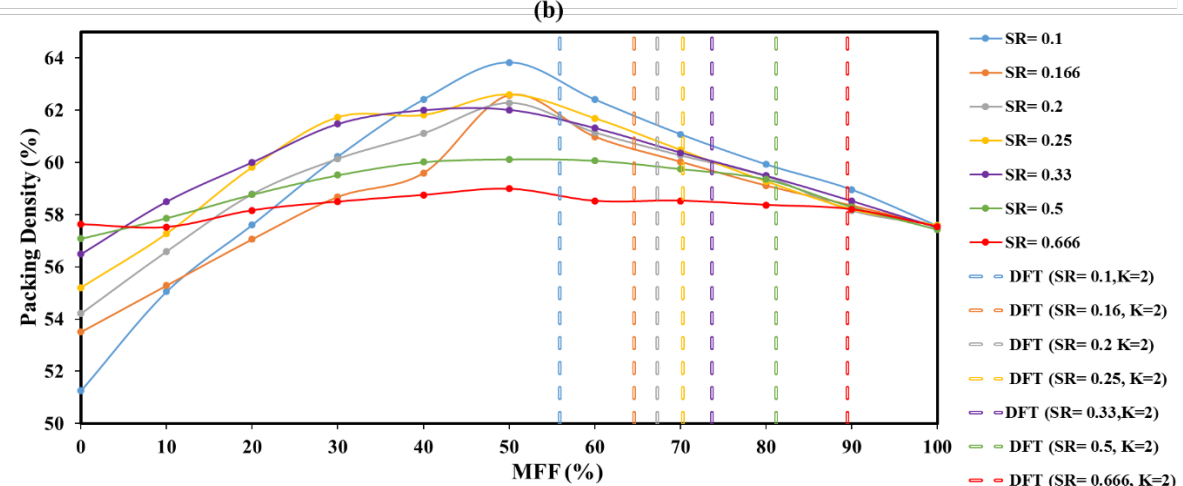
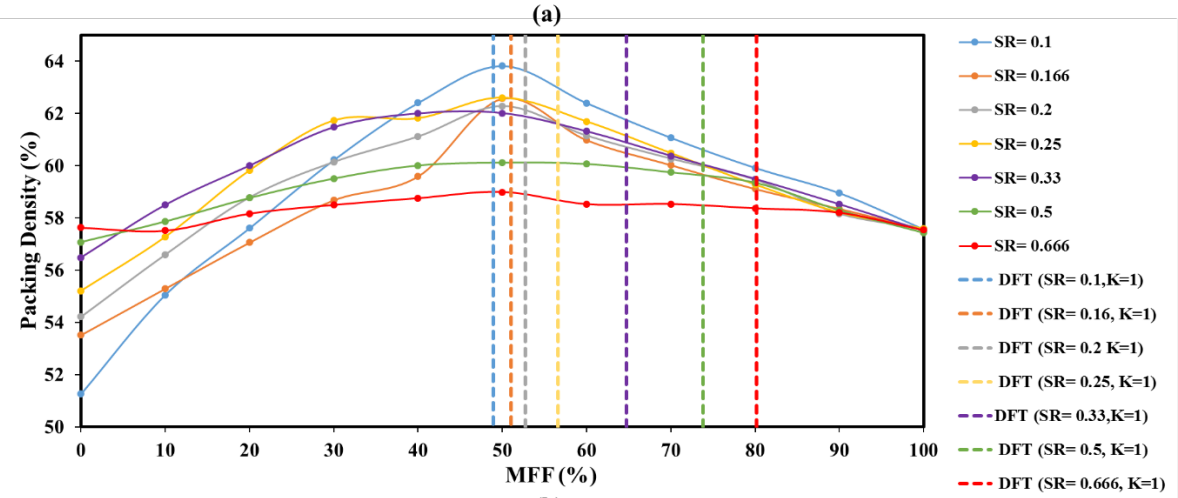
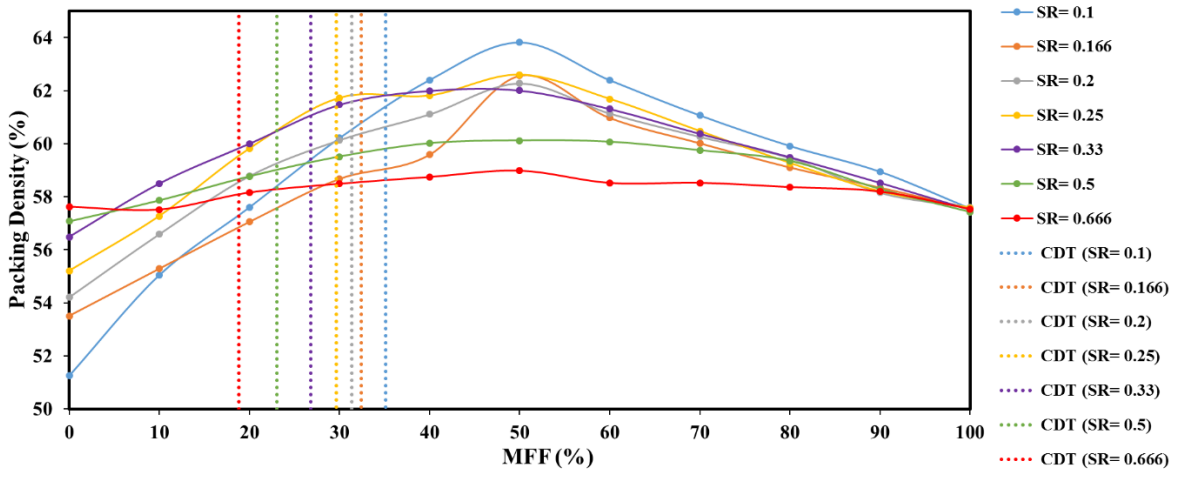
$$CN_c = \frac{2C_c}{N_c} \quad (3.12)$$

where,  $C_c$  and  $N_c$  are the numbers of contact points and coarse particles, respectively. In order to eliminate the boundary effects (wall effects) on the calculation of coordination number, the particles within a zone ( $0 < r < 3/4R$ ) and height ( $1/4H_{max} - 3/4H_{max}$ ) were selected, where  $R$  and  $H_{max}$  are the container radius (75 mm) and maximum packing height, respectively.

Blumenfeld et al. (2005) suggested that particles with fewer than two contact points in 2D and three contact points in 3D are mechanically unstable. Therefore, a  $CN_c$  of three was considered as the stability threshold of the coarse particles. Figure 3.10 shows the values of  $CN_c$  as a function of MFF after compaction. These results indicate the average coordination number of coarse

particles at CDT for size ratios of 0.100, 0.166, 0.200, 0.250, 0.330, 0.500 and 0.660 are respectively 3.15, 3.05, 3.00, 2.75, 2.50, 2.50 and 2.35. These values are greater than or equal to 3 for size ratios less than 0.25 and between 2.35 and 2.75 for the remaining size ratios. Therefore, for size ratios less than 0.25, it was concluded the analytical model accurately estimates the maximum mass of fine particles that can be added into coarse particles without disruption of coarse particle structure (e.g. CDT).

Additionally, the analysis of the  $CN_c$  values at DFT ( $k=1$ ) indicates these values are close to 1, especially for size ratios of less than 0.25. This means at the DFT ( $k=1$ ) threshold, there is still contact between coarse particles, and consequently, DFT ( $k=1$ ) threshold cannot appropriately determine the condition in which the contact between coarse particles begins to disappear. Thus, it cannot be a good estimate of the border between the fine and dense pack areas. Furthermore, in DFT ( $k=1$ ) threshold, the coarse particles are unable to establish a stable main structure (average  $CN_c \sim 1$ ), but they have a significant contribution to the main structure of mixtures. At DFT ( $k=2$ ), the  $CN_c$  values are less than 0.50 and, for size ratio less than 0.250, they are very close to zero. This shows the effect of coarse particles in the development of the main aggregate structure is not significant; the main aggregate structure of mixture is formed by fine particles. Therefore, the DFT ( $k=2$ ) threshold can be used as a separator between fine and dense pack areas.



(c)

Figure 3.9 Packing Density Values for Different Size Ratios and Corresponding Mass of the Fine Fraction at (a) CDT, (b) DFT ( $k=1$ ), and (c) DFT ( $k=2$ ).

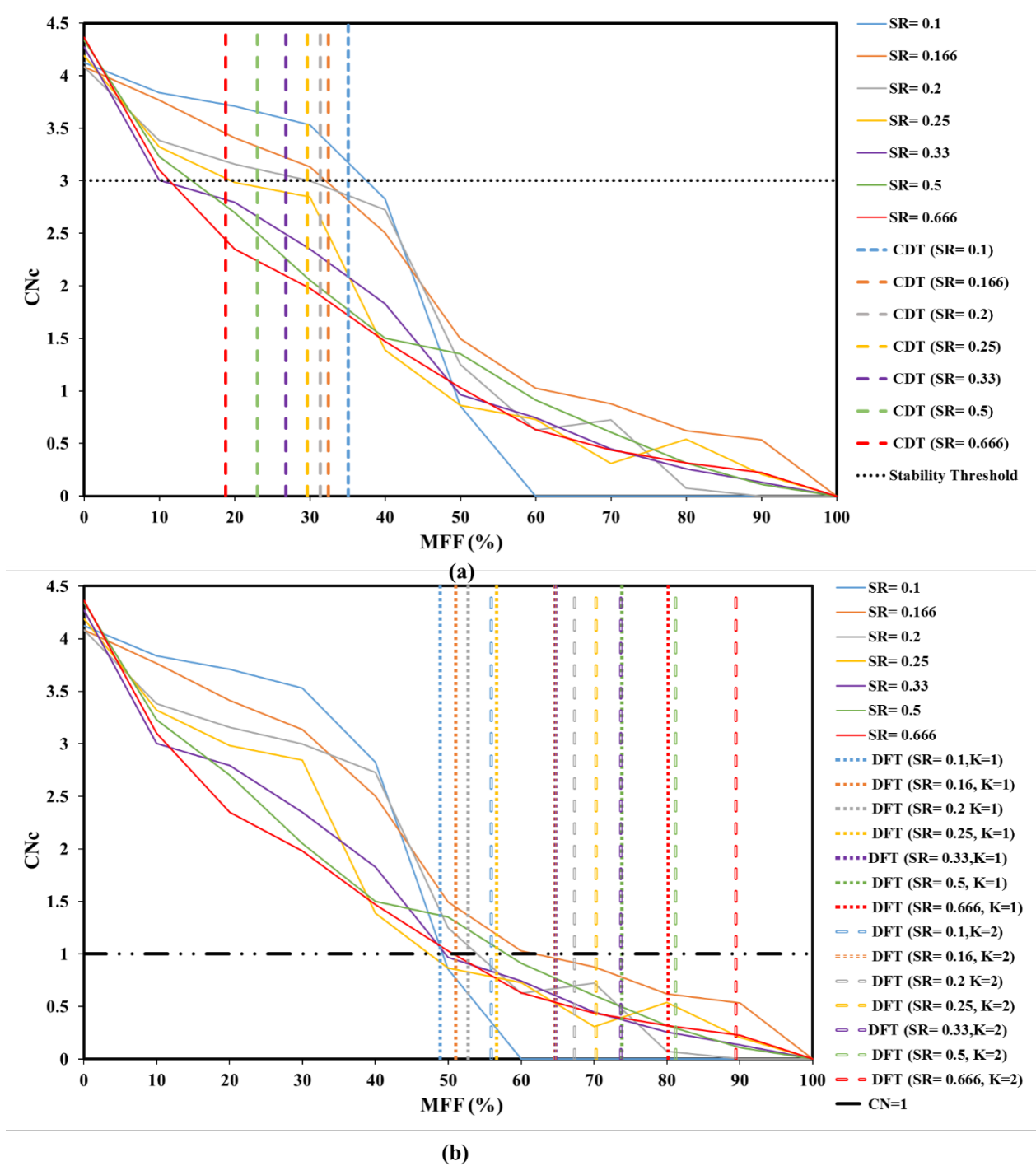


Figure 3.10 Analytical Model  $CN_c$  Values for all Size Ratios and Corresponding Mass of Fines Fraction at (a) CDT and (b) DFT.

### 3.3.3 Radial Distribution Function

The radial distribution function (RDF) is another criterion that can be used to examine the contribution of coarse and fine particles to the structure of particle mixtures. The RDF is a popular measurement for geometrical characterization of packing structures in the field of statistical mechanics. It is defined as the probability of finding the center of a particle exactly at distance ( $r$ ) from the center of a reference particle (Aste et al., 2005; Isola, 2008). Considering each particle of an aggregate blend as a reference particle, and finding if there is at least one particle at the distance  $r$ , the probability for every distance of  $r$  can be computed for the whole mixture as shown in Figure 3.11. Notably, for coarse particles,  $r$  is twice the coarse particle radius, while for fine particles  $r$  is twice the fine particle radius. These are important to ensure the contact of spherical particles. The higher the probability of contact between coarse particles, the stronger the structure. Figure 3.11 shows the result of RDF for coarse and fine particles for a size ratio of 0.500 ( $D_c = 2$  mm and  $D_f = 1$  mm). In this case, the normalized probabilities of existing contact between coarse particles at CDT, DFT ( $k=1$ ) and DFT ( $k=2$ ) are 64, 11, and 7%, respectively. Additionally, the probabilities for fine particles at CDT, DFT ( $k=1$ ) and DFT ( $k=2$ ) are 35, 83, and 91%, respectively.

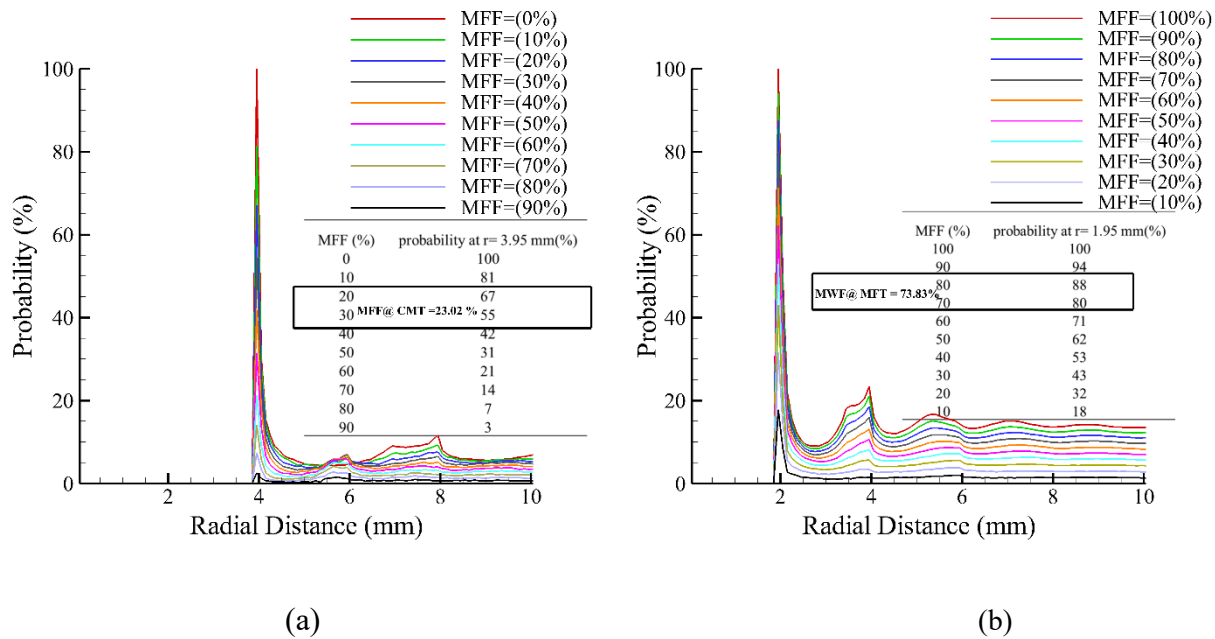


Figure 3.11 Radial Distribution Function for (a) Coarse Particles (size = 2 mm) and (b) Fine Particles (size = 1 mm).

The RDF results for fine and coarse particles in different size ratios are shown in Table 3.3. The RDF results imply the probabilities of contact between coarse particles at CDT for all size ratios are greater than 50%, and for size ratios less than 0.250 are greater than 70 percent. The probabilities of contact between coarse particles are less than 40% (varying from 7% to 38%) at the DFT ( $k=1$ ) boundary. For DFT ( $k=2$ ), the probability of contact between coarse particles reduces to 14 percent. Furthermore, the probabilities of contact between fine particles at DFT ( $k=1$ ) and DFT ( $k=2$ ) are higher than 80%, but at CDT they are 27 to 37 percent.

Table 3.3 Radial Distribution Function Probabilities.

Size Ratio	Probability of Contact between Coarse Particles (%)			Probability of Contact between Fine Particles (%)		
	CDT	DFT ( $k=1$ )	DFT ( $k=2$ )	CDT	DFT ( $k=1$ )	DFT ( $k=2$ )
<b>0.100</b>	94	38	14	31	89	95
<b>0.166</b>	88	32	12	33	88	94
<b>0.200</b>	77	26	10	24	88	92
<b>0.250</b>	70	22	10	37	86	92
<b>0.330</b>	66	15	8	27	84	91
<b>0.500</b>	64	11	7	35	83	91
<b>0.660</b>	52	7	5	29	82	89

### 3.4 Proposed Aggregate Structure Definition

Results of packing density, coordination number, and RDF analyses reveal the CDT suggested by the proposed analytical model can appropriately determine the boundary between coarse- and dense-pack areas, especially for size ratios less than 0.250. Additionally, the boundary between dense- and fine-pack areas can be determined by DFT ( $k=2$ ). The packing density at the DFT ( $k=1$ ) is higher than the CDT and DFT ( $k=2$ ) thresholds and can therefore be used as a criterion to divide the dense-pack area into two sub-areas, coarse-dense-pack (CDP) and fine-dense-pack (FDP). The former addresses the area between coarse and dense pack. In this area, although the main mixture structure is developed using both coarse and fine particles, the contribution of coarse particles to the main mixture structure is more significant than the contribution of the fine particles ( $CN_c$  between 1 and 3 and  $0 < k < 1$ ). The fine-dense-pack area can be defined as the area between DFT ( $k=1$ ) and DFT ( $k=2$ ) and describes the transition area between dense-pack and fine-pack areas ( $1 < k < 2$ ). In this area, the fine particles are more influential than the coarse particles in constructing the main particle structure of the mixture; the

effect of coarse particles is negligible ( $CN_c < 0.5$ ). Therefore, based on the amount of MFF percentage, the following aggregate structure definitions are proposed (Figure 3.12):

- Coarse-pack (CP) area: The main mixture structure is created by coarse particles and bears any applied loads. This area falls between MFF=0 and MFF at CDT. Within this area the variation of packing density is linear.
- Dense-pack (DP) area: This area falls between MFF at CDT and DFT ( $k=2$ ). The main mixture structure is built from both coarse and fine particle sizes and the variation of packing density is non-linear. Based on packing density and coordination number analysis results, this area can be divided into two sub-areas using MFF at DFT ( $k=1$ ), CDP ( $0 < k < 1$ ) and FDP ( $1 < k < 2$ ).
- Fine-pack (FP) area: In this area, the fine particles construct the main mixture structure and the mixture falls within MFF at DFT ( $k=2$ ) and MFF of 100 percent. In this area, the change in packing density decreases linearly with the increase of MFF.

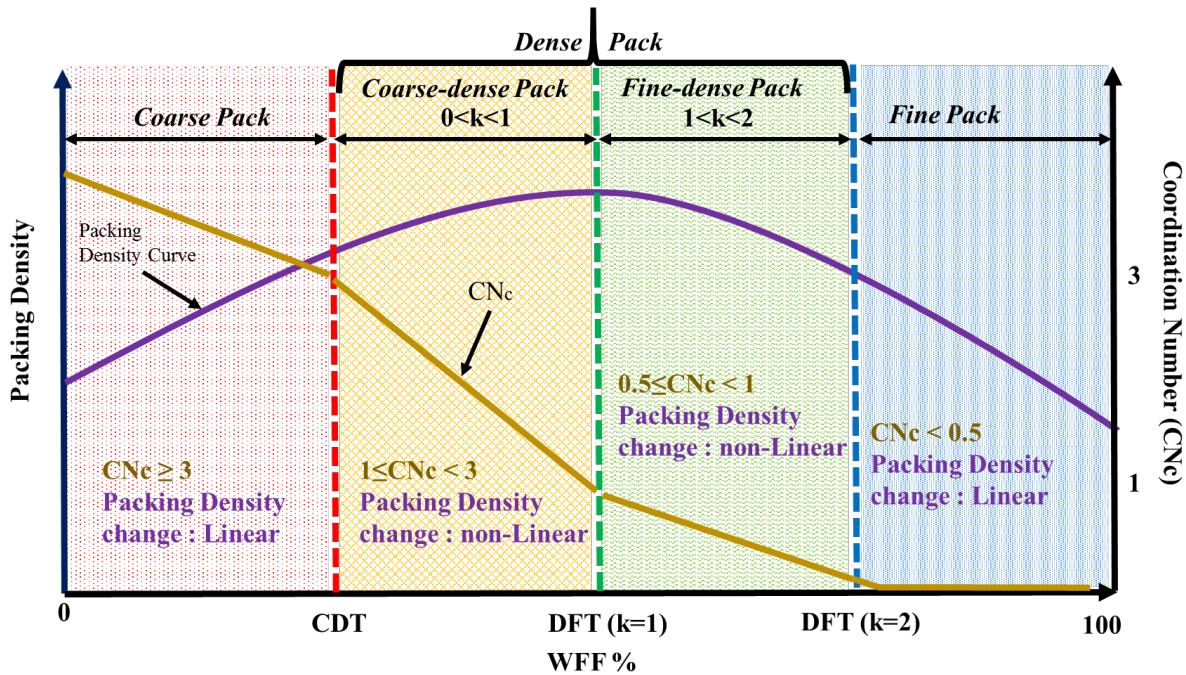


Figure 3.12 Proposed Aggregate Structure Definition Illustration.

### 3.5 Application of Analytical Model to Multi-Sized Aggregate Stockpiles

As shown earlier, the analytical model was developed for binary mixtures. However, in practice, aggregate stockpiles used to produce asphalt mixtures have multi-sized particles. It is therefore necessary to modify the binary approach to be applicable to multi-sized aggregate stockpiles. This can be done by employing the idea of representative size in a multi-sized aggregate stockpile. As stated in chapter 2, the size distribution of most crushed aggregate stockpiles can be represented by the Rosin-Raimmmler-Sperling-Bennett (RRSB) distribution, as shown in Equation 3.13:

$$P(s)=100-e^{-\left(\frac{s}{s_{rp}}\right)^n} \quad (3.13)$$

where,  $P(r)$  is the cumulative probability that the size is less than  $S$  (%),  $S$  is the particle size,  $n$  is a shape parameter, and  $S_{rp}$  is the position parameter of the distribution and has a cumulative probability of 0.368.  $S_{rp}$ , the mid-size in the RRSB distribution, can be selected as a representative size for aggregate stockpiles. Thus, the RRSB model is utilized to determine a representative size for aggregate stockpiles.

To evaluate the applicability of the proposed representative size approach, a number of DEM simulations were conducted using a series of multi-sized particle mixtures, similar to what was done for binary mixtures. The particle size distributions of the coarse and fine stockpiles are shown in Table 4. Based on the different combinations of the two stockpiles, eleven mixtures were considered. These were determined by changing the percentage of the fine stockpile from 0 to 100%, in 10% increments. In each mixture, the number of particles for both the coarse and fine sizes was estimated based on the final gradation curve and the following equation (Cai et al., 2014):

$$N=\frac{3 \times V(p_{m+1}-p_m)}{4 \pi((D_{m+1}+D_m)/2)^3} \quad (3.14)$$

where  $N$  is the number of particles with a size of  $(D_{m+1}+D_m)/2$ ,  $P$  is the volume percentage of the particles in the mixture, and  $p_{m+1}$  and  $p_m$  are the aggregate volume percentages passing through the  $D_{m+1}$  and  $D_m$  sieve sizes, respectively. The material properties and simulation specifications were those presented in Table 3.1.



Table 3.4 Coarse and Fine Stockpile Size Distributions.

Size (mm)	Coarse Stockpile (% Passing)	Fine Stockpile (% Passing)
12.5	100	100
9.5	97	100
4.75	30	97
2.36	16	82.5
1.18	2	65
0.600	1	45
0.300	0	16
0.150	0	1.9
0.075	0	0.2

Based on the RRSB model, the representative sizes for the coarse and fine stockpiles are respectively 6.54 and 1.11 mm. The values of MFF at CDT, DFT (k=1), and DFT (k=2) obtained from the analytical model are 18, 46, and 74%, respectively. The definition of the coarse and fine aggregates is based on the Baily method, in which coarse and fine aggregates are defined by a sieve size known as the Primary Control Sieve (PCS) (Vavrik, 2000; Pine, 2016). The PCS is a function of the nominal maximum aggregate size (NMAS) and is calculated as:

$$\text{PCS} = \text{NMAS} \times 0.22 \quad (3.15)$$

Particles sizes greater than PCS are considered coarse particles, while those smaller than PCS are fine particles. The  $\text{CN}_c$  and the change of packing density at different MFF percentages are illustrated in Figure 3.13.

Results of the analysis indicate that  $\text{CN}_c$  at CDT is equal to 2.85, which is close to three. Additionally, the mixture at DFT (k=1) shows a packing density close to the maximum value. At DFT (k=2), the  $\text{CN}_c$  value is less than 0.1. Therefore, the proposed analytical model does appear to reasonably determine the aggregate structure of multi-sized mixtures using the proposed representative size approach.

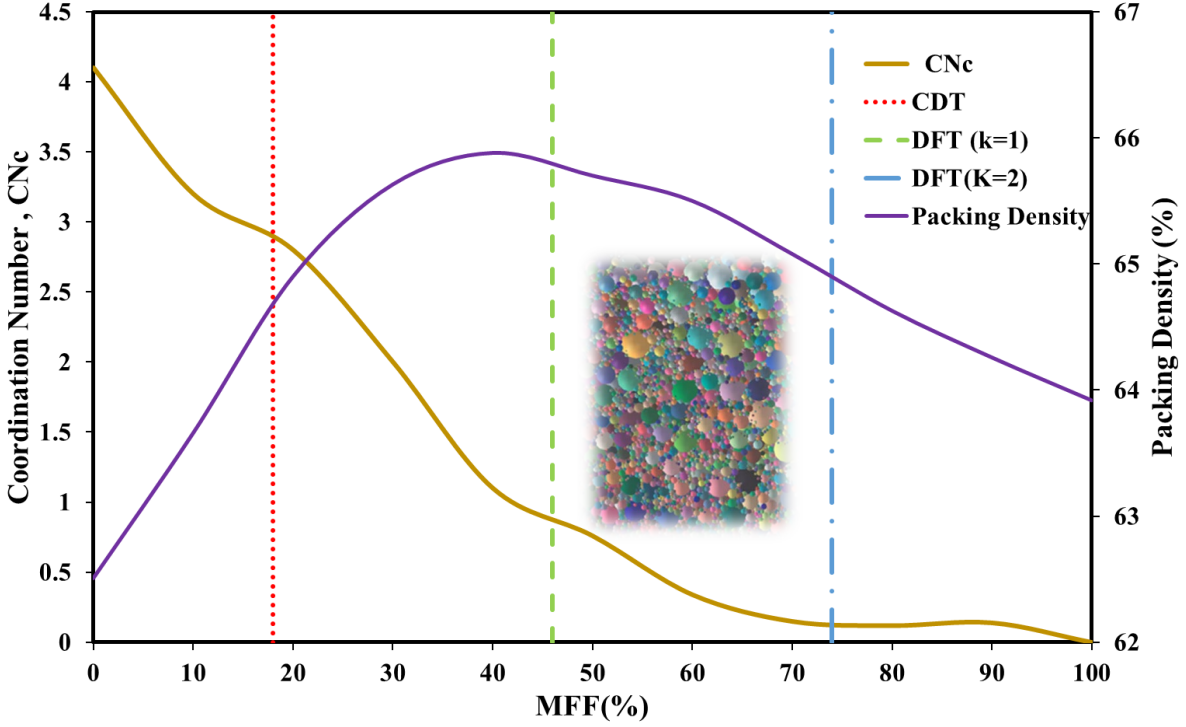


Figure 3.13 Variation of  $CN_c$  and Packing Density for Coarse and Fine Stockpile Mixtures.

### 3.6 Summary

The work presented in this chapter draw attention to the aggregate structure as a major load-bearing constituent of asphalt mixtures. Depending on the mass fraction of fine particles (MFF) in a binary mixture, the particle structure of a mixture can be divided into three areas: coarse pack (CP), dense pack (DP) and fine pack (FP). Boundaries between these areas (CDT and DFT) were determined using a proposed analytical model. A series of numerical simulations to determine the packing behavior of binary mixtures was conducted on various aggregate blends using the discrete element method (DEM). Based on the simulation results, the proposed analytical model could appropriately define the particle structure of binary mixtures especially when the size ratio between fine and coarse particles is less than 0.25.

In order to apply the developed approach for the multi-sized aggregate blends, the Rosin-Raimmler-Sperling-Bennett (RRSB) distribution was employed to find aggregate sizes representing fine and coarse aggregate stockpiles. Based on the DEM simulation for multi-sized aggregate blends, it can be concluded that the proposed aggregate structure can be satisfactorily applied to the blending of multi-sized aggregate stockpiles.

## CHAPTER 4. EFFECT OF AGGREGATE STRUCTURE ON ASPHALT MIXTURE COMPACTION PARAMETERS

*This chapter is under review in Journal of Materials in Civil Engineering*

### 4.1 Introduction

Compactability, defined as the effort needed to compact an asphalt mixture in the field, is a defining characteristic of asphalt mixtures during construction. Achieving an acceptable level of density during field compaction has a direct bearing on an asphalt mixture's in-service performance. Insufficient density has a detrimental effect on fatigue and rutting performance, and on moisture damage resistance (NCAT, 2011). It is therefore vital to understand factors that may affect compactability, factors such as binder content and type, compaction temperature and effort, and aggregate gradation, shape and texture. Additionally, research has shown that asphalt mixture compactability can provide information about an asphalt mixture's rutting performance, rutting being an all too often asphalt pavement distress type (Zaniewski and Srinivasan, 2004).

Several compactability studies have been conducted and various parameters introduced to better clarify it. Terms such as compaction energy index (CEI) and traffic densification index (TDI) (Bahia et al., 1998), compaction force index (CFI) and traffic force index (TFI) (Delage, 2000), locking point and compaction slope (CS) (Vavrik and Carpenter, 1998; Anderson et al., 2002; Leiva and West, 2008), and initial density ( $\%G_{mm}$  at  $N_{ini}$ ) (Leiva and West, 2008; Awed et al., 2015) have been proposed. CEI and TDI are energy-based parameters, while CFI and TFI are force-based parameters for addressing the compaction energy required during construction and densification under traffic, respectively. The locking point evaluates aggregate structural resistance against compaction, while CS and initial density are helpful parameters that can be used to predict volumetric properties at different compaction levels. Kassem et.al (2012) reported a good correlation between these two parameters (CS and initial density) and field compactability. Furthermore, CS was found to have a good correlation with the permanent deformation and shear stiffness of asphalt mixtures (Zaniewski and Srinivasan, 2004).

Apart from temperature, binder type and content and aggregate shape and texture are the most common parameters affecting asphalt mixture compaction. Additionally, the aggregate gradation plays a key role in compactability, but there is no consensus on which parameters best

explain how gradation affects compactability. The Bailey method proposed three parameters, coarse aggregate (CA), fine aggregate-coarse fraction ( $FA_c$ ), and fine aggregate-fine fraction ( $FA_f$ ) to define the packing of the coarse portion of the aggregate gradation, the coarse portion of the fine aggregate, and the fine portion of the fine aggregate, respectively (Pine, 2016). Mohammad and Al-Shamsi (2007) reported that using the Bailey method parameters of CA and  $FA_c$  did not result in a good correlation with the asphalt mixture volumetric properties, while Leiva and West (2008) noted that the Bailey parameters did not correlate well with the compactability parameters such as CEI, locking point, CS, initial density, and air voids content. Awad et al., (2015) have reported that applying the Weibull distribution function to define scale and shape parameters of the aggregate gradation curve is useful for predicting CS and the initial air voids content at the gyration ( $N_{ini}$ ).

Most previous studies performed on asphalt mixture compactability incorporated several factors into compactability modeling, including gradation parameters. The influence of aggregate gradation on asphalt mixture compactability is heavily dependent on other factors such as aggregate morphological properties and binder content and type. However, while aggregate morphological properties cannot be engineered during the mixture design procedure (other than by changing aggregate types), gradation can be engineered, within limits. It is therefore important to assess the effect of aggregate gradation on asphalt mixture compactability independently of aggregate morphological properties, binder content, and binder type.

Given the importance of asphalt mixture compactability to ensuring adequate asphalt mixture density and thereby performance, an investigation of how asphalt mixture aggregate gradation affects compactability seems prudent. Therefore, the main objective of the work presented in this chapter is to evaluate the effect of aggregate gradation on asphalt mixture compactability. This effect was studied using two different approaches. One approach used asphalt mixtures of coarse and fine aggregates, without the addition of aggregate filler, and all mixtures having the same effective binder type and content. The second approach used asphalt mixtures of coarse and fine aggregates, included aggregate filler, and a constant effective binder type and content for all mixtures. All mixtures were designed with the design binder content being chosen at 4% air voids.

To design mixtures with a constant effective binder and air voids contents a standard mixture design procedure was developed and implemented. To find the relationships between

asphalt mixture aggregate gradation and compaction parameters, the most meaningful and practical compaction parameters were selected for use in the study. Correlations between the selected compaction parameters and the proposed gradation indices addressing gradation curve shape and proximity to the maximum line density were then established for the two mixture approaches. Finally, the models developed were evaluated using laboratory and field data to ensure their effectiveness.

## 4.2 Materials

The aggregates used in the study were limestone and blast furnace slag (BFS) coarse aggregates with natural sand and filler being the fine aggregates. The filler material was obtained from the asphalt plant baghouse. The coarse aggregates both had a nominal maximum aggregate size (NMAS) of 9.5 mm. The coarse aggregate fractions of the mixtures were divided such that 50% by mass was limestone and 50% was BFS, a common practice for surface mixtures. The aggregate properties are shown in Table 4.1. The binder used in all the mixtures was a PG 70-22 obtained from a local supplier.

Table 4.1 Aggregate Stockpile Properties.

Sieve Size (mm)	Coarse Stockpiles		Fine Stockpile	Mineral Filler
	Limestone	Blast Furnace Slag	Natural Sand	
12.5	100	100		
9.5	90.1	89.3	100	
4.75	19.4	22.8	99.9	
2.36	3.5	8.7	89.1	
1.18	1.7	6.7	70.1	
0.600			47.7	100
0.300			17	99.4
0.150			2.2	97.8
0.075			0.8	94.6
Gsb	2.681	2.442	2.612	2.800 <sup>a</sup>
Representative Size (mm)	7.427	7.295	1.056	----

<sup>a</sup>Mineral filler apparent specific gravity.

### 4.2.1 Aggregate Gradations

The aggregate stockpiles shown in Table 4.1 were blended to yield the 15 gradations plotted in Figure 4.1. These gradations were determined based on the approach developed in chapter 3 cover three main aggregate structures, coarse-pack (CP), dense-pack (DP) and fine-pack (FP). CP is defined as the condition in which all coarse particles are in direct contact with each other (stone-on-stone contact) creating the asphalt mixture's main aggregate skeleton with the fine particles simply filling voids in the skeleton. In DP mixtures, the asphalt mixture aggregate structure is controlled by both fine and coarse particle sizes. FP indicates the condition in which the fine particles dominate the main aggregate skeleton of the mixture and the coarse particles float in the fine particles. Equation 4.1 was used to design CP mixtures, while Equation 4.2 was used to develop DP and FP mixtures.

$$\text{MFF@CDT}=100 \times \left\{ \frac{G_{\text{sf}}(e_c - \text{SRF}(\text{sr}))}{G_{\text{sbc}}(1+e_f) + G_{\text{sf}}(e_c - \text{SRF}(\text{sr}))} \right\} \quad (4.1)$$

$$\text{MFF@DFT}=100 \times \left\{ \frac{G_{\text{sf}}[(1+e_c)(1+k \times \text{sr})^3 - 1]}{G_{\text{sbc}}(1+e_f) + G_{\text{sf}}[(1+e_c)(1+k \times \text{sr})^3 - 1]} \right\} \quad k=1,2 \quad (4.2)$$

In these two equations, MFF is the percent by mass of fine aggregate that should be added to coarse aggregate by the total aggregate mass,  $e_c$  and  $e_f$  are the void ratio of coarse and fine aggregates, respectively,  $\text{sr} = \frac{D_f}{D_c}$ , where  $D_c$  and  $D_f$  are the representative sizes of coarse and fine stockpiles, respectively,  $\text{SRF}(\text{sr})$  is the size ratio function  $(0.3087\text{sr} - 0.0207) \times (15.75 - 10.74e_c)$ ,  $k$  is the fine aggregate coefficient that defines the number of fine particles between two coarse particles ( $k=1$  for DP and  $k=2$  for FP mixtures), and  $\gamma_c$  and  $\gamma_f$  are the specific gravities of the coarse and fine aggregates, respectively.

The void ratio of only coarse and only fine aggregates (i.e.  $e_c$  and  $e_f$ , respectively) for Equations 4.1 and 4.2 were calculated at different packing densities achieved by using 0, 8, 15 and 25 gyrations of the Superpave Gyratory Compactor (SGC). After determining  $e_c$  and  $e_f$  at different gyration numbers, four gradations for each CP and FP ( $k=2$ ) mixtures were found based on 0, 8, 15 and 25 gyrations. Initial assessment revealed that the DP can be divided into two categories, namely fine dense pack (FDP), with  $1 < k < 2$ , and coarse dense pack (CDP), with  $0 < k < 1$ . There are

four gradations for FDP mixtures, according to the gyration number at which  $e_c$  and  $e_f$  were determined.

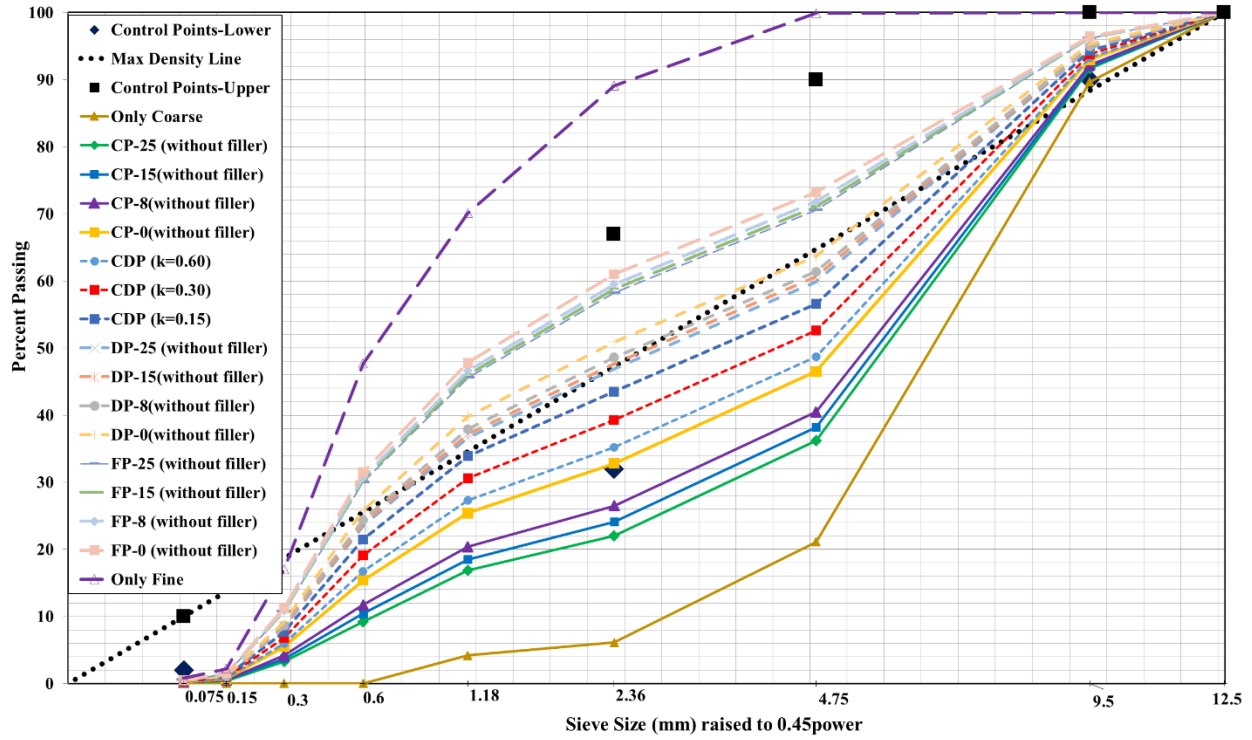


Figure 4.1 Selected Aggregate Blend Gradations (without filler).

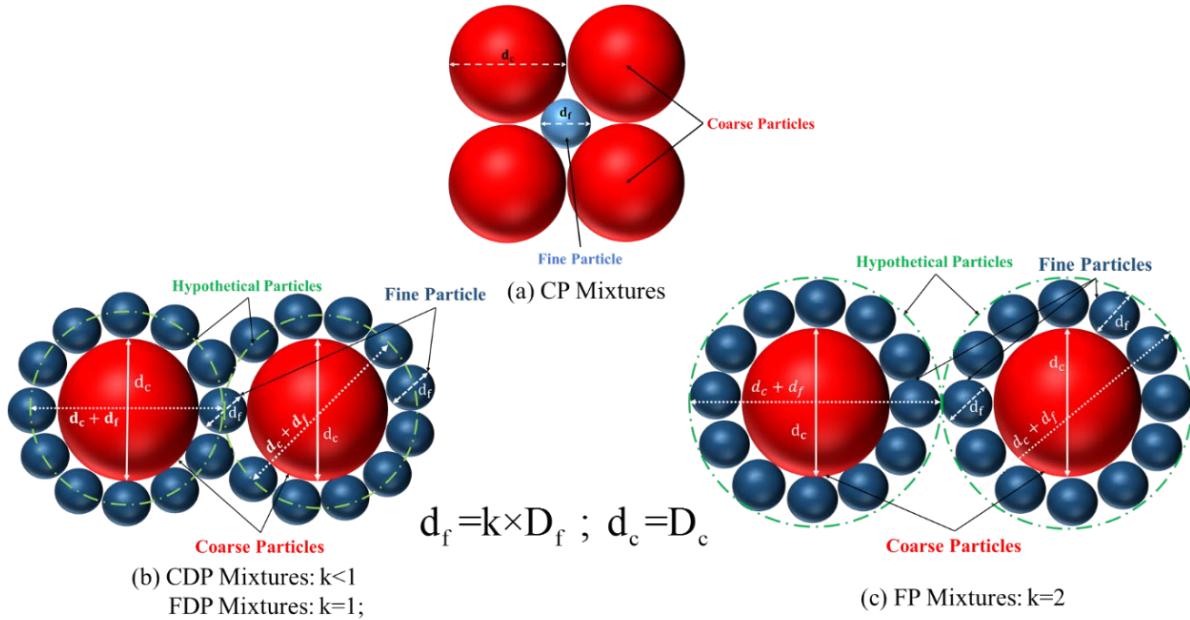


Figure 4.2 Schematic of Coarse Pack, Coarse Dense Pack, Fine Dense Pack, and Fine Pack.

With regard to CDP, three k values of 0.150, 0.300 and 0.600 were used for the gradation within CDP. These three k values represent the situation in which aggregates of sizes 0.150, 0.300 and 0.600 mm were placed between the coarse aggregates. Figure 4.2 indicates the arrangement of CP, DP, FDP, and FP schematically. Also, Table 4.2 shows the tabulated gradation information.

Table 4.2 Gradation information.

Mixture ID	Gyrations Number	Void Ratio		% Fine	% Coarse	Threshold
		Fine	Coarse			
CP-0	0	0.55	0.88	32.2	67.8	CDT
FDP-0	0	0.55	0.88	54	46	DFT (k=1)
FP-0	0	0.55	0.88	66.1	33.9	DFT (k=2)
CP-8	8	0.69	0.42	24.6	75.4	CDT
FDP-8	8	0.69	0.42	51.2	48.8	DFT (k=1)
FP-8	8	0.69	0.42	64.3	35.7	DFT (k=2)
CDP-8 (k=0.600)	8	0.69	0.42	35.1	64.9	DFT (k=0.600)
CDP-8 (k=0.300)	8	0.69	0.42	40.1	59.9	DFT (k=0.300)
CDP-8 (k=0.150)	8	0.69	0.42	45.2	54.8	DFT (k=0.150)
CP-15	15	0.6	0.4	21.7	78.3	CDT
FDP-15	15	0.6	0.4	50.1	49.9	DFT (k=1)
FP-15	15	0.6	0.4	63.5	36.5	DFT (k=2)
CP-25	25	0.55	0.38	19.2	80.8	CDT
FDP-25	25	0.55	0.38	49.2	50.8	DFT (k=1)
FP-25	25	0.55	0.38	62.8	37.2	DFT (k=2)

### 4.3 Specimen Preparation

Determining the optimum binder content (OBC) for a target air voids is the aim of all asphalt mixture design methods, including Hveem, Marshall and Superpave (Asphalt Institute, 1997; Asphalt Institute, 2001; Robert et al., 2002). Apart from the aggregate source properties that help ensure sufficient durability, toughness, cleanliness, shape, and texture, the selected gradation needs to fall within the upper and lower limits of the mixture design specification. Among the volumetric properties, air voids content of asphalt mixtures is of great importance, since the OBC is determined at 4% air voids content. Air void value is an indicator of compactability of asphalt mixtures that is affected by binder content and particle size distribution (Muras, 2010). Unlike the standard Superpave mixture design, for the work reported herein, the design air voids content (4%) and effective binder content are considered fixed. This is accomplished by varying the aggregate



gradation, especially filler content, and total binder content simultaneously. Applying this concept, it is possible to design various mixtures with different aggregate structures (CP, CDP, FDP and FP) while maintaining approximately equivalent air voids and binder contents.

#### 4.3.1 Mixture Design Approach

Figure 4.3 shows the summary of the approach that was developed and used to design mixtures based on the desirable air voids design ( $V_a$ ), voids-in-the-mineral-aggregate (VMA) the volume of air voids and effective binder content, design gyration ( $N_{des}$ ) and mixture type (CP, CDP, FDP or FP). To complete the mixture designs, for each gradation, two compacted and two loose (un-compacted) specimens were fabricated using 4-5% binder and the appropriate mixture of coarse and fine aggregates without filler. The 4-5% binder content of was chosen because visual inspection revealed this amount sufficient to coat the aggregate particles. The loose specimens were used for measuring maximum theoretical specific gravity ( $G_{mm}$ ) and the compacted specimens' bulk specific gravity ( $G_{mb}$ ) in accordance with AASHTO T209, "Standard Method of Test for Maximum Theoretical Specific Gravity ( $G_{mm}$ ) and Density of Hot Mix Asphalt (HMA)" and AASHTO T-166, "Standard Method of Test for Bulk Specific Gravity ( $G_{mb}$ ) of Compacted Hot Mix Asphalt (HMA) Using Saturated Surface-Dry Specimens," respectively. All mixtures were designed using 100 SGC gyrations.

Using the  $G_{mm}$ ,  $G_{mb}$ , aggregate bulk specific gravity ( $G_{sb}$ ), and binder specific gravity ( $G_b$ ), the latter two being supplied by the contractor who furnished the materials, the following steps were taken to estimate required binder and filler contents:

Calculate the total volume of compacted samples using the following Equation 4.3,

$$V_T = \frac{W_T}{G_{mb} \gamma_w} \quad (4.3)$$

where,  $V_T$  and  $W_T$  are the total volume and weight of compacted sample, respectively and  $\gamma_w$  is the specific weight of water, 9.807 kN/m<sup>3</sup>.

Determine VMA of compacted samples (VMA) according to (AASHTO M323, 2015):

$$VMA = 100 - \left[ \frac{(G_{mb} P_s)}{G_{sb}} \right] \quad (4.4)$$

where,  $P_s$  is the percentage of aggregate (coarse and fine).

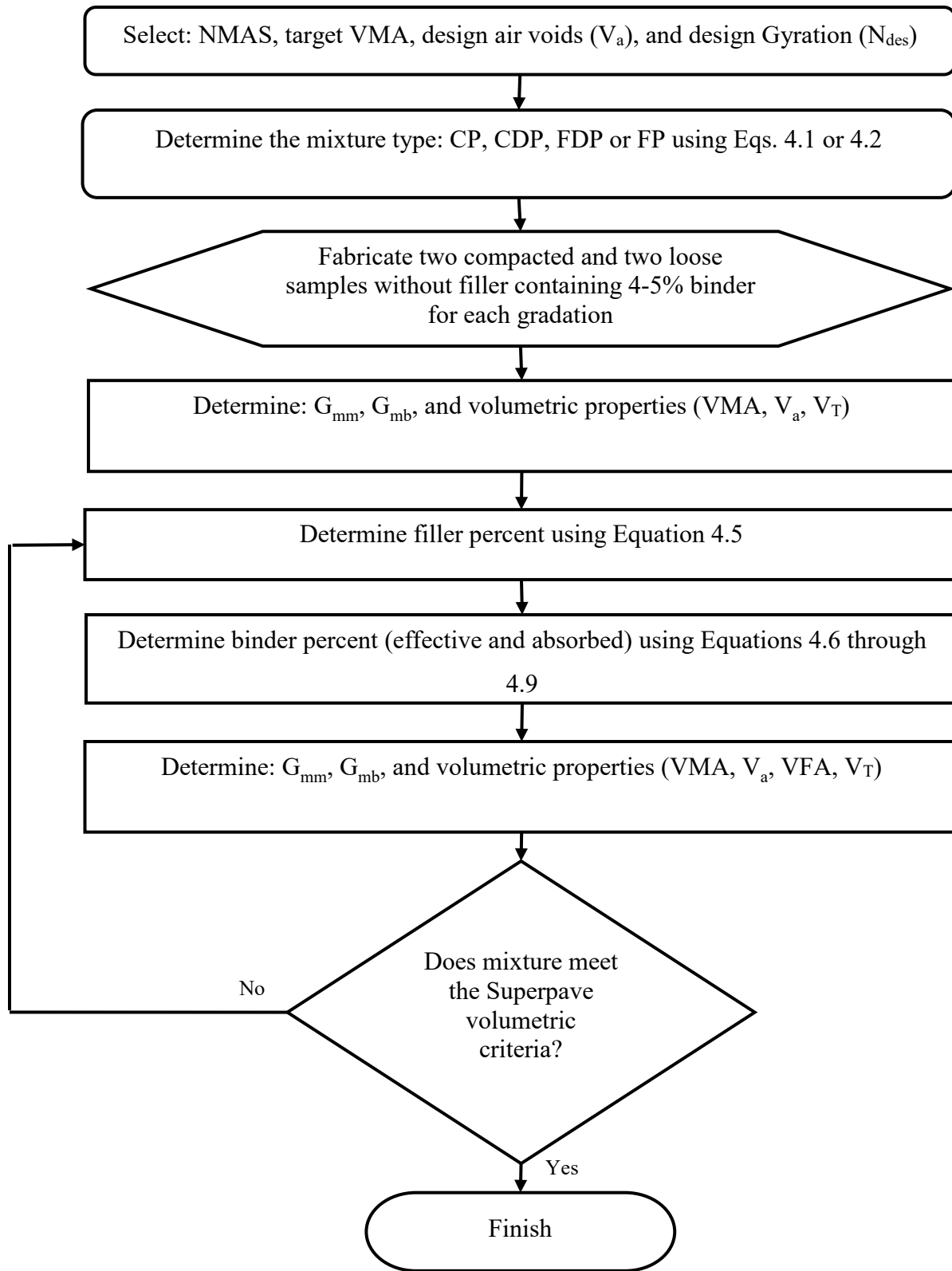


Figure 4.3 Flowchart of Mixture Design Approach.

Determine initial filler percentage: By knowing a target VMA (15% for 9.5-mm mixtures) and design air voids content (4%) for the final mixture design, the amount of filler (% filler) required for the mixture can be estimated based on the target VMA ( $VMA_t$ ), volume of required filler ( $V_f$ ), weight of required filler ( $W_f$ ), weight of fine and coarse aggregates ( $W_s$ ) and specific gravity of filler ( $G_{sbf}$ ) as follows:

$$V_f = \frac{(VMA_m - VMA_t)(V_T)}{100}; W_f = V_f \times (G_{sb})_f \times \gamma_w$$

$$\% \text{filler} = \frac{W_f}{(W_f + W_s)}; W_s = P_s \times W_T \quad (4.5)$$

1. Estimate the mass of optimum binder content. First, the mass of absorbed binder and volume of effective binder of previously compacted samples is calculated. Given this data, the total required mass of the OBC can be estimated using the target VMA and design air voids content as follows:

- a. Calculate effective specific gravity ( $G_{se}$ ) and determine percent absorbed asphalt ( $P_{ba}$ ) using the following equations (AASHTO, 2015):

$$G_{se} = \frac{100 - P_b}{\left[ \frac{100}{G_{mm}} \right] - \left[ \frac{P_b}{G_b} \right]}; \quad P_{ba} = \frac{(100G_b)(G_{se} - G_{sb})}{(G_{se}G_{sb})} \quad (4.6)$$

- b. Estimate the volume and mass of optimum effective binder content ( $V_{be}$ ,  $M_{be}$ ).

$$V_{be} = \frac{(VMA_t - V_a) \times V_T}{\left(1 - \frac{\% \text{filler}}{100}\right)}; \quad M_{be} = V_{be} \times G_b \times \gamma_w \quad (4.7)$$

- c. Find the total mass of optimum absorbed binder ( $M_{ba}$ ).

$$M_{ba} = P_{ba} \times (W_s + W_f) \times \left(1 - \frac{\% \text{filler}}{100}\right) \quad (4.8)$$

- d. Estimate the total mass of optimum binder as a summation of optimum absorbed and effective binder.
- e. Determine the total binder percentage.

$$P_{obc} = \frac{(100 \times M_{obc})}{(W_s + W_f + M_{obc})} \quad (4.9)$$

After determining the required amounts of filler and asphalt binder to meet the target VMA and design air voids content, two compacted and one loose specimen are prepared. The volumetric properties of these specimens are then measured and compared to the desired values. If additional modifications are necessary, steps 1 through 4 can be repeated as needed based on the volumetrics.

#### **4.3.2 Mixture Design Results**

The mastic (combination of binder and filler) partially fills the voids between aggregate particles allowing the target air voids content of 4% to be achieved. It is assumed the total volume of mastic is equal to the binder and filler volumes. Therefore, the initial VMA without filler (Table 4.3) must be deducted from the minimum allowable VMA (15% for 9.5-mm mixture) to find the volume of required filler. The minimum allowable VMA was selected so as to provide the smallest allowable VFA and thus require the least binder to obtain 4% air voids. As expected, and as indicated in Table 4.3, coarser aggregate gradations have higher VMA and therefore require larger amounts of filler. Also, the VMA increases with increasing number of gyrations at which  $e_c$  and  $e_f$  are determined. The lowest VMA and air voids content occur between CDP ( $k=300$ ) and CDP ( $k=150$ ), as it results in the densest aggregate packing. It is noteworthy that finer aggregate gradations do not lead to less VMA and air voids, but rather they tend to reduce the amount of absorbed binder, likely due to fewer pores and cavities of the smaller aggregate particles.

After using Equation 4.5 to determine the filler mass, 11% binder by volume of total mixture plus absorbed binder is required to fulfill the VMA and absorption requirements. Using Equations 4.6 through 4.9, the amount of binder was calculated and is shown in Table 4.4. Because of higher absorbed binder, the first estimated total binder percentages for coarser aggregate gradations are higher than those for finer gradations.

The results of the first trial (Table 4.5) indicate the air voids contents are not satisfactorily close to 4% for the CP and FP mixtures. For CP mixtures, the difference between the target VMA and the results of first trial can be explained by the lubricating effect of filler. This effect acts to “extend” the binder and facilitates the compaction. Also, comparing the volume of effective binder and its target value (11%), it can be seen that the selected binder contents for CP mixtures were overestimated. Thus, the air voids content is lower than anticipated (Table 4.5).

Table 4.3 Initial Volumetric Data (without filler).

Mixture	G <sub>mm</sub>	G <sub>mb</sub>		Total Volume (cm <sup>3</sup> )		VMA (%)		V <sub>a</sub> (%)		P <sub>ba</sub> (%)	
	Ave.	Ave.	Std.	Ave.	Std.	Ave.	Std.	Ave.	Std.	Ave.	Std.
CP-25	2.550	2.048	0.014	2277.58	13.37	24.3	0.50	19.65	0.55	1.74	0.090
CP-15	2.543	2.091	0.011	2204.54	10.20	22.8	0.11	17.77	0.12	1.68	0.010
CP-8	2.536	2.131	0.001	2190.30	2.62	21.3	0.10	16.00	0.10	1.49	0.005
CP-0	2.541	2.179	0.002	2125.95	1.24	19.6	0.05	14.25	0.05	1.55	0.001
CDP-8 (k=0.600)	2.526	2.195	0.001	2101.45	1.45	18.9	0.01	13.12	0.10	1.37	0.002
CDP-8 (k=0.300)	2.527	2.227	0.001	2096.75	2.50	17.7	0.10	11.65	0.15	1.28	0.005
CDP-8 (k=0.150)	2.526	2.221	0.001	2100.32	4.45	17.9	0.02	12.01	0.11	1.22	0.004
FDP-25	2.527	2.219	0.001	2107.58	5.00	18.1	0.05	12.18	0.01	1.19	0.001
FDP-15	2.526	2.217	0.002	2105.37	2.45	18.1	0.04	12.23	0.01	1.20	0.004
FDP-8	2.524	2.215	0.007	2104.80	5.74	18.3	0.31	12.20	0.30	1.21	0.010
FDP-0	2.521	2.204	0.003	2114.68	1.59	18.7	0.15	12.55	0.15	1.16	0.003
FP-25	2.521	2.198	0.005	2131.52	2.41	18.8	0.14	12.81	0.14	0.94	0.001
FP-15	2.52	2.178	0.003	2142.78	5.92	19.6	0.11	13.57	0.18	0.23	0.002
FP-8	2.490	2.151	0.004	21.68.45	7.15	20.6	0.17	13.61	0.20	0.62	0.004
FP-0	2.481	2.143	0.007	2173.70	6.54	21.1	0.25	13.75	0.25	0.51	0.005

On the other hand, for FP mixtures, the higher air void and VMA contents are results of underestimated binder and filler contents. After two to four trials the final filler and binder contents were determined, as shown in Table 4.6. As seen in the table, the resulting air voids content ( $4\pm0.2\%$ ), VMA ( $15\pm0.2\%$ ), VFA ( $65\leq VFA\leq75$ ), and dust ratio ( $0.6\leq DP\leq2$ ) meet the Superpave mixture design volumetric specifications.

Table 4.4 Initial Results of Required Filler and Binder Contents.

Mixture	VMA (%)	Total Volume (cm <sup>3</sup> )	Filler Volume (cm <sup>3</sup> )	Filler Mass (g)	Percent Filler	Required Effective Binder Volume (cm <sup>3</sup> )	Required Effective Binder Mass (g)	Absorbed Binder Mass (g)	Total Binder Mass (g)	Percent Binder
CP-25	24.3	2277.58	200.41	561.0	12.5	219.2	225.81	74.6	300.4	6.3
CP-15	22.8	2204.54	172.10	481.6	10.7	216.6	223.13	72.7	295.8	6.2
CP-8	21.3	2190.30	138.04	386.4	8.6	220.2	226.81	65.1	291.9	6.1
CP-0	19.5	2125.95	96.70	270.8	6.0	219.8	226.42	68.3	294.7	6.1
CDP-8 (k=0.600)	18.9	2101.45	83.00	232.4	5.2	219.1	225.71	60.5	286.2	6.0
CDP-8 (k=0.300)	17.7	2096.75	56.62	158.5	3.5	222.6	229.3	57.1	286.4	6.0
CDP-8 (k=0.150)	18.0	2100.32	62.63	175.3	3.9	222	228.7	54.1	282.8	5.9
FDP-25	18.	2107.58	64.51	180.6	4.0	222.6	229.3	52.8	282.1	5.9
FDP-15	18.1	2105.37	66.14	185.1	4.1	222.1	229.81	53.2	283	5.9
FDP-8	18.3	2104.80	69.51	194.6	4.3	221.6	230.22	53.6	283.8	5.9
FDP-0	18.8	2114.68	79.32	222.0	4.9	221.2	230.81	51.3	282.1	5.9
FP-25	18.8	2131.52	81.90	229.3	5.1	222.5	231.25	41.5	272.8	5.7
FP-15	19.6	2142.78	98.09	274.7	6.1	221.3	231.94	36.1	268.0	5.6
FP-8	20.6	2168.45	120.79	338.2	7.5	220.6	232.22	27.2	259.4	5.5
FP-0	21.1	2173.7	131.53	368.2	8.2	219.5	233.14	22.3	255.4	5.4

Table 4.5 Volumetric Results of First Trial.

Mixture Type	VMA (%)		Va (%)		Effective Binder Volume (%)		Pba (%)	
	Ave.	Std.	Ave.	Std.	Ave.	Std.	Ave.	Std.
CP-25	13.7	0.51	1.5	0.24	12.20	0.21	1.12	0.04
CP-15	14.1	0.14	2.5	0.12	12.11	0.24	1.04	0.05
CP-8	14.3	0.20	2.9	0.14	11.82	0.15	1.01	0.03
CP-0	14.6	0.10	3.1	0.15	11.53	0.11	0.97	0.03
CDP -8(k=0.600)	14.7	0.07	3.4	0.08	11.25	0.06	0.98	0.04
CDP-8 (k=0.300)	14.9	0.08	3.7	0.10	11.24	0.05	0.99	0.05
CDP-8 (k=0.150)	14.9	0.10	3.6	0.12	11.33	0.14	1.01	0.02
FDP-25	15.8	0.11	4.4	0.12	11.42	0.12	0.85	0.06
FDP-15	15.9	0.21	4.4	0.14	11.50	0.14	0.81	0.07
FDP-8	15.7	0.14	4.6	0.15	11.11	0.20	0.81	0.02
FDP-0	15.5	0.15	4.5	0.17	11.24	0.22	0.75	0.08
FP-25	15.5	0.12	4.6	0.14	11.15	0.15	0.74	0.04
FP-15	15.4	0.14	5.0	0.11	10.51	0.26	0.71	0.03
FP-8	15.4	0.16	4.7	0.17	10.60	0.25	0.67	0.06
FP-0	15.3	0.23	4.9	0.20	10.47	0.25	0.64	0.07

Table 4.6 Final Mixture Design Results.

Mixture	Percent Filler	Percent Binder	Pbe (%)	VMA (%)	Va (%)	VFA (%)	Dust Ratio	No. of Trials
CP-25	9.3	5.8	4.73	15.1	4.3	71.9	2.0	4
CP-15	8.2	5.8	4.79	15.1	4.0	73.5	1.7	4
CP-8	7.9	5.8	4.84	14.9	3.9	74.2	1.6	3
CP-0	4.6	5.6	4.88	14.9	3.9	73.9	0.9	2
CDP (k=0.600)	4.1	5.6	4.85	14.9	3.9	73.8	0.8	2
CDP (k=0.300)	3.7	5.6	4.81	15.0	3.9	73.9	0.8	2
CDP (k=0.150)	4.3	5.6	4.85	15.1	4.0	73.5	0.9	2
DP-25	4.9	5.6	4.78	15.1	4.0	73.8	1.0	2
DP-15	4.9	5.5	4.76	15.2	4.1	73.1	1.0	2
DP-8	4.9	5.7	4.77	15.1	4.1	72.8	1.0	2
DP-0	5.3	5.6	4.66	15.2	4.1	73.4	1.1	2
FP-25	6.4	5.7	4.75	15.0	3.9	74.2	1.3	3
FP-15	7.6	5.8	4.78	15.1	4.1	72.8	1.6	3
FP-8	8.0	5.8	4.70	14.9	4.0	73.2	1.7	3
FP-0	8.5	5.9	4.76	15.1	4.2	72.0	1.8	3

## 4.4 Gradation and Compactability

### 4.4.1 Compaction Parameters

Indices such as the locking point, initial density, compaction slope (CS) and compaction energy index (CEI) have been suggested to measure laboratory compactability. The locking point identifies the gyration number at which the aggregate structure begins resisting compaction and has been defined in different ways by various researchers:

Original: The locking point is the gyration number of the first three gyrations with the same sample height preceded by two gyrations of the same sample height (Vavrik and Carpenter, 1998; Anderson et al., 2002).

Locking Point 2-1: The locking point is the gyration number at which the first two consecutive gyrations with the same sample height occur (Leiva and West, 2008).

Locking Point 2-2: The locking point is the gyration number at which the second two consecutive gyrations with the same sample height occur (Leiva and West, 2008).

Locking Point 2-3: The locking point is the gyration number at which the third two consecutive gyrations with the same sample height occur (Leiva and West, 2008).

The second approach (Locking Point 2-1) has been widely used by highway agencies (Leiva and West, 2008) and was therefore selected to determine the locking point in this work. Initial density is defined as the %G<sub>mm</sub> at N<sub>ini</sub> (at the 8th gyration for this study), while CS is the slope of semi-log %G<sub>mm</sub> as a function of the number of gyration curve from 8 to 100 gyrations (Leiva and West, 2008) (Figure 4.4a). CEI, as shown in Figure 4.4b, is the area under the compaction curve from the N<sub>ini</sub> (8<sup>th</sup> gyration) to the gyration corresponding to 92% of G<sub>mm</sub> (Bahia et al., 1998).

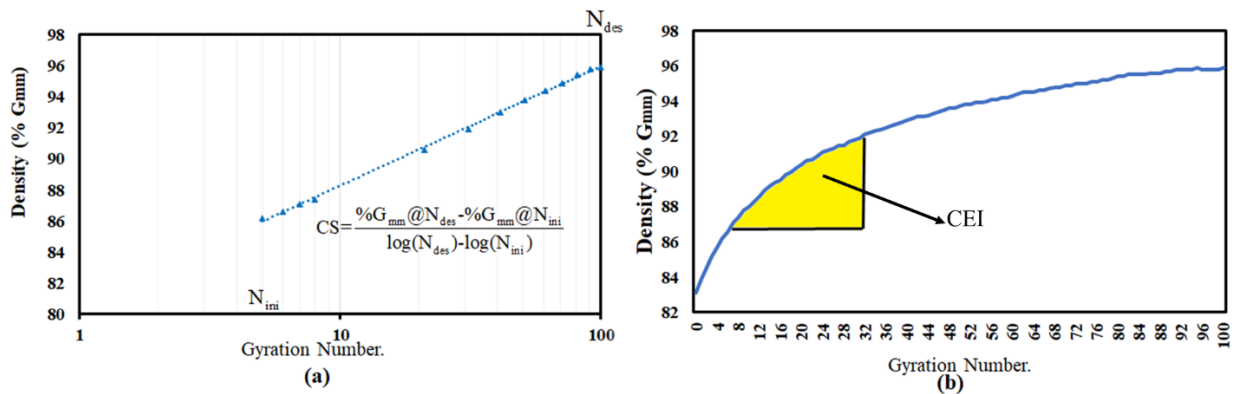


Figure 4.4 Definition of (a): Compaction Slope and; (b): Compaction Energy Index.



#### 4.4.2 Gradation Parameters

To establish a relationship between the mixture gradation and the laboratory compaction parameters, it is necessary to define independent qualitative variables that represent the gradation characteristics. Therefore, two groups of parameters are used to address the general shape of the gradation curve and the closeness of the gradation to the maximum density line (MDL). The overall gradation shape can be characterized using a power distribution function:

$$P(d)=100 \times e^{-\left(\frac{d}{d_r}\right)^n} \quad (4.10)$$

where,  $d$  is the aggregate size of each sieve used in the gradation (mm),  $P(d)$  is the cumulative retained percentage for each sieve size,  $d_r$  is the size considered to be the representative gradation size (mm), and  $n$  is a scale to describe the gradation uniformity. The  $d_r$  and  $n$  parameters are determined using curve fitting techniques. The parameter  $d_r$  is also used to determine the representative size of each stockpile shown in Table 4.1.

The Bailey method suggests four control sieves to describe the packing condition of the coarse and fine portions of any gradation (Vavrik et al., 2002), half control sieve (HCS), primary control sieve (PCS), secondary control sieve (SCS) and tertiary control sieve (TCS). The HCS is defined as the closest sieve to one-half the NMA (0.5×NMA), while the PCS is the closest sieve to 0.22×NMA. The SCS is the closest sieve to 0.22×PCS and the TCS is the closest sieve to 0.22×SCS. The PCS, SCS, and TCS are used to determine the break points between the coarse and fine portions of the gradation, the coarse and fine parts of the fine aggregate and, the coarse and fine parts of fine portion of fine aggregate, respectively. Also, the HCS is defined so as to describe the aggregate size distribution of coarse aggregates. Based on the newest version of the Bailey method, the NMA is defined as the first sieve larger than the first sieve to retain more than 15% (Pine, 2016). Table 4.7 presents the recommended HCS, PCS, SCS and TCS for different NMA.

Table 4.7 Half Sieve and Control Sieve Sizes based on the Bailey Method (Pine, 2016).

Control Sieve	Nominal Maximum Aggregate Size (mm)					
	37.5	25.0	19.0	12.5	9.5	4.75
	Sieve Size (mm)					
Half (HCS)	19.0	12.5	9.5	6.25	4.75	2.36
Primary (PCS)	9.5	4.75	4.75	2.36	2.36	1.18
Secondary (SCS)	2.36	1.18	1.18	0.600	0.600	0.300
Tertiary (TCS)	0.600	0.300	0.300	0.150	0.150	0.075

The preliminary statistical analysis to find a relationship between the Bailey method control sieves and compactability parameters revealed the control sieves could not satisfactory describe the compactability parameters of CS and initial density. Therefore, a new parameter, the relative difference packing index (RDPI), is proposed to characterize the relative difference between the packing condition of the coarse and fine portions of an aggregate gradation (Figure 4.5). The RDPI can be calculated using Equations 4.11 and 4.12.

$$\text{Diff (d)} = P(d) - P_{\text{Dens}} \quad (4.11)$$

$$\text{RDPI} = \text{Diff (HCS)} - \{ \text{Diff (PCS)} + \text{Diff (SCS)} + \text{Diff (TCS)} \} \quad (4.12)$$

where, Diff (d) is the deviation of the aggregate percentage of size d from the MDL (0.45 power line), P(d) is the percentage of aggregates passing sieve size d (%), and  $P_{\text{Dens}}$  is the corresponding passing percent on the MDL which it can be estimated using Equation 4.13.

$$P_{\text{Dens}} = 100 \left( \frac{d}{\text{NMAS}} \right)^{0.45} \quad (4.13)$$

In this study, because the NMAS of all the mixtures is 9.5 mm, the sieve sizes of 4.75, 2.36, 0.600 and 0.150 mm are selected as the HCS, PCS, SCS and TCS, respectively. The gradation parameter values for the various asphalt mixtures have been calculated and are shown in Table 4.8. As seen in the table, increasing the fine aggregate percentage in an asphalt mixture results in decreasing  $d_r$  and  $n$  values. In the case of RDPI, the CP, CDP, and two of the FDP mixtures have negative RDPI values, while it is positive for FP and two FDP mixtures.

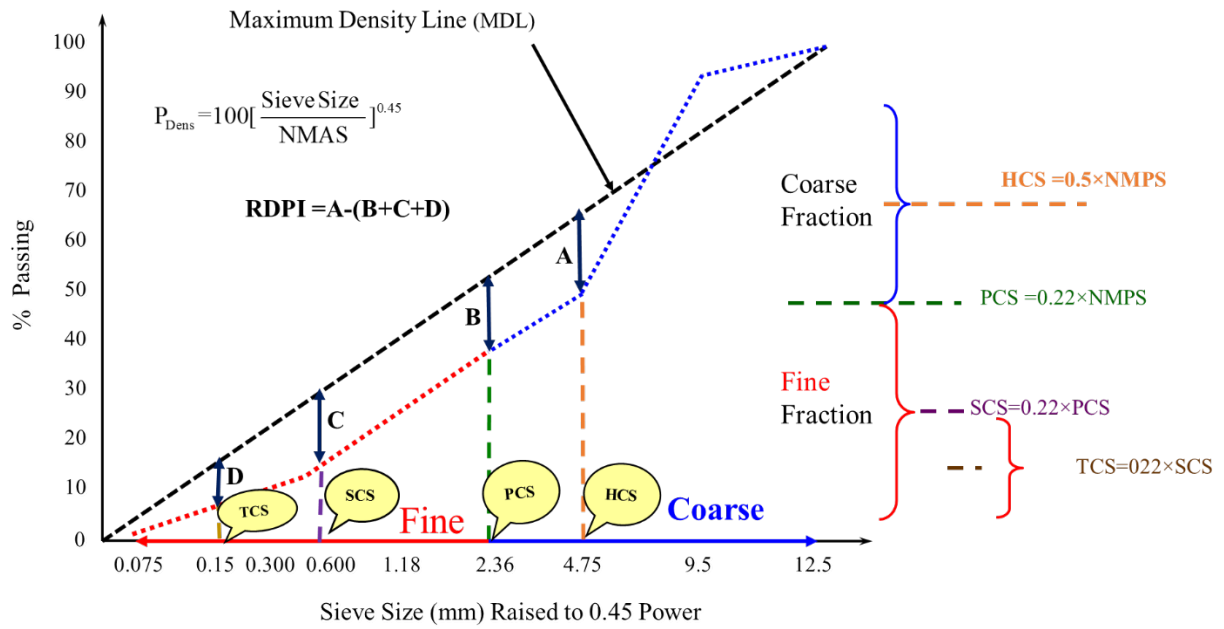


Figure 4.5 Illustration of RDPI and Bailey Control Sieves.

Table 4.8 Gradation Parameters.

Mixture Type	RDPI	dr	n
CP-25	-6.1	5.91	0.86
CP-15	-8.6	5.81	0.90
CP-8	-7.7	5.61	0.86
CP-0	-10.2	5.17	0.87
CDP-8 (k=0.150)	-9.9	4.95	0.85
CDP-8 (k=0.300)	-8.4	4.55	0.82
CDP-8 (k=0.600)	-3.9	4.03	0.77
FDP-25	-0.3	3.62	0.74
FDP-15	-0.6	3.57	0.74
FDP-8	0.0	3.48	0.74
FDP-0	1.5	3.26	0.73
FP-25	6.9	2.58	0.73
FP-15	8.9	2.49	0.72
FP-8	10.7	2.4	0.71
FP-0	13.8	2.24	0.72

#### 4.4.3 Mixtures without Filler

The compaction parameter results for mixtures not containing filler are shown in Table 4.9. In addition to the aforementioned gradations, only coarse and fine mixtures were included in order to more widely observe the compactability trend.

Table 4.9 Compaction Parameters for Mixtures without Filler.

Mixture Type	Initial Density		Compaction Slope		Locking Point		CEI	
	Average	COV (%)	Average	COV (%)	Average	COV (%)	Average	COV (%)
Only Coarse	62.15	0.43	3.76	0.98	72	1.39	613.5	0.39
CP-25	70.50	0.61	3.75	0.52	66	2.27	605.9	1.65
CP-15	72.78	0.57	3.68	0.04	64	1.56	596.9	3.22
CP-8	75.05	0.11	3.62	0.14	59	4.24	588.5	1.16
CP-0	77.30	0.51	3.43	0.43	52	2.88	562.4	2.08
CDP-8 (k=0.150)	79.45	0.84	3.06	0.99	46	1.09	500.4	0.89
CDP-8 (k=0.300)	81.6	0.52	2.69	0.88	41	1.22	437.9	3.43
CDP-8 (k=0.600)	81.95	0.43	2.46	0.07	37	1.35	402.1	1.27
FDP-25	82.55	0.22	2.35	0.43	33	0.01	332.9	3.04
FDP-15	82.55	0.33	2.21	0.95	31	1.61	354.8	3.94
FDP-8	82.43	0.48	2.17	0.54	33	3.03	360.1	4.95
FDP-0	82.3	0.55	2.16	0.82	36	1.39	366.2	5.24
FP-25	82.12	0.63	2.13	0.86	34	1.47	352.8	3.1
FP-15	82.02	0.42	2.11	0.19	32	3.13	344.9	0.8
FP-8	81.95	0.17	2.08	0.18	33	1.52	339.4	0.88
FP-0	81.65	0.94	1.95	0.84	32	0.05	316.3	1.63
Only Fine	75.11	0.14	1.91	0.19	29	3.45	307.7	5.46

Increasing the amount of fine aggregates in the mixtures results in increasing initial density up to the FDP-25 mixture, after which it remains fairly constant for all the fine mixtures. For CP and CDP mixtures, the rate of change in initial density is much higher than for FP and FDP mixtures (Figure 4.6). With regard to CP, CDP and FP mixtures, the decreasing trend of CS, locking point, and CEI are similar when the amount of fine aggregates increases. However, a different behavior can be observed for FDP mixtures.

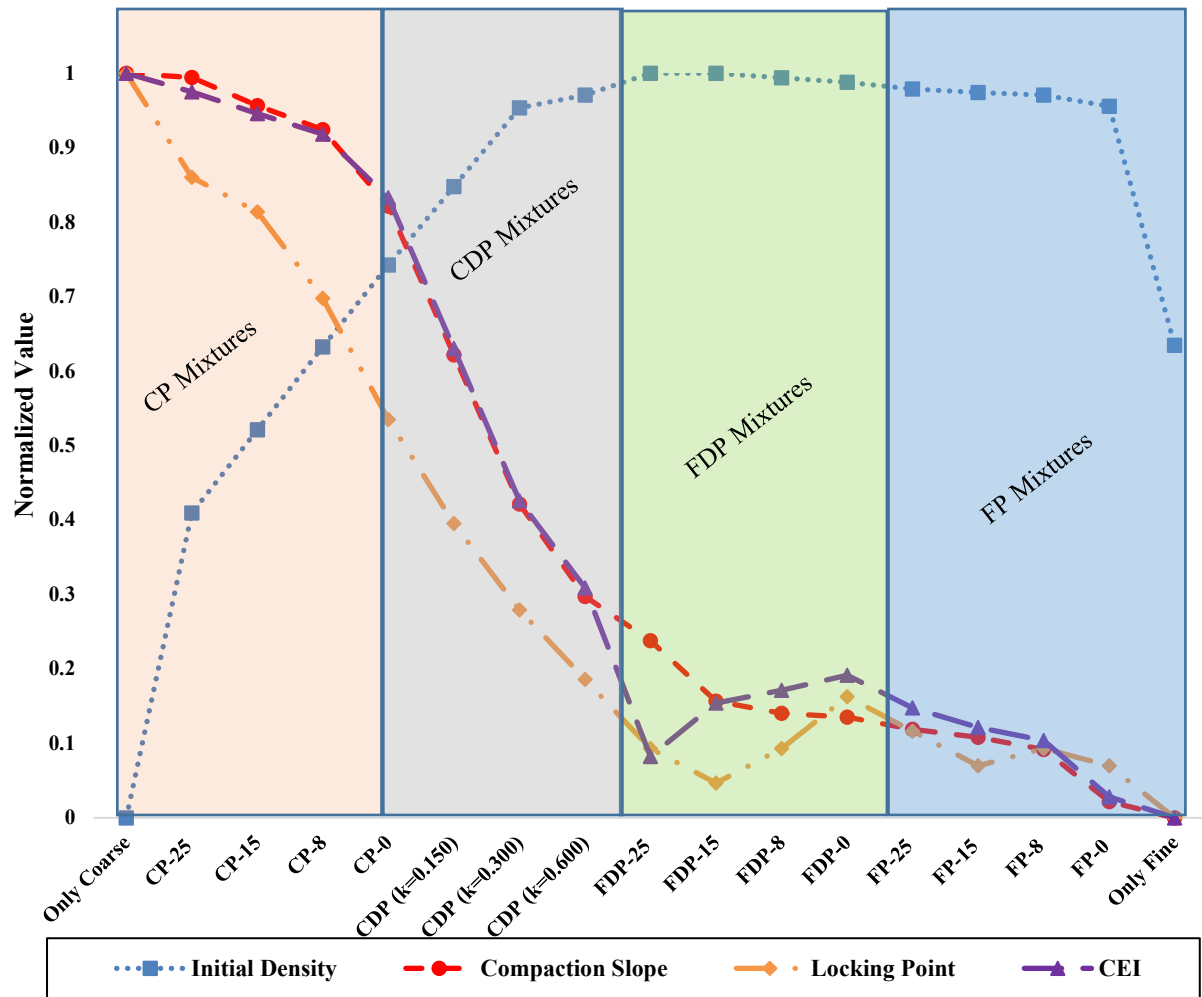


Figure 4.6 Normalized Compaction Parameters for Various Gradation Types (without filler).

To establish a relationship between mixture gradation and compactability parameters, an analysis of variance (ANOVA) was performed to determine if the gradation parameters could predict the normalized values of initial density and CS. The ANOVA F-test provides a p-value based on a chosen significance level,  $\alpha$ . If the p-value is less than the chosen  $\alpha$ , 5% in this case, the null hypothesis that there is not relationship is rejected and consequently, it can be concluded that the explanatory variables are statistically significant. In this study, laboratory CS and initial density were selected as the dependent variables, since they were found to have good correlation with field densities (Kassem et al., 2012; Awed et al., 2015).

Table 4.10 shows the ANOVA results for both compaction parameters (initial density and CS) and Student's t-tests for each model's explanatory parameters. The results indicate that all gradation parameters (RDPI,  $d_r$ , and  $n$ ) have a significant effect on the predicted values of initial

density at a significance level of 5% (P-values  $\leq 0.05$ ). For CS values, the gradation parameters of RDPI and  $d_r$  are significant.

Table 4.10 ANOVA Results for Normalized Initial Density and Compaction Slope Models (without filler).

Normalized Initial Density	Normalized Initial Density = 2.14 - 0.039(RDPI) - 0.315(d <sub>r</sub> ) - 0.416n					
	Root MSE	0.06535	R2	0.9557	Adjusted R2	0.9454
	Variable	DF	Parameter Estimate		t Value	Pr >  t
	Intercept	1	2.14262		11.33	<0.0001
	RDDI	1	- 0.03943		-4.27	0.0009
	dr	1	- 0.31517		-4.52	0.0006
	n	1	-0.41555		-11.44	<0.0001
Normalized Compaction Slope	Normalized CS = -1.60 + 0.055(RDPI) + 0.623(d <sub>r</sub> )					
	Root MSE	0.09067	R2	0.9539	Adjusted R2	0.9432
	Variable	DF	Parameter Estimate		t Value	Pr >  t
	Intercept	1	-1.60681		-6.13	<0.0001
	RCI	1	0.05505		4.30	0.0009
	dr	1	0.61004		6.31	<0.0001
	n	1	0.05268		1.05	0.3148

Additionally, the compaction parameters results were used to classify the mixtures using a self-organizing map (SOM) method. The various SOM methods are popular artificial neural network (ANN) approaches for clustering multi-dimensional data (Map and Kohonen, 1990; Van Hulle, 2012). The SOM method chosen for use is a powerful tool for data clustering based on multi-input parameters. It considers the input parameters as the topological information to determine which mixtures (classes) are most like others using an unsupervised, competitive learning algorithm.

The classification results are shown in Table 4.11. The method indicates the CP mixtures are all in Class A, while all the FP and FDP mixture fall into Class D. The CDP mixtures fall into two classes, Classes B and C, indicating a variation in compaction behavior of these mixtures. They compact differently than do the CP, FP, and FDP mixtures. Compared to the other classes, class A mixtures have the highest compaction slope (stronger aggregate structure), however, they

have the lowest initial density values. Therefore, they show the worst compactability (the highest compaction energy index and locking point) compared to other classes. Additionally, although the initial density of CPD mixtures is approximately same, the high variation between the compaction slope of CDP ( $k=0.600$ ) mixture and two other CPD mixtures ( $k=0.300$  and  $k=0.150$ ) leads to two different classes (B and C). The Class B mixture has a stronger aggregate skeleton than the Class C mixtures, while the Class C mixtures have better compactability than the Class B mixture. Class D mixtures show better compactability in term of CEI, locking point and initial density than other classes, but they have the weakest aggregate structure due to the lowest compaction slope. By considering a balance between compaction slope and initial density, it seems that CDP mixtures offer the strongest aggregate structure and along with adequate compactability.

Table 4.11 Classification Analysis using the Self Organizing Map Method.

Mixture Type	% Fine	Class	Compaction Parameter			
			Initial Density	Compaction Slope	Locking Point	Compaction Energy Index
Only Coarse	0	A	71.55±5.22	3.65±0.12	63±6.7	593.4±17.7
CP-25	19.2	A				
CP-15	21.7	A				
CP-8	24.6	A				
CP-0	32.2	A				
CDP ( $k=0.600$ )	35	B	79.45±0.66	3.06±0.03	46±0.5	500.4±4.5
CDP ( $k=0.300$ )	40	C	81.80±0.18	2.58±0.11	39±2	420±17.9
CDP ( $k=0.150$ )	45	C				
FDP-25	49.2	D	81±2.24	2.11±0.12	33±1.8	341±18.6
FDP-15	50.1	D				
FDP-8	51.2	D				
FDP-0	54	D				
FP-25	62.8	D				
FP-15	63.5	D				
FP-8	64.3	D				
FP-0	66.1	D				
Only Fine	100	D				

#### 4.4.4 Mixtures with Fillers

Table 4.12 presents the compaction parameter results for “final” mixtures containing filler. The data clearly indicate that filler facilitates compaction. This is shown graphically in Figure 4.7 where compaction parameters for mixtures with and without filler are compared. The lubricating effect of filler on all compaction parameters is more significant for CP mixtures than for the others. Also, the rate of change in initial density and CS is higher in CP and CDP mixtures as compared to FP and FDP mixtures. In the case of CS, there is a slight difference between the mixtures with and without filler for FP and FDP mixtures. With respect to the locking point, there is a range from CDP ( $k=0.300$ ) and FDP-15 where mixtures without filler have lower locking points than those with filler. Also, the addition of filler notably reduces compaction energy within all the gradation areas.

Table 4.12 Compaction Parameters for Mixtures Containing Filler.

Mixture Type	Initial Density		Compaction Slope		Locking Point		CEI	
	Average	COV (%)	Average	COV (%)	Average	COV (%)	Average	COV (%)
CP-25	85.9	1.11	4.97	1.25	48	3.13	270.9	1.99
CP-15	86.1	1.32	4.87	1.53	48	2.08	258.3	3.84
CP-8	86.3	0.39	4.75	0.42	45	3.33	244.6	1.36
CP-0	87.4	0.64	4.24	0.78	46	2.17	183.6	2.34
CDP-8 ( $k=0.600$ )	88.3	1.04	3.81	1.23	41	1.22	168.4	1.92
CDP-8 ( $k=0.300$ )	89.3	0.89	3.37	0.94	41	2.44	105.1	3.01
CDP-8 ( $k=0.150$ )	90.2	0.34	2.93	0.35	41	1.22	59.8	1.02
FDP-25	91.1	0.81	2.49	0.84	36	1.39	32.2	2.02
FDP-15	91.2	0.58	2.43	0.57	32	3.13	35.7	2.81
FDP-8	91.3	0.40	2.37	0.41	31	1.61	37.0	3.56
FDP-0	91.5	0.69	2.29	0.72	33	1.52	37.7	3.84
FP-25	91.7	0.25	2.27	0.23	27	5.56	31.0	2.19
FP-15	91.9	0.62	2.26	0.61	25	2.04	30.0	1.55
FP-8	92.0	0.24	2.27	0.21	24	4.17	30.1	1.64
FP-0	92.2	0.34	2.24	0.35	24	2.08	21.5	1.03



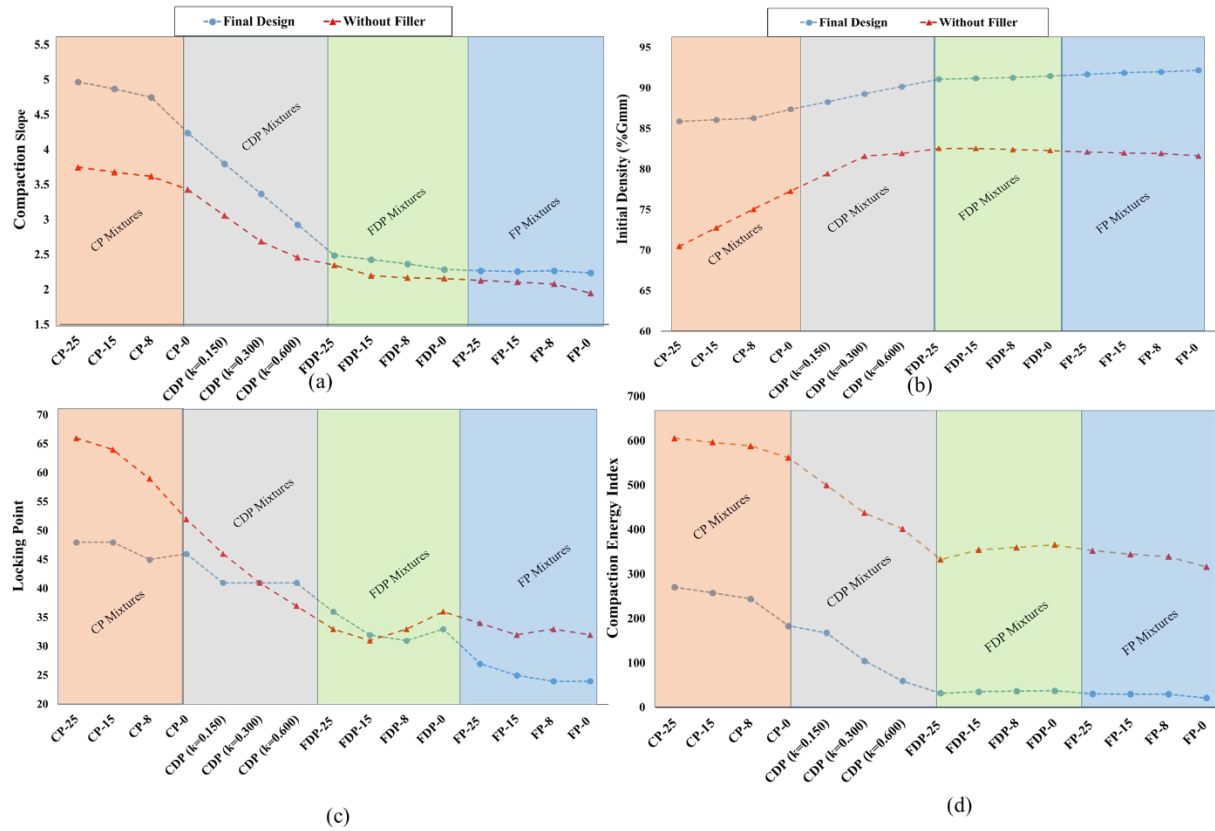


Figure 4.7 Comparison of Compaction Parameters for Mixtures with and without Filler: (a) Initial Density; (b) Compaction Slope; (c) Locking Point and; (d) Compaction Energy Index.

Similar to the mixtures without filler, statistical models were developed for the mixtures containing filler (Table 4.13). All the gradation parameters were found to be significant with regards to CS and initial density. The results illustrate that decreasing  $d_r$  and  $n$  values results in increasing initial density and decreasing CS values. For CP and CDP mixtures, a decrease of RDPI increases initial density and decreases CS, while for FP and FDP mixtures the reverse is true. Additionally, the plot of predicted versus actual values of initial density and CS confirms both regression equations are well-fit to the data (Figure 4.8). With such a high  $R^2$ , it can be concluded that using three gradations is enough to develop the models for prediction of change in CS and initial density. This can lead to far fewer samples required for evaluating the compactability of a wide range of gradation types.

Table 4.13 ANOVA Results for the Normalized Initial Density and Compaction Slope Models (with filler).

Normalized Initial Density	Normalized Initial Density = 3.75 - 0.022(RDPI) - 0.266(d <sub>r</sub> ) - 2.69n					
	Root MSE	0.03051	R2	0.9947	Adjusted R2	0.9933
	Variable	DF	Parameter Estimate		t Value	Pr >  t
	Intercept	1	3.75499		14.11	<0.0001
	RDPI	1	- 0.02186		-8.33	<0.0001
	dr	1	- 0.26609		-9.34	<0.0001
	n	1	-2.68853		-5.98	<0.0001
Normalized Compaction Slope	Normalized CS = -3.50 + 0.030(RDPI) + 0.28(d <sub>r</sub> ) + 3.53n					
	Root MSE	0.03381	R2	0.9941	Adjusted R2	0.9925
	Variable	DF	Parameter Estimate		t Value	Pr >  t
	Intercept	1	-3.49674		-11.86	<0.0001
	RDPI	1	0.02974		10.22	<0.0001
	dr	1	0.27663		8.76	<0.0001
	n	1	3.53239		7.09	<0.0001

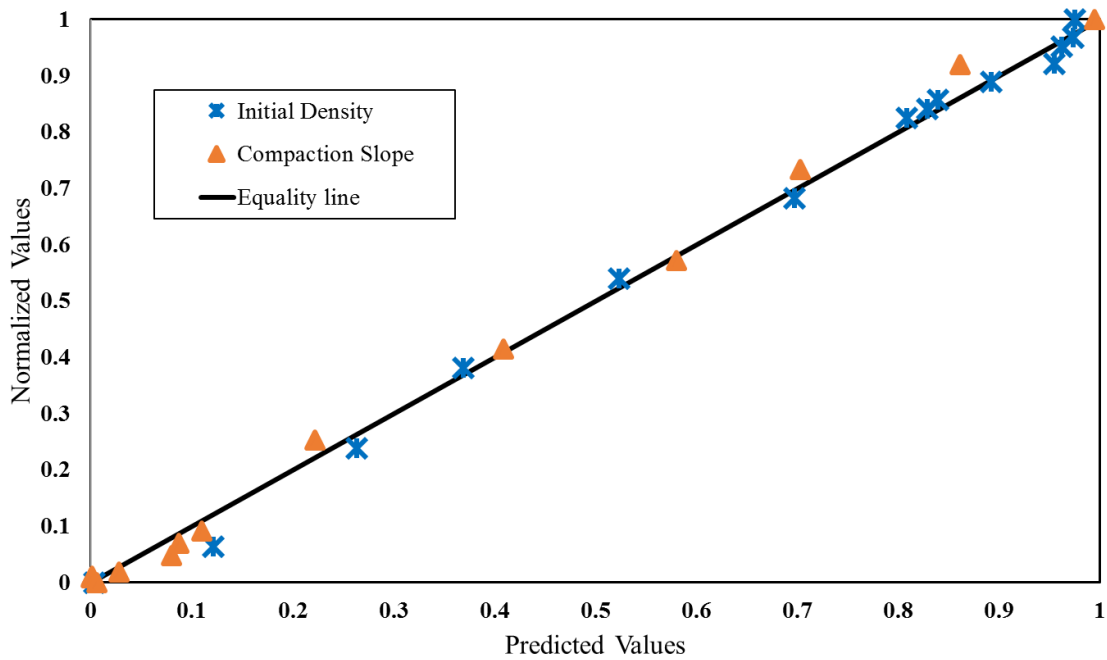


Figure 4.8 Predicted and Laboratory Normalized Initial Density and Compaction Slope Values for Mixtures Containing Filler.

From the models developed for the initial density and CS (equations in Table 4.13), it can be observed that the signs of the coefficients are opposite. Thus, in order to achieve a gradation with high packing capability (i.e. high initial density), as well as strong aggregate structure (i.e. high CS) (Vavrik, 2000; Leiva and West, 2008), the intersection of the two equations must be determined. Equating the two and simplifying results in Equation 4.14.

$$0.062(RDPI)+0.54(d_r)+6.22n-7.25=0 \quad (4.14)$$

As shown by the Equation 4.14, the result is a plane with three unknowns (i.e. RDPI,  $d_r$  and  $n$ ). It is clear that each mixture satisfying this equation has high initial density and an appropriate compaction slope. Applying Equation 4.14 to the mixture gradations reveals the gradation parameters meeting Equation 4.14 fall between a CDP of 0.150 and 0.300. Therefore, any gradation having a  $k$  value between 0.150 and 0.300 should have both a high packing capacity and a strong structure that can resist deformation under loading. In Figure 4.9, the difference line shows the values obtained from applying the gradation parameters of each mixture to Equation 4.13.

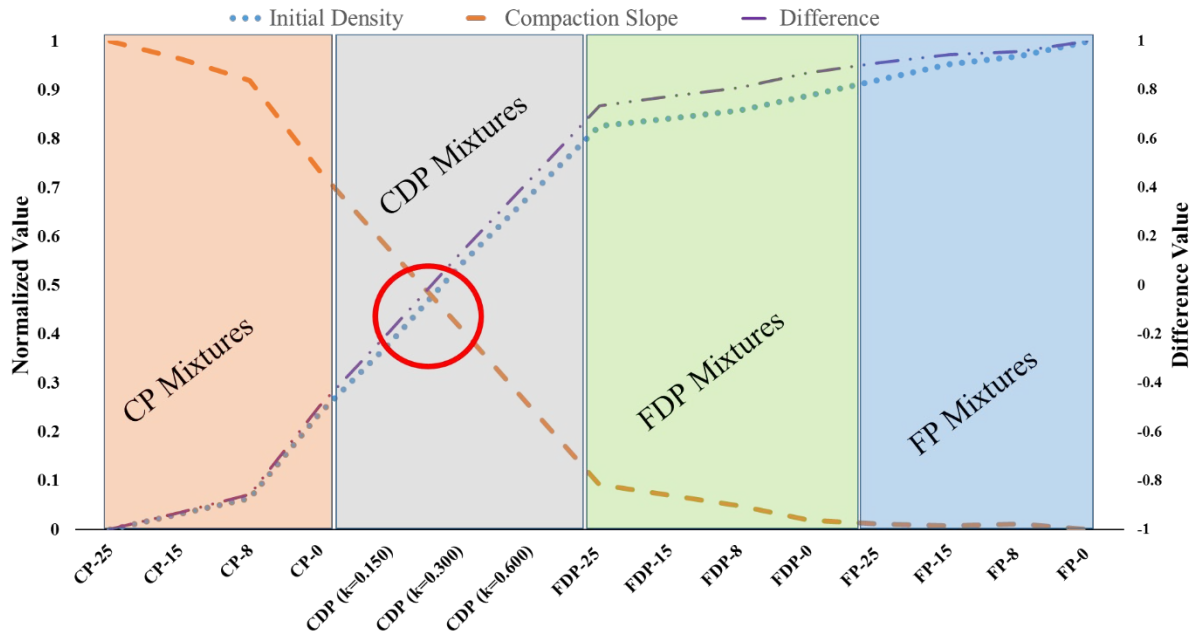


Figure 4.9 Recommended Gradation based on Initial Density and Compaction Slope.

## 4.5 Evaluation of Compactability Models

To assess the proposed relationship between compaction parameters (initial density and compaction slope (CS)) and the gradation parameters, two independent sets of data, one set of laboratory data and one set of field data, were used.

### 4.5.1 Laboratory Data

In 2000, a comprehensive experiment to establish a relationship between the Bailey method parameters and the volumetric properties of asphalt mixtures was completed (Vavrik, 2000). These experimental data are used here because they include compaction parameters and, more importantly, all mixtures were fabricated from the same stockpiles with constant binder and filler contents. In the experiment, the original coarse and fine stockpiles were divided into three parts, coarse, medium, and fine. Based on the different stockpile combinations and five coarse aggregate chosen unit weight (CUW) levels, 90, 95, 100, 105 and 110 percent, twenty-five mixture designs were completed, and specimens fabricated. All mixtures contained 5% filler by total aggregate mass and 5.5% asphalt binder (PG 64-22) by total mixture mass. Mixture specimens were compacted using 100 SGC gyrations. Tables 4.14 and 4.15 show the coarse and fine stockpile gradations of each mixture type (Block 1 through 5) and the corresponding compaction and gradation parameters of each mixture.

Table 4.14 Aggregate Gradations and Properties (after Vavrik, 2000).

Coarse Stockpile				Fine Stockpile			Filler
Sieve (mm)	Coarse	Medium	Fine	Coarse	Medium	Fine	
12.50	100.0	100.0	100.0	100.0	100.0	100.0	100.0
9.50	94.0	97.0	100.0	100.0	100.0	100.0	100.0
4.75	15.0	30.0	45.0	94.0	97.0	100.0	100.0
2.38	7.0	16.0	25.0	81.0	82.5	84.0	100.0
1.18	—	2.0	4.0	62.0	65.0	68.0	100.0
0.60	—	1.0	1.0	30.0	45.0	60.0	100.0
0.30	—	—	—	3.0	16.0	29.0	100.0
0.15	—	—	—	1.9	1.9	1.9	99.0
0.08	—	—	—	0.2	0.2	0.2	88.0
Gsb	2.692	2.692	2.692	2.572	2.572	2.572	2.755

Table 4.15 Gradation and Compaction Parameters (after Vavrik, 2000).

Mixture Name		Stockpiles		Gradation Parameters			Compaction Parameters	
		Coarse	Fine	RDPI	dr	n	Initial Density	CS
Block 1	LUW1 -10	Med	Med	-7.7	4.15	0.86	82.8	7.4
	LUW -5	Med	Med	-7.7	4.4	0.88	81.7	7.6
	LUW1	Med	Med	-9.7	4.63	0.93	80.8	7.9
	LUW +5	Med	Med	-10.7	4.83	0.97	79.6	8.3
	LUW +10	Med	Med	-13.7	5.06	1.05	78.4	8.7
Block 2	LUW -10	Coarse	Med	-2.7	4.36	0.8	84.6	6.6
	LUW -5	Coarse	Med	-2.7	4.63	0.82	84.2	7.0
	LUW	Coarse	Med	-3.7	4.96	0.85	83.4	7.8
	LUW +5	Coarse	Med	-5.7	5.21	0.89	82.9	8.2
	LUW +10	Coarse	Med	-6.7	5.41	0.95	81.0	9.0
Block 3	LUW -10	Fine	Med	-12.7	4.5	0.78	79.4	8.0
	LUW -5	Fine	Med	-14.7	4.85	0.79	79.5	8.1
	LUW	Fine	Med	-16.7	5.29	0.81	79.2	8.7
	LUW +5	Fine	Med	-17.7	5.6	0.82	77.9	8.8
	LUW +10	Fine	Med	-19.7	5.81	0.85	76.7	8.9
Block 4	LUW -10	Med	Coarse	-10.7	4.31	0.93	82.4	7.8
	LUW -5	Med	Coarse	-12.7	4.56	0.97	81.3	8.1
	LUW	Med	Coarse	-13.7	4.76	1.02	80.7	8.3
	LUW +5	Med	Coarse	-14.7	4.95	1.07	79.6	8.5
	LUW +10	Med	Coarse	-15.7	5.13	1.11	77.8	8.7
Block 5	LUW -10	Med	Fine	-2.7	4.07	0.78	86.1	7.4
	LUW -5	Med	Fine	-4.7	4.31	0.82	84.4	8.3
	LUW	Med	Fine	-6.7	4.53	0.86	83.2	8.9
	LUW +5	Med	Fine	-7.7	4.79	0.91	81.9	9.5
	LUW +10	Med	Fine	-10.7	5.03	0.98	80.5	9.6

1: LUW stands for the loose unit weight of coarse aggregates

As shown in Figures 4.10 and 4.11, the trends of change in estimated CS and initial density (normalized values) using the equations from Table 4.13 are similar to the trends of the laboratory data. However, the laboratory values of CS and initial compaction are somewhat different from those predicted by the proposed models, most likely because the laboratory mixtures were not designed at constant air voids content.

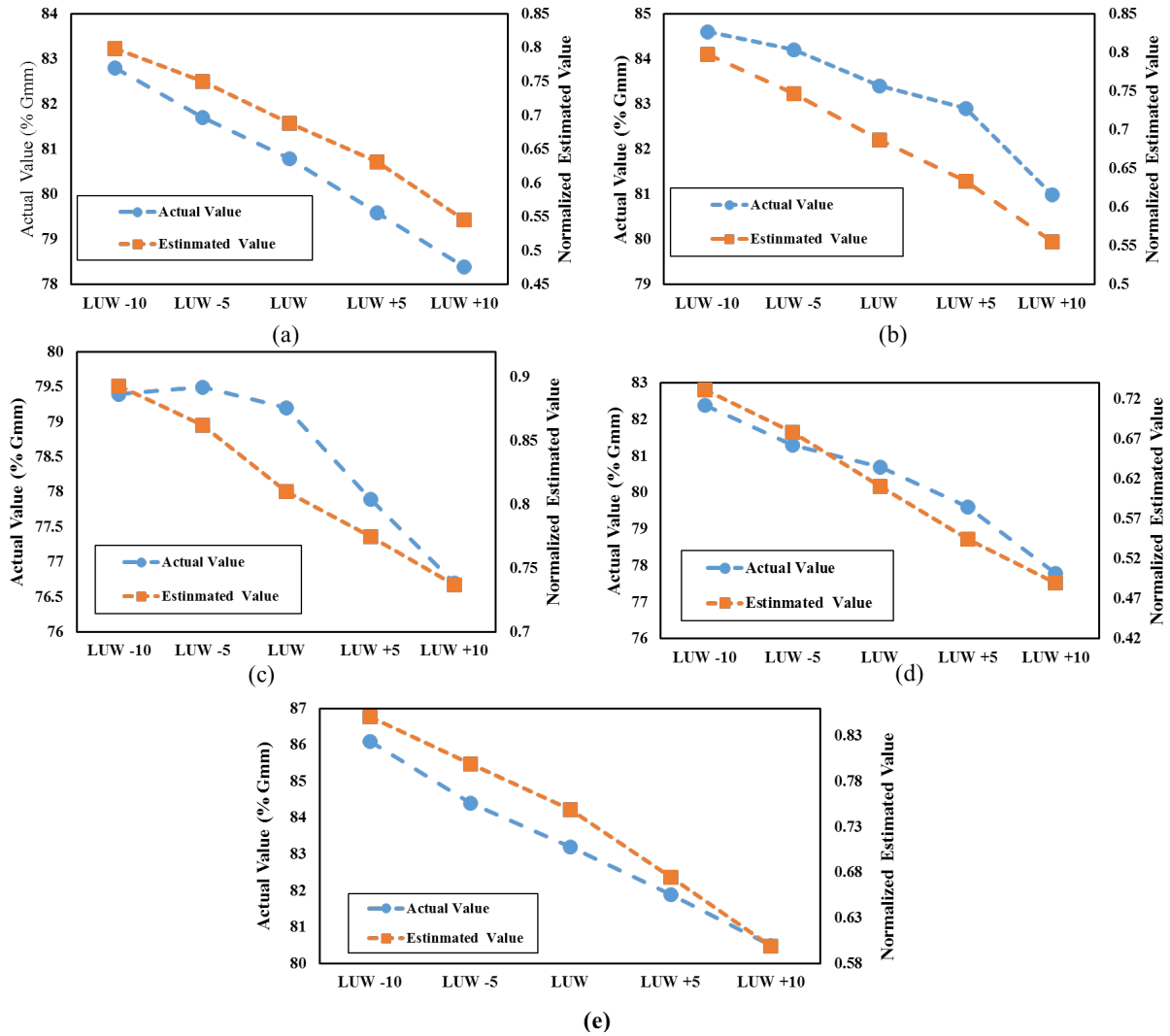


Figure 4.10 Comparison of Laboratory Initial Density and Corresponding Predicted Normalized Values for: (a) Block 1; (b) Block 2; (c) Block 3; (d) Block 4; (e) Block 5.

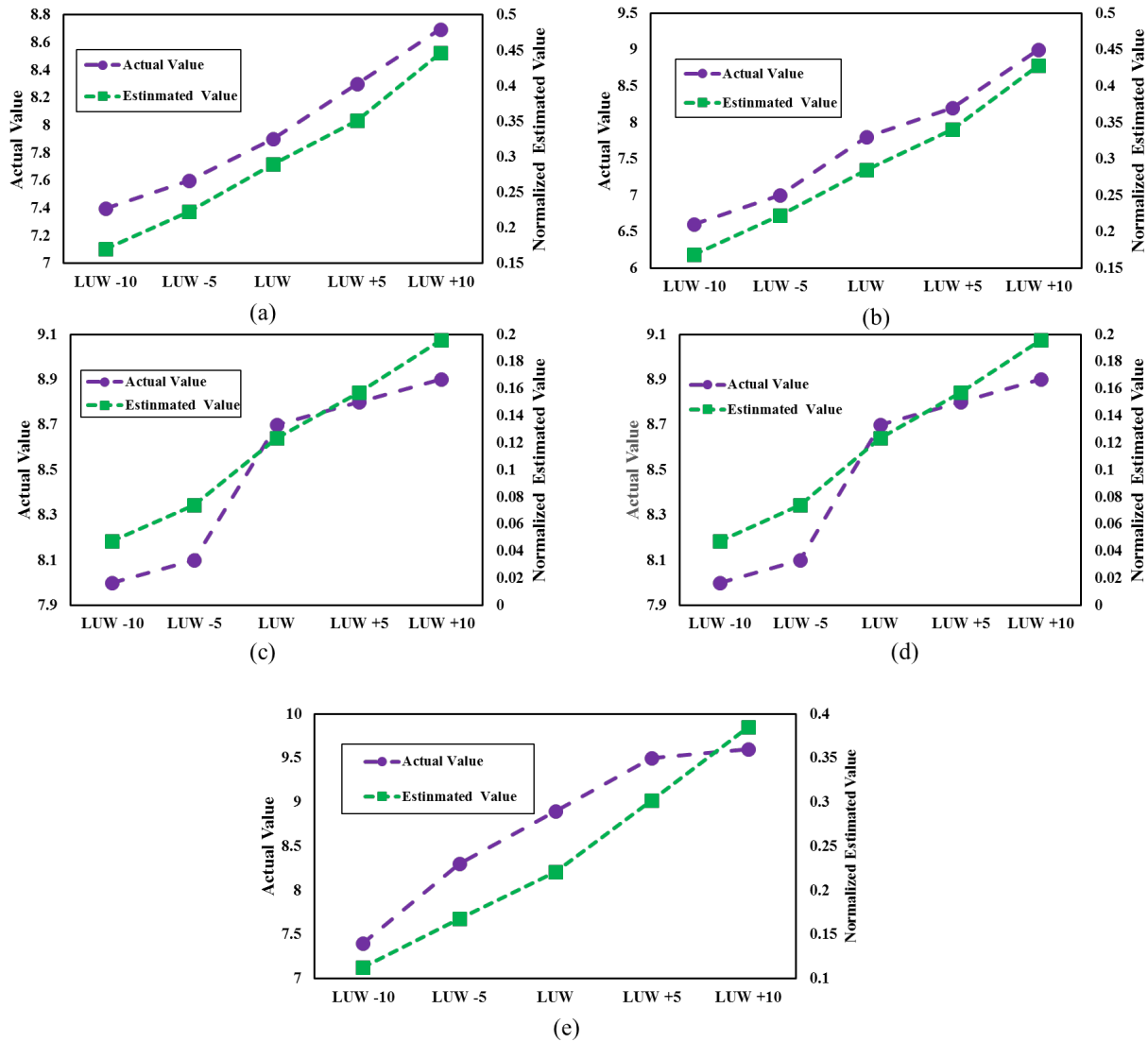


Figure 4.11 Comparison of Laboratory Compaction Slope and Corresponding Predicted Normalized Values for: (a) Block 1; (b) Block 2; (c) Block 3; (d) Block 4; (e) Block 5.

#### 4.5.2 Field Data

In early 2016, a trial project demonstrating how in-place asphalt pavement density could be achieved using a modified Superpave mixture design procedure was completed on a section of US 40 in Richmond, Indiana and involved milling approximately 38 mm (1.5 in.) of existing asphalt surface and applying 38 mm (1.5 in.) of new asphalt mixture. Two different sections were constructed, one using the modified mixture design and second using a standard Superpave-designed mixture. The modified mixture was designed by choosing OBC at 5% air voids and

reducing the number of design gyrations to 50 ( $N_{des}=50$ ). The control mixture was designed with OBC chosen at 4% air voids and a  $N_{des}$  of 100.

Field compaction was achieved using three vibratory, steel-wheeled rollers having an approximate 9 tonne mass (10 tons) (Figure 4.12). Six vibratory passes were applied followed by one static pass. The compaction temperature was approximately  $127 \pm 28^{\circ}\text{C}$  ( $260 \pm 25^{\circ}\text{F}$ ) (Montoya et al., 2018).

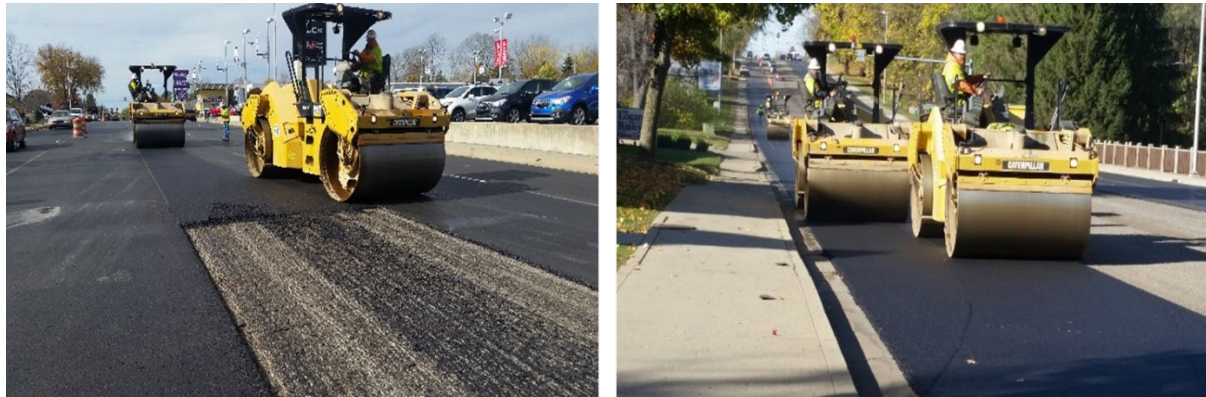


Figure 4.12 Compaction on US 40 Field Project.

As shown in Figure 4.13, changes in the SGC gyrations and design air voids content resulted in a slight gradation difference between the two mixtures. The laboratory and field compaction parameters for the mixtures are shown in Table 4.16. Although there are small differences in the mixture gradations and they have nearly identical binder contents, the gradation parameters and laboratory compaction parameters indicate the modified mixture has better compactability than does the standard mixture, a fact that is observed from the field densities of the two mixtures. The modified mixture yielded over 2% higher density than the standard mixture, both mixtures having been densified with the same compaction effort.

Using the equations from Table 4.13 with the gradation parameters of the standard and modified mixture shows both the initial laboratory density and CS due to gradations can be closely approximated using the proposed relationships (Figure 4.14).



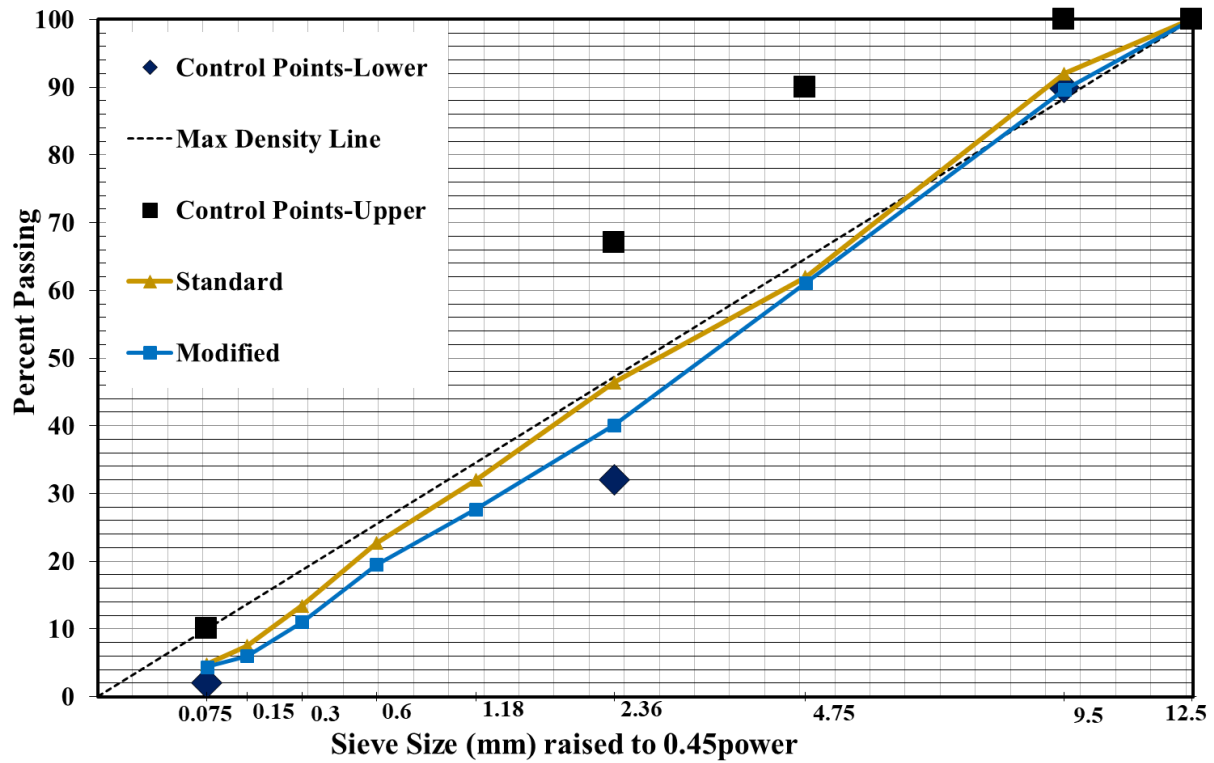


Figure 4.13 Gradation of US 40 Mixtures.

Table 4.16 Laboratory and Field Compaction Parameters.

Mixture	Gradation Parameters			Lab Compaction Parameters		Binder Content (%)	Field Density (% G <sub>mm</sub> )
	RDPI	d <sub>r</sub>	n	Initial Density (% G <sub>mm</sub> )	Compaction Slope		
Standard	-27.195	4.743	1.066	81.69	5.12	6.5	93.27
Modified	-25.995	4.339	1.011	85.89	4.34	6.7	95.35

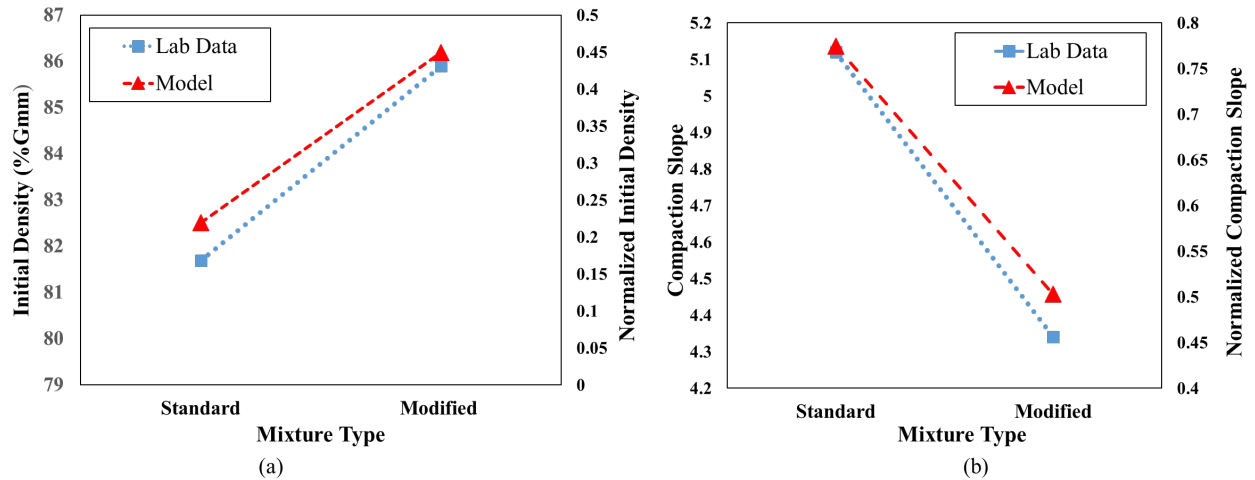


Figure 4.14 Comparison of Laboratory Compaction and Corresponding Normalized Estimated Parameters for: (a) Initial Density; and (b) Compaction Slope.

## 4.6 Summary

The objective of the work presented in this chapter was to evaluate the effect of asphalt mixture aggregate gradation on laboratory compaction parameters using a comprehensive experiment. This evaluation was performed in two stages in order to observe the effect of filler on the compaction parameters. To fabricate various mixtures with approximately equal effective binder and design air voids content (4%), a different mixture design approach was used. Rather than choosing a gradation and varying binder content to achieve required air voids content, the amount of filler and the aggregate gradation were adjusted to reach the desired volumetric properties.

Furthermore, three gradation parameters, RDPI,  $d_r$ , and  $n$  and were proposed to predict initial mixture density and compaction slope (CS), these being considered two indicators of compactability. Based on, the findings, the following conclusions are drawn:

- Filler affects asphalt mixture compactability and its effects are more significant for coarser gradations. This explains why more trials were required to reach desirable volumetric properties for coarse-graded mixtures than for fine-graded.
- The proposed parameters of RDPI,  $d_r$ , and  $n$  cannot only be used to accurately predict compactability parameters such as initial density and compaction slope, but they thereby can predict the compactability of asphalt mixtures.
- The prediction models developed in the study accurately predict the effects of gradation changes on mixture compactability.

- Based on the defined gradation zones, CDP mixtures are the most efficient mixtures with respect to compactability.
- Using the parameters proposed in this experiment, the compactability of an asphalt mixture can be predicted during the mixture design process, allowing the designer to develop mixtures that can be more easily compacted during construction.

## CHAPTER 6. IMPACT OF THE COARSE AGGREGATE SHAPE PARAMETERS ON COMPACTION CHARACTERISTICS

*This chapter is under revision in Powder Technology Journal*

### 6.1 Introduction

Under normal environmental conditions, the aggregate matrix within an asphalt mixture is responsible to carry the loads imposed by traffic. Thus, aggregate characteristics such as shape, size distribution, texture, and strength directly affect asphalt mixture performance and are key factors in asphalt mixture durability, workability, permeability, and rutting and cracking resistance. Compactability, defined as how easily asphalt mixtures reach the desired level of density during and after field compaction, is an important measure of asphalt mixture adequacy. Some researchers have reported that after aggregate gradation, aggregate shape characteristics, especially of the coarse aggregates, is the most important parameter influencing the aggregate skeleton and consequently the compactability and performance of asphalt mixtures (Moavenzadeh and Goetz, 1963; Brown et al., 1997; Aho et al., 2001; Zhou et al., 2017). Some research indicates that the aggregate shape, the number of fractured aggregate faces, and coarse aggregate surface texture have significant effects on asphalt mixture laboratory compaction characteristics and field density (Brown et al., 1997; Leiva and West 2008; Muras, 2010). Results of these studies also revealed an increase in aggregate surface roughness and angularity can result in the need for increased compaction energy to achieve a specific mixture density.

The Superpave asphalt mixture design method considers aggregate angularity, flatness and elongation, and clay content as important properties to help achieve well performing asphalt mixtures. These morphological tests are usually applied to the aggregate blend of the asphalt mixture rather than to the individual components. Therefore, many studies have concluded the morphological tests are not accurate enough and do not necessarily apply to the broad range of aggregate materials (Garboczi, 2002; Pan and Tutumluer, 2006; Masad et.al 2007). Therefore, various alternative methods have been proposed to better measure both coarse and fine aggregate shape, angularity, and texture (Garboczi, 2002; Garboczi et al., 2006; Pan and Tutumluer, 2006; Masad et al., 2007; Wang et al., 2007a and 2007b; Wang et al., 2012). Although some researchers have found relationships between aggregate morphological properties and asphalt mixture

performance using laboratory tests, the tests were often time-consuming and expensive (Chen et al. 2001; Masad et al. 2007; Tutumluer et al., 2005).

Numerical solutions can be considered as an alternative to laboratory experiments, costing less and requiring less time. Among the common numerical methods used in materials engineering, discrete element modeling (DEM) can be considered the most effective to analyze asphalt mixture mechanical behavior, due to discontinuities in the asphalt mixture microstructures (Abbas et al., 2005; Arasan et al., 2011; Bessa et al., 2014). Additionally, asphalt mixture microstructure properties are highly dependent on the degree of aggregate packing during the compaction process. In DEM, a solid material is represented by a collection of discrete particles that can model the macro-mechanical response of a material through their motions and interactions (Cook and Jensen, 2002). Therefore, DEM is able to consider the discontinuities of microstructure and the changes in particle packing density due to aggregate particles movement, simultaneously. However, one major challenge for numerical analysis of real aggregates is to accurately define the complex shapes of real aggregate particles in the DEM modeling.

DEM modeling is based on two-dimensional discs or three-dimensional spheres due to their computational efficiency. In reality, the aggregate shapes are highly irregular and such simplified modeling could be unrealistic (McDowel et al., 2011). To overcome this limitation, various approaches have been conducted to add the effect of particle shape using non-circular or spherical particles. Among these are, ellipsoids (Ouadfel and Routhenburg, 2001; Ng, 2009), cylinders (Pournin et al., 2005), polyhedrons (Azema et al., 2009; Galindo and Pedroso, 2010), pentagons (Azema et al., 2007), glue-sphered (Taghavi, 2011; Zhou et al., 2017), and clusters of discs or spheres (Salot et al., 2009; Matsushima et al., 2009; Katagiri et al., 2010). While an improvement over discs or spheres, these were unable to accurately model the effect of particle shape properties on the mechanical and packing behavior of granular systems due to oversimplification.

In 2007, Das proposed the overlapping discrete element cluster (ODEC) method as a more accurate clumping technique in two and three dimensions to model angularity in particle shapes. In this method, the particle shape is modeled by clumping a number of overlapping disc (2D) or sphere (3D) elements within the particle boundary to approximate the outline of the real sand particles. This technique has successfully been used to model the mechanical behavior of irregular sand particles observed in experiments. Mollon and Zhao (2012 and 2014) modified the Das

method and proposed a systematic and broader method to describe particle shape for discrete element modeling. They applied the discrete random fields theory based on spherical harmonics (SH) to generate star-like granular particles.

## 6.2 Shape Parameters

In granular material science “morphology” is defined as the overall geometrical characteristics of particles. Particle morphology can be expressed by two main parameters, shape and surface texture (Blott and Pye, 2008). Shape parameters describe the large- to intermediate-scale external features of a particle, while surface texture represents the surface features of a particle at small-scale. In this study, only shape parameters were considered.

A search of the literature revealed four important shape parameters proposed to describe the shape features of a particle: form, roundness, regularity, and sphericity (Sneed and Folk, 1958; Barrett, 1980; Orford, 1983; Blott and Pye, 2008; Mollon and Zhao, 2012). Form parameters describe the dimensional characteristic of a particle using ratios of its three linear dimensions, length, width, and thickness. Two well-known form parameters are flatness and elongation, and can be calculated using Equations 1a and 1b.

$$\text{Flatness} = \frac{S}{I} \quad (5.1a)$$

$$\text{Elongation} = \frac{I}{L} \quad (5.1b)$$

where, S, I and L are the small, intermediate and large dimension of the particles, respectively (Figure 5.1a).

Roundness determines how rounded or angular a particle is (sharpness of corners and edges) and can be determined using Equation 2 (Wadell, 1932; Mollon and Zhao, 2012).

$$\text{Roundness} = \frac{\sum_{i=1}^{n_c} R_{ci}}{n_c \times R_{\text{insc}}} \quad (5.2)$$

where,  $n_c$  is the number of overlapping spheres used to accurately fill the volume of the particle,  $R_c$  are the radii of the overlapping spheres, and  $R_{\text{insc}}$  is the radius of the largest sphere size that can be inscribed in the considered particle (Figure 5.1b).

Regularity indicates the deviation of particle shape from that of a regular shape, either curved or straight-sided, and is defined as (Mollon and Zhao, 2012):

$$\text{Regularity} = \log\left(\frac{P}{P - P_{\text{convex}}}\right) \quad (5.3)$$

where,  $P$  and  $P_{\text{convex}}$  are the perimeter and convex perimeter of a particle as shown in Figure 5.1c.

Lastly, sphericity expresses how closely a particle shape mirrors an ideal sphere and can be determined using the following equation (Riley, 1941):

$$\text{Sphericity} = \sqrt{\frac{R_{\text{inse}}}{R_{\text{circ}}}} \quad (5.4)$$

where,  $R_{\text{circ}}$  is the radius of the smallest circumscribed sphere to the considered particle (Figure 5.1d).

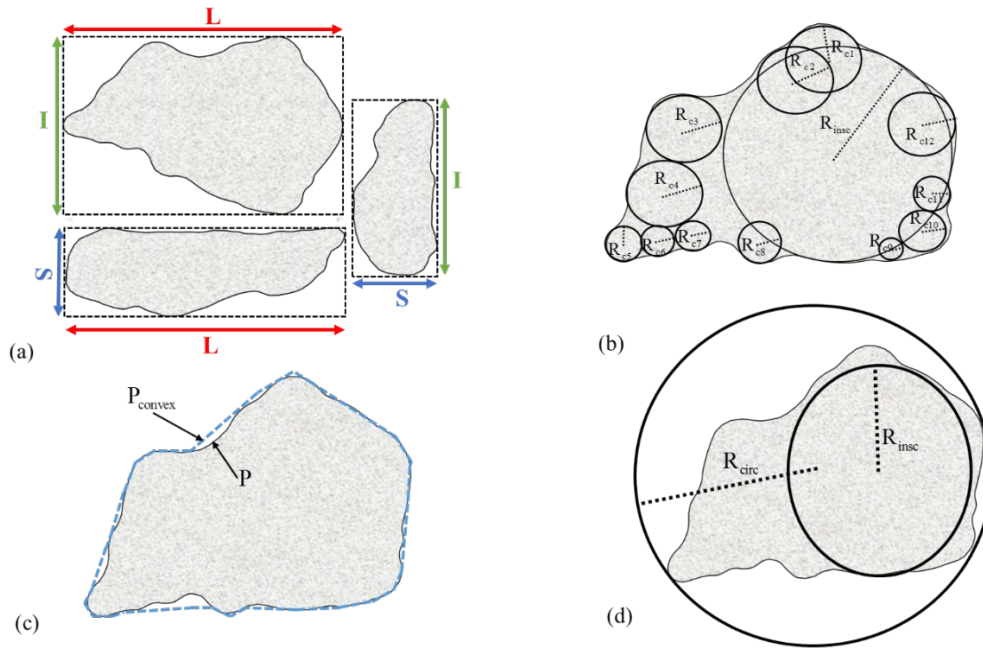


Figure 5.1 Form Parameter Definitions.

Flatness and elongation ratios have been used by researchers to develop particle classification systems (Zingg, 1935; Benn and Ballantyne, 1992; Blott and Pye, 2008). The system proposed by Blott and Pye (2008) is shown in Table 5.1. In this system, five categories, or classes describe the form of a particle based on elongation and flatness. Figure 5.2 graphically illustrates 25 possible classifications for spherical particles. In this figure, the “ExFy” designation represents the particles with elongation and flatness classes of  $x$  and  $y$ , respectively.

Table 5.1 Particle Classification Based on Form Parameters (after Blott and Pye, 2008).

Elongation			Flatness		
Range	Class	Term	Range	Class	Term
0.0-0.2	5	Extremely elongate	0.0-0.2	5	Extremely flat
0.2-0.4	4	Very elongate	0.2-0.4	4	Very flat
0.4-0.6	3	Moderately elongate	0.4-0.6	3	Moderately flat
0.6-0.8	2	Slightly elongate	0.6-0.8	2	Slightly flat
0.8-1.0	1	Not elongate	0.8-1.0	1	Not flat

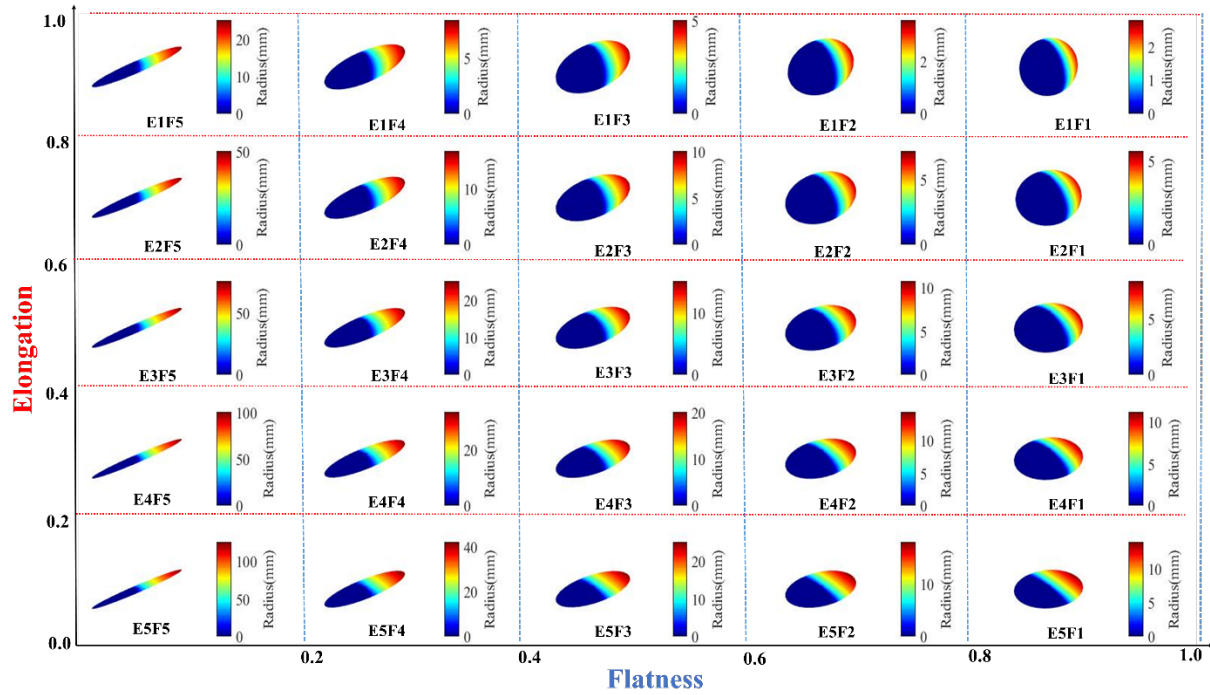


Figure 5.2 Spherical Particle Classification based on Flatness and Elongation.

Similar classifications for roundness have been proposed (Russell and Taylor, 1937; Pettijohn, 1949; Powers, 1953; Blott and Pye, 2008), as shown in Table 5.2. Figure 5.3 illustrates a classification system proposed by Blott and Pye (2008) for two particle types, square and an eight-point star.

Riley (1941) proposed ranges to classify particle sphericity (Table 5.3). The proposed system has five classes of sphericity: very high, high, moderate, low, and very low sphericity, depending on the sphericity value determined from Equation 5.4. Figure 5.4 illustrates the graphical definition of sphericity classification for round particles.



Table 5.2 Particle Roundness Classification.

Source	Class					
	R6	R5	R4	R3	R2	R1
	Very angular	Angular	Subangular	Sub-rounded	Rounded	Well Rounded
Russell and Taylor (1937)	--	0.0-0.15	0.15-0.30	0.30-0.50	0.50-0.70	0.70-1.0
Pettijohn (1949)	--	0.0-0.15	0.15-0.25	0.25-0.40	0.40-0.60	0.60-1.0
Powers (1953)	0.12-0.17	0.17-0.25	0.25-0.35	0.35-0.49	0.49-0.70	0.70-1.0
Blott and Pye (2008)	--	0.0-0.13	0.13-0.25	0.25-0.50	0.50-1.0	--






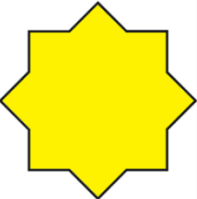
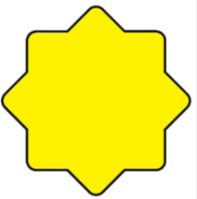
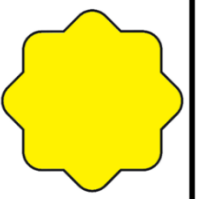
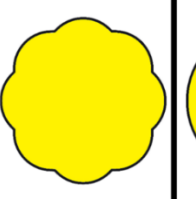
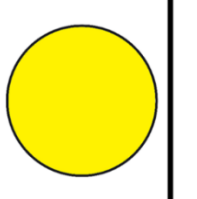
Particle Type	Roundness Class				
	Perfectly Angular	Angular	Sub-Angular	Sub-Rounded	Rounded
Square					
Eight-pointed star					

Figure 5.3 Roundness Classes (Blott and Pye 2008).

Table 5.3 Sphericity Classification (Riley, 1941).

Class		Sphericity Range
Code	Description	
S1	Very High	0.894-1.000
S2	High	0.775-0.894
S3	Moderate	0.632-0.775
S4	Low	0.447-0.632
S5	Very Low	0.000-0.447


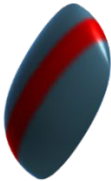
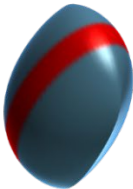

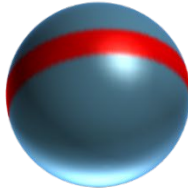
S5	S4	S3	S2	S1
Very Low Sphericity	Low Sphericity	Moderate Sphericity	High Sphericity	Very High Sphericity
				

Figure 5.4 Sphericity Classification for Round Particles.

Although there is no classification for regularity, Mollon and Zhao (2012) explained that regularity greater than 3 or 4, meaning  $P-P_{\text{convex}}$  is less than  $10^{-3}$  or  $10^{-4}$ , can be effectively considered as perfect regularity.

In this study, the flatness, elongation, roundness, sphericity, and regularity shape parameters are considered as particle shape descriptors and the corresponding classifications (Tables 5.1 through 5.3) used to classify the effect of particle shape features on mixture packing density and compactability.

## 6.3 Generation of 3D Particles

### 6.3.1 Computational Modeling

The algorithm utilized to generate 3D particles with controllable shape descriptors is based on discrete random fields theory and spherical harmonics as proposed by Mollon and Zhao (2014). The star-like class of shapes satisfactorily covers most mineral aggregate particles (crushed and rounded) used in asphalt mixture production. For this shape class, the external surface of a particle can be determined using the center of the particle,  $O$ , and distance,  $R(\theta, \varphi)$ , from this center (Figure 5.5).  $\theta$  and  $\varphi$  are the angular coordinates used to determine the position of a point on the surface of the particle. For the simplest case, a perfect sphere can be produced if all  $R$  values are equal to a constant number.

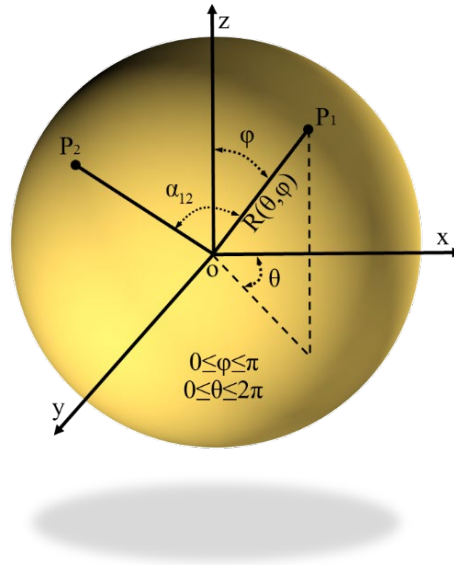


Figure 5.5 Spherical Coordinate System.

By changing the  $R$  values, it is possible to produce a particle with predefined shape parameters. Additionally, as observed by Mollon and Zhao (2014), 2,562 points on the surface of a particle are enough to define a particle shape. The random values of  $R$  for all 2,562 points on the surface of a particle can be determined using Equation 5.5:

$$[R] = [\mu] + \sum_{i=1}^{2562} \xi_i \cdot \sqrt{\lambda_i} \cdot [\psi_i] \quad (5.5)$$

where,  $\mu$  is the average of R values, and  $\lambda_i$  and  $\psi_j$  are the  $i^{\text{th}}$  eigenvalue and eigenvector of covariance matrix (C), respectively and  $\xi_i$  is a Gaussian random variable with zero-mean and unit variance. The covariance matrix (C) can be determined using a discrete normalized Fourier spectrum of 64 independent amplitude modes ( $D_k$  with  $0 \leq k \leq 127$ ) (Equation 5.6). The normalized Fourier spectrum ( $D_0=1$ ) is considered as symmetric, therefore, the normalized Fourier spectrum is a function of 63 independent modes ( $D_k=D_{128-k}$  for  $2 \leq k \leq 64$ ).

$$C(\alpha_n) = \sum_{k=1}^{127} D_k^2 \cdot e^{2i\pi n \frac{k}{128}} \quad 0 \leq n \leq 127 \quad (5.6)$$

where,  $\alpha_n$  is the angle between a pair of points at the  $n^{\text{th}}$  mode and can be determined using Equation 5.7:

$$\alpha_n = \frac{2\pi n}{128} \quad 0 \leq n \leq 127 \quad (5.7)$$

For sand materials, Das (2007) showed the relationship between the Fourier spectrum modes and the number of mode descriptors is log-log linear and therefore, the surface roughness of sand aggregates can be estimated by the slope and intercept of this linear relationship. For simplicity, Mollon and Zhao (2014) suggested that using only the values of  $D_2$ ,  $D_3$ , and  $D_8$  can result in particles with different shape parameters. All eight mode descriptors can be determined using Equation 5.8:

$$D_k = \begin{cases} 2^{\log_2(\frac{k}{3}) + \log_2(D_3)} & \text{for } 3 < k < 8 \\ 2^{\log_2(\frac{k}{8}) + \log_2(D_8)} & \text{for } k > 8 \end{cases} \quad (5.8)$$

where, a and b are the slopes of the log-log linear relationships between the Fourier spectrum modes and the number of mode descriptors between modes 3-8 and 8-63, respectively. Das (2007) proposed that a and b both equal to -2 result in the best estimation for sand aggregates.

Figure 5.6 shows that different combinations of the three main spectrum mode descriptors ( $D_2$ ,  $D_3$  and  $D_8$ ) can result in particles with different flatness, elongation, roundness, sphericity and regularity. These can be used to select particles with desirable shape parameters. Furthermore, the sensitivity analysis of mode descriptor  $D_2$  reveals that it has a significant influence on particle flatness and elongation if the  $D_3$  and  $D_8$  modes are zero (see Figure 5.7 a). Increases in the  $D_2$  parameter result in decreasing flatness and elongation form parameters and increases in dispersions

between them. Although an increase in  $D_2$  can decrease the sphericity and regularity of the generated particles, it has a negligible effect on particle roundness.

An increase in  $D_3$  creates a decreasing trend in all five shape descriptors, especially roundness, sphericity, and regularity if the  $D_2$  and  $D_8$  modes are set to be zero. Changes in  $D_8$  have a notable effect on surface roughness (regularity), but a negligible and limited effect on the flatness and elongation form parameters and sphericity, respectively. An increase in  $D_8$  also leads to a significant decrease in particle roundness.

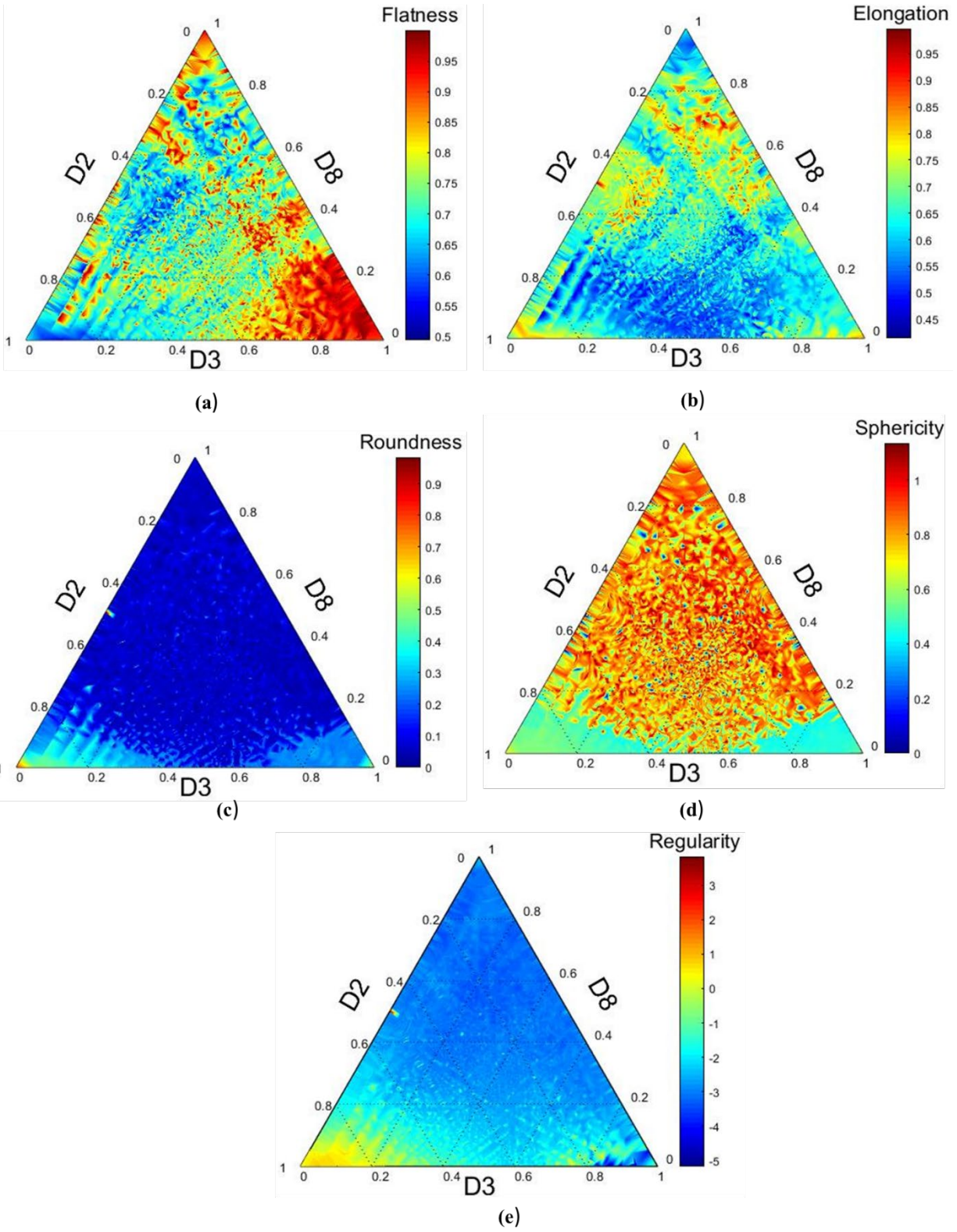


Figure 5.6 Effect of Change in  $D_2$ ,  $D_3$ , and  $D_8$  on: (a) Flatness, (b) Elongation, (c) Roundness, (d) Sphericity, and (e) Regularity of a Particle.

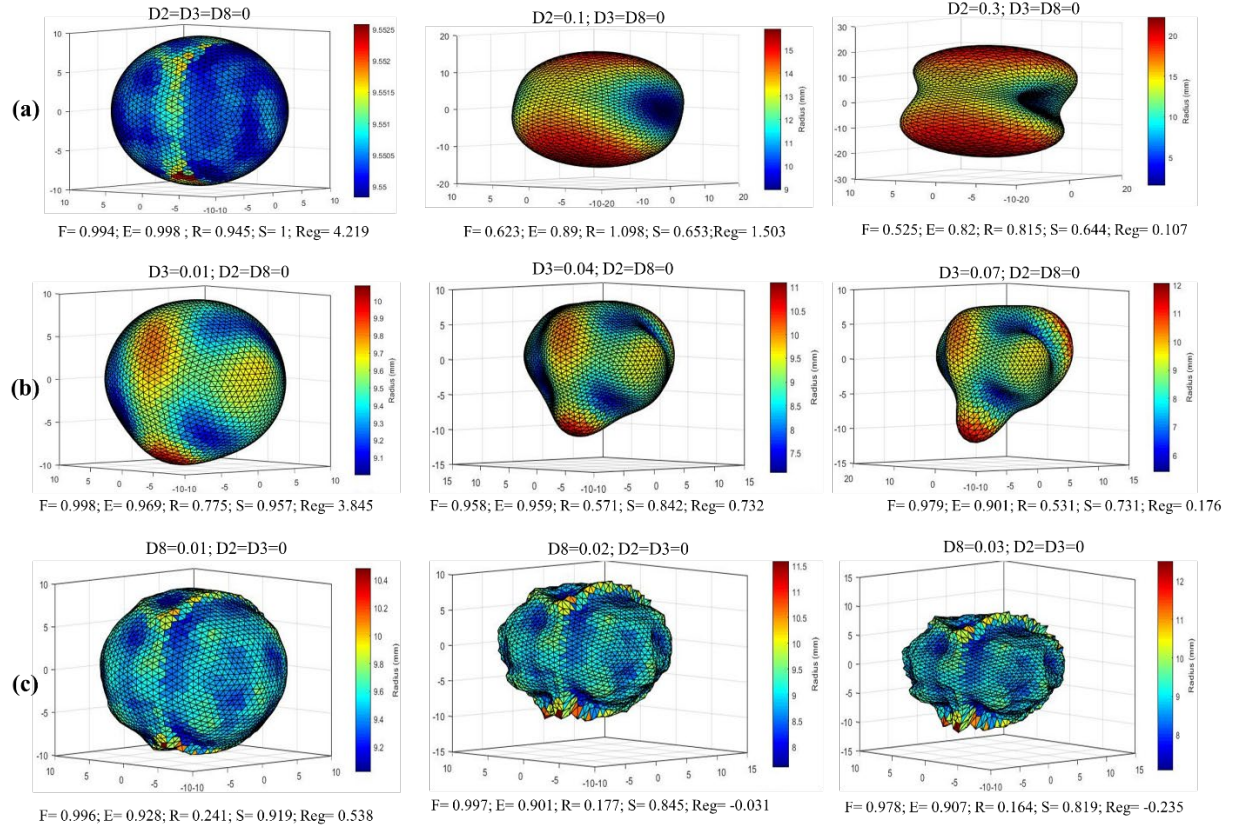


Figure 5.7 Illustrative Example of Change in Three Selected Spectrum Mode Descriptors ( $D_2$ ,  $D_3$  and  $D_8$ ) on Shape Parameters (Flatness (F); Elongation (E); Roundness (R); Sphericity (S); and Regularity (R)).

### 6.3.2 Sample Preparation

After computer generation of particles, it is necessary to pack them in a given container for discrete modeling. In this study, the container was partitioned using a Constrained Voronoi Tessellation (CVT) method. Generally, VT is a powerful geometric approach to partition a space with a dimension  $n$  into cells or convex polyhedrons (Aurenhammer, 1991). The CVT is a special version of the VT method with the capability to control all cells properties, such as cell size or volume distribution. As asphalt mixtures are multi-sized particle mixtures, the CVT approach is an effective approach for packing particles with a predetermined size or volume distribution.

As a first step, the bonded VT for a random set of points in a given domain is calculated. Then, based on a criterion parameter, for example, the volume distribution of cells, the corresponding statistical property of the parameter is calculated and compared to the target parameter to determine the error level. Depending on the error level, one of the seeding points



randomly moves to another random position and a new bonded VT of the new cells and their statistical properties are computed, and the level of error is determined. If the current error is less than the one previously found, the modification is accepted and compared to the target error. This approach continues until the desirable error level is reached.

After determination of polyhedral convex cells with the desired size distribution, the 3D particle can be generated in each cell to fill it using the approach explained in Section 5.3.1. During the cell filling stage, it is necessary to make sure the same volume fraction between the generated and convex cells is obtained and no part of the generated particle is outside the cell after the filling. Figure 5.8 shows an example of the developed polyhedral convex cell and the 2000 generated particles with flatness, elongation, roundness, sphericity, and regularity of 0.86, 0.81, 0.36, 0.78, and 1.30, respectively, in the unit cubic container. The normal volume distribution with covariance of 0.8 and error level of 10% was assumed as the volume distribution of the generated particles.

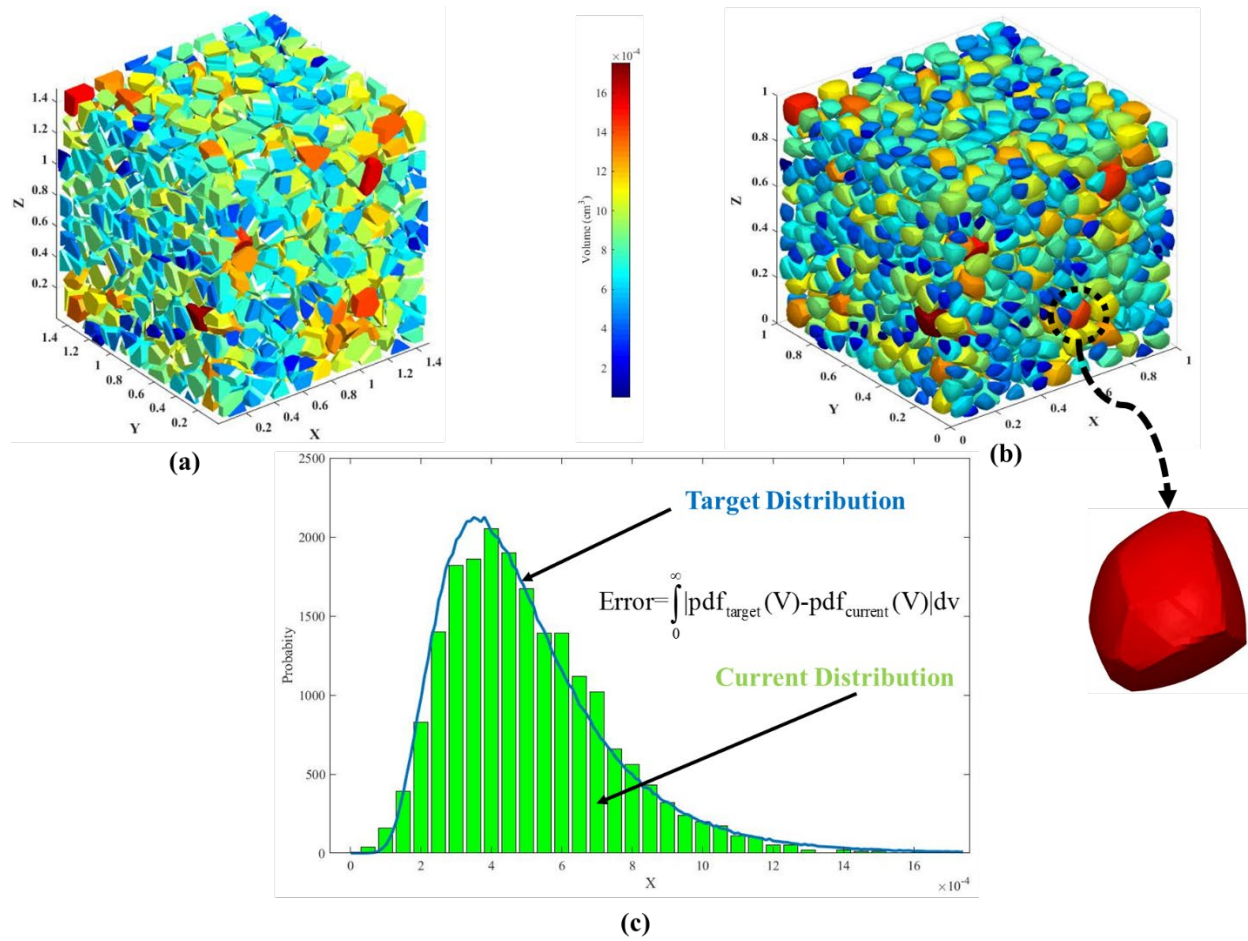


Figure 5.8 (a) Convex Polyhedral Cells; (b) Corresponding 2000 Generated 3D Particles; (c) Normal Distribution (Covariance = 0.80) at 10% Error.



## 6.4 Discrete Element Method Simulation

Based on the approaches previously explained, 100 mixtures with 2000 particles each were selected for the study. Figure 5.9 shows the selected gradation (size distribution) for all virtual mixtures. To increase the efficiency of simulations, the particles above the primary control sieve (PCS) were selected and the effect of the rest of sizes was considered in the constitutive mechanical interaction between the coarse particles, those larger than the PCS. Based on the Bailey method, the PCS is used as a break between the coarse and fine part of an aggregate gradation and is a function of the nominal maximum aggregate size (NMAS) of the mixture ( $PCS = 0.22 \times NMAS$ ) (Vavrik et al., 2002). Previous studies have revealed the overall shape of a gradation can be characterized using a power function, Equation 5.9 (Goltermann et al., 1997; Pouranian and Haddock, 2018, 2019):

$$P(d) = 100 \times e^{-\left(\frac{d}{d_r}\right)^n} \quad (5.9)$$

where,  $d$  is the aggregate size of each sieve used in the gradation (mm),  $P(d)$  is the cumulative percentage retained on each sieve size, and  $d_r$  is the size considered to be representative of the gradation (mm). The gradation selected for this study is a 12.5 mm NMAS and therefore the PCS is 2.36 mm. The larger particles were simulated according to the RRD distribution with  $d_r$  and  $n$  equal to 8.58 and 0.746, respectively.

As previously discussed, DEM is based on spherical particles. To insert irregular-shaped particles into DEM the overlapping discrete element cluster (ODEC) algorithm proposed by Ashmawy et al. (2003) and Das (2007) is used. In this algorithm, a number of overlapping spherical discrete elements is used to create illustrative assemblies of irregular-shaped particles for DEM simulations. Figure 5.10 shows an irregular particle assembled using this technique.

An open source 3D DEM code was used to perform discrete element analysis. The code is a numerical package developed in the c++ Object and Python programming languages (Kozicki and Donzé, 2009). Based on the different values of particle shape descriptors, 100 simulations were performed to cover all the shape parameter combinations. The numerical simulations were conducted using the soft-particle approach, where all particles are allowed to deform and overlap numerically.

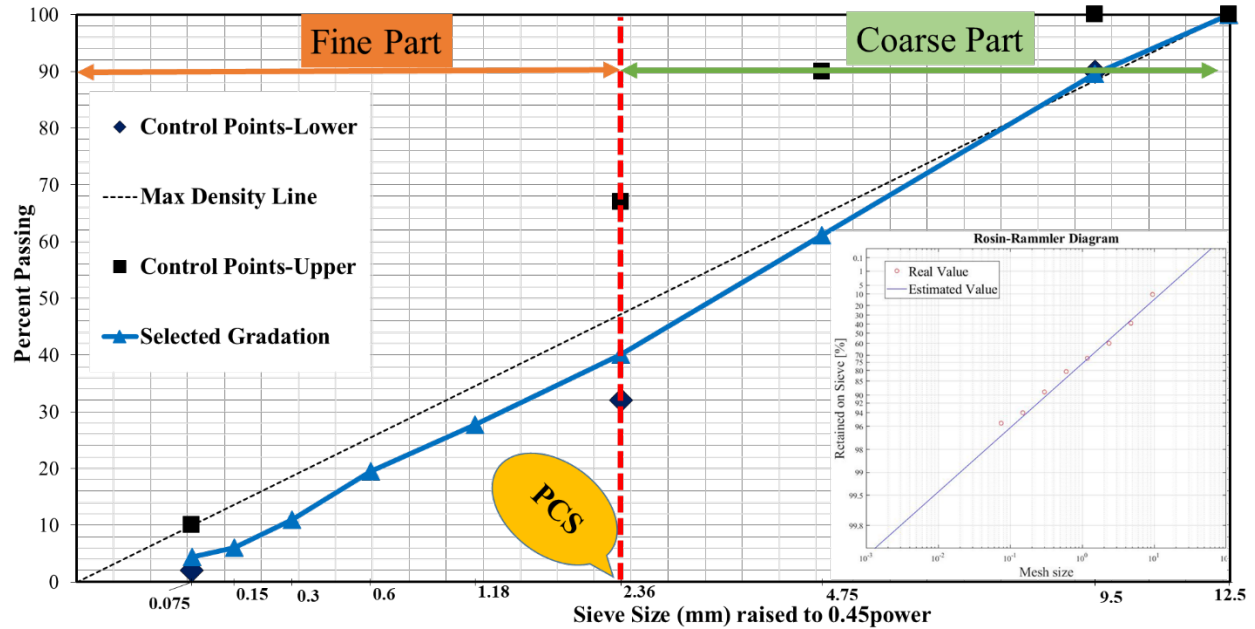


Figure 5.9 Selected Gradation (Size Distribution) Simulated.

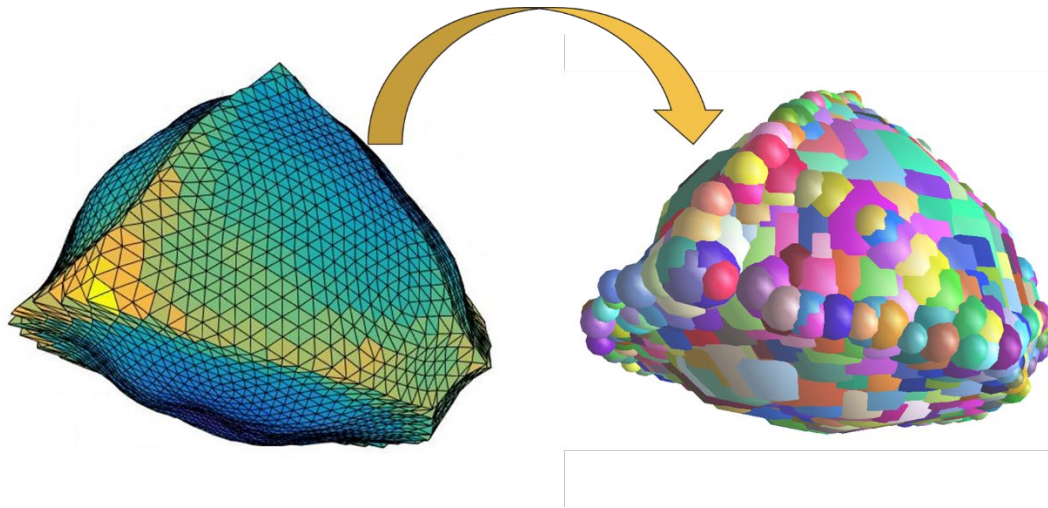


Figure 5.10 Applying the Overlapping Discrete Element Cluster Algorithm to Import a 3D Irregular Particle into the Discrete Element Model Package.

The dynamic behavior of particles was considered using a force-displacement Lagrangian approach to determine the position, velocity, and the acceleration of each particle. The normal and shear forces between particles were computed using Burger's viscoelastic model. The Burgers' model is a popular viscoelastic model that has been used to study the rheological behavior of asphalt mixtures (Abbas et al., 2005; Chen et al., 2014). The model is comprised of Maxwell and Kelvin materials in series, making it possible to consider creep and relaxation behaviors, as well

as the dynamic properties of the asphalt mixture. Figure 5.11(a) illustrates the Burger's constitutive model and corresponding parameters ( $E_m$ ,  $\eta_m$ ,  $E_k$ , and  $\eta_k$ ). Previous studies have shown the Burger's model parameters can be determined using the dynamic modulus test results, i.e.  $|E^*|$  master curve (Chen et al., 2014; Ma et al., 2018; Pouranian et al., 2019). In this study, the asphalt mastic, a mixture of the fine portion of the selected gradation and asphalt binder, was used to define the viscoelastic mechanical contact model between coarse aggregates.

For asphalt mixtures, the typical compaction temperature is 120-135°C. Therefore, the  $|E^*|$  master curve should be shifted to the compaction temperature using the time-temperature superposition principle. In this study, four mastic mixtures of the aggregate (crushed sand) with 6% asphalt binder (PG 70-22) by total mixture mass were fabricated and their dynamic moduli values determined at three temperatures (Figure 5.12). These were then used to establish a master curve for the mastic. The Burger's parameters at 130°C can be determined from the master curve using curve fitting techniques from Equation 5.10.

$$|E^*| = \frac{1}{\sqrt{\left(\frac{1}{E_m} + \frac{E_k}{E_k^2 + \omega^2 \eta_k^2}\right)^2 + \left(\frac{1}{\omega \eta_m} + \frac{\omega \eta_k}{E_k^2 + \omega^2 \eta_k^2}\right)^2}} \quad (5.10)$$

where,  $E^*$  is the complex modulus and  $\omega$  is the radial frequency. Based on the Burger's parameters, the mechanical contact model for the normal ( $E_{mn}$ ,  $\eta_{mn}$ ,  $E_{kn}$ , and  $\eta_{kn}$ ) and shear ( $E_{ms}$ ,  $\eta_{ms}$ ,  $E_{ks}$  and  $\eta_{ks}$ ) directions can be determined using Equations 5.11 and 5.12, respectively.

$$E_{mn} = \frac{4E_m E_{Agg}}{E_m + E_{Agg}} R_{ave} ; \eta_{mn} = 4\eta_m R_{ave} ; E_{kn} = 4E_k R_{ave} ; \eta_{kn} = 4\eta_k R_{ave} \quad (5.11)$$

$$E_{ms} = \frac{4E_m E_{Agg}}{E_m(1+\nu) + E_{Agg}(1+\nu_m)} R_{ave} ; \eta_{ms} = \frac{2\eta_m R_{ave}}{(1+\nu_m)} ; E_{ks} = \frac{2E_k R_{ave}}{(1+\nu_m)} ; \eta_{ks} = \frac{2\eta_k R_{ave}}{(1+\nu_m)} \quad (5.12)$$

where,  $R_{ave}$  is the average of two particle radii in contact,  $E_{Agg}$  is the elastic modulus of coarse aggregates, and  $\nu$  and  $\nu_m$  are the poisson ratio of coarse aggregate and asphalt mastic mixture, respectively. The parameters of the contact model are shown in Table 5.4.

Table 5.4 Contact Model's Parameters.

Parameters	$E_{Agg}$ (GPa)	$\nu$	$\nu_m$	$E_m$ (MPa)	$\eta_m$ (MPa.s)	$E_k$ (MPa)	$\eta_k$ (MPa.s)
Value	55	0.3	0.50	22.973	1389.33	21.84	9.69

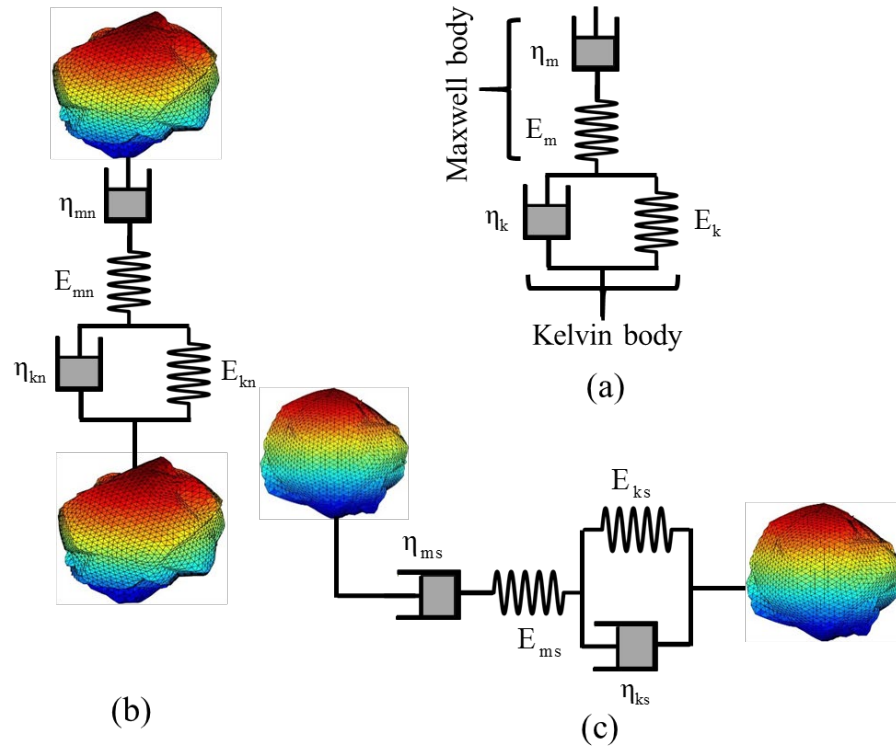


Figure 5.11 (a) Burger's Contact Model; (b) Normal and (c) Shear Aggregate Contact Models.

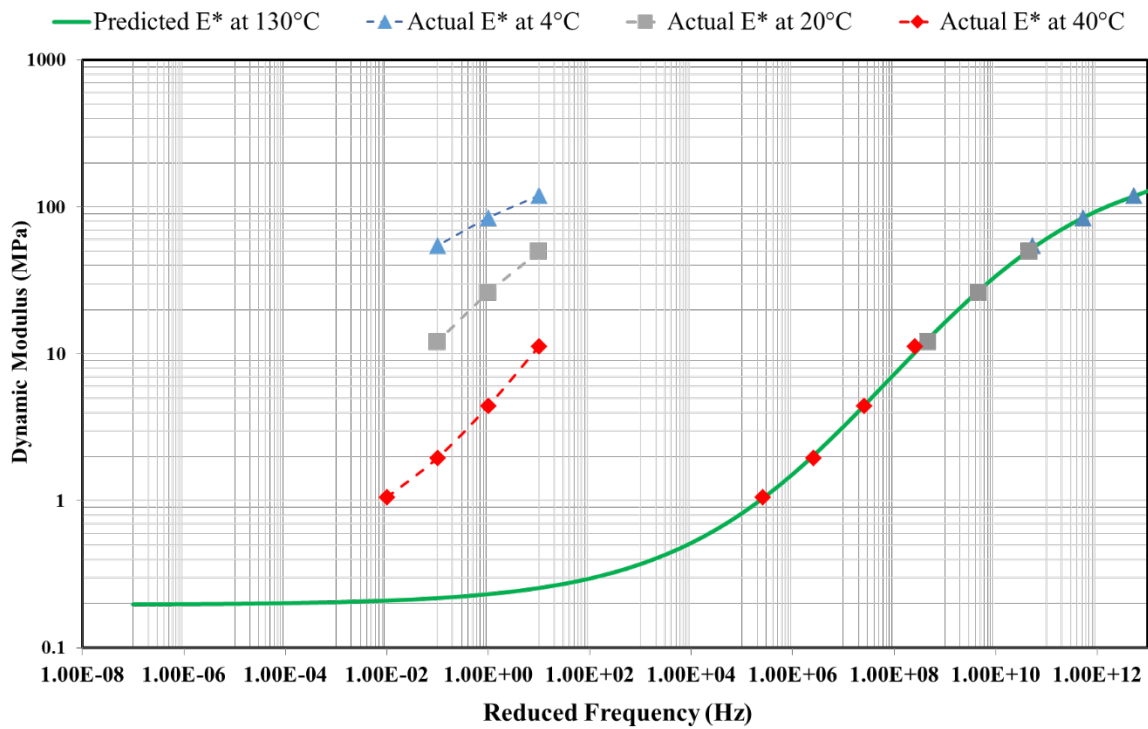


Figure 5.12 Asphalt Mastic Mixture  $|E^*|$  Master Curve.

To simulate the SGC compaction mechanism for each mixture, first an initial package (cloud) of particles, based on the approach explained in section 5.3.2, is prepared in a container (Figure 5.13a). Cloud packing refers to a condition in which there is no contact between particles. Gravity force is then applied, and the particles are allowed to settle in a cylindrical mold beneath the container (Figures 5.13b and c). Once the particles are in the compaction mold a 600 kPa vertical pressure is applied using a virtual loading plate. The mold is then tilted to a 1.16-degree angle and rotated the desired number of gyrations (Figures 5.13d and e). Seventy-five gyrations was selected for this work because it takes less computational time than would 100 or 125 gyrations. Seventy-five is the recommended design gyration number ( $N_{des}$ ) for asphalt mixtures placed for traffic of 0.3 to 3 million equivalent single axle load (ESAL) (AASHTO, 2015).

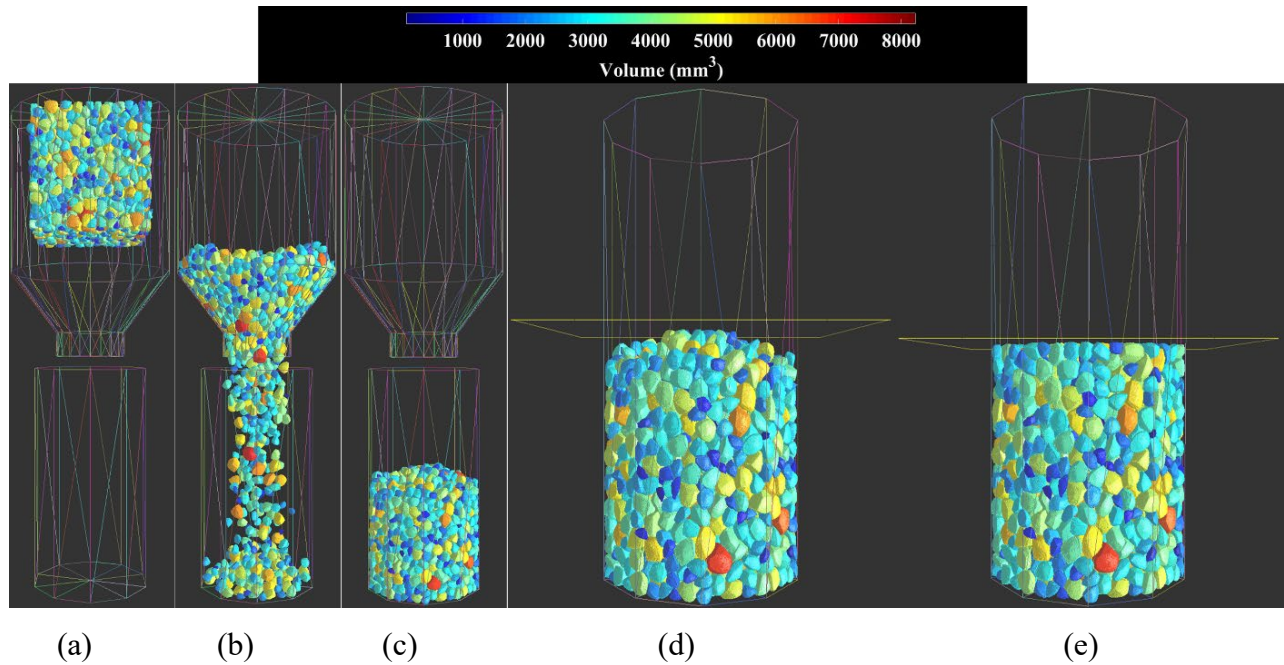


Figure 5.13 Compaction Simulation Process: (a) Cloud Condition; (b) Applying Gravity Force; (c) Settlement in the Mold; (d) Applying Vertical Load; and (e) Final Compaction Condition.

Two important SGC compaction parameters (initial density and compaction slope) can be obtained from the virtual compaction curve. As in actual practice, the virtual compaction curve shows the change in density as a function of the number of gyrations applied. Based on the Superpave mixture design method, for a  $N_{des}$  of 75, the initial gyration number ( $N_{ini}$ ) is 6. Therefore, 6 gyrations were selected as the point to measure initial density. The compaction slope

is defined as the slope of density change divided by the log of gyrations from  $N_{ini}$  to  $N_{des}$ . An example of compaction curve for two mixtures is shown in Figure 5.14.

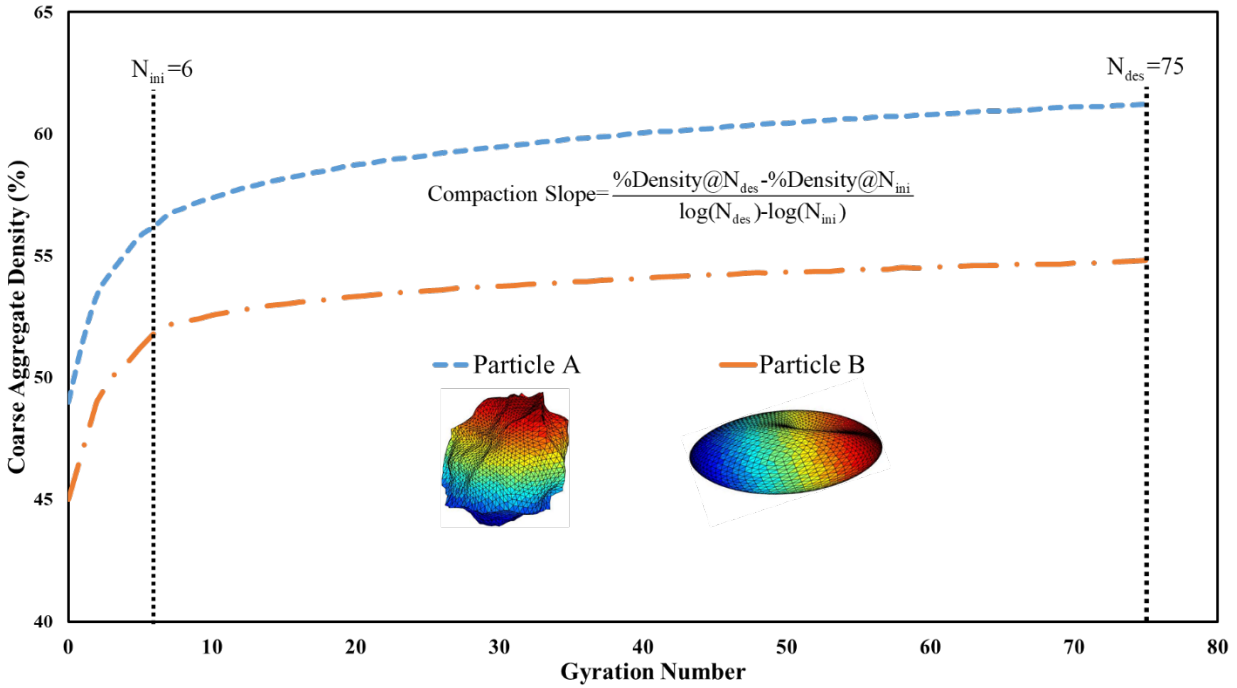


Figure 5.14 Example Compaction Curve.

## 6.5 Results and Discussion

### 5.1 Compaction Parameters

In order to determine the relationship between the shape descriptors as explanatory variables and the compaction parameters, a statistical regression analysis was conducted. In statistical analyses, before establishing a statistical relationship, it is necessary to determine if the regression assumptions are violated. This is done by first evaluating the normality assumption and correlation between the explanatory variables. When done for the compaction data in this experiment, a high correlation between flatness and elongation and sphericity is revealed (see Figure 5.15). This means the variables of flatness and elongation and sphericity cannot simultaneously be used in a regression analysis,

In the Box-Cox transformation, there is an exponent parameter ( $\lambda$ ) that can vary from -5 to 5; all  $\lambda$  values should be tested to find the optimum value, the  $\lambda$  value which results in the best

approximation of a normal distribution. The Box-Cox transformation of Y, the response variable, can be expressed by Equation (5.13) (Neter et al., 1996):

$$Y(\lambda) = \begin{cases} \frac{Y^\lambda - 1}{\lambda}, & \text{if } \lambda > 0; \\ \log Y, & \text{if } \lambda = 0; \end{cases} \quad (5.13)$$

The Box-Cox results indicated that  $\lambda=3$  and  $\lambda=2.75$  are the best values for the two regression analyses, initial density as a function of (1) flatness and elongation, and (2) roundness, sphericity and regularity, respectively. Using initial density raised to the 3<sup>rd</sup> power and initial density raised to the 2.75 power as response variables allows the use of linear regression analysis for both models. Results of ANOVA analyses are shown in Table 5.5. The results for both models indicate the Student's t-tests for each model's explanatory parameters and overall model are significant at a significance level of  $\alpha = 5\%$  ( $P\text{-values} \leq 0.05$ ). Figure 5.16 graphically shows how well the proposed regression models predict the initial density change due to changes in particle shape parameters.

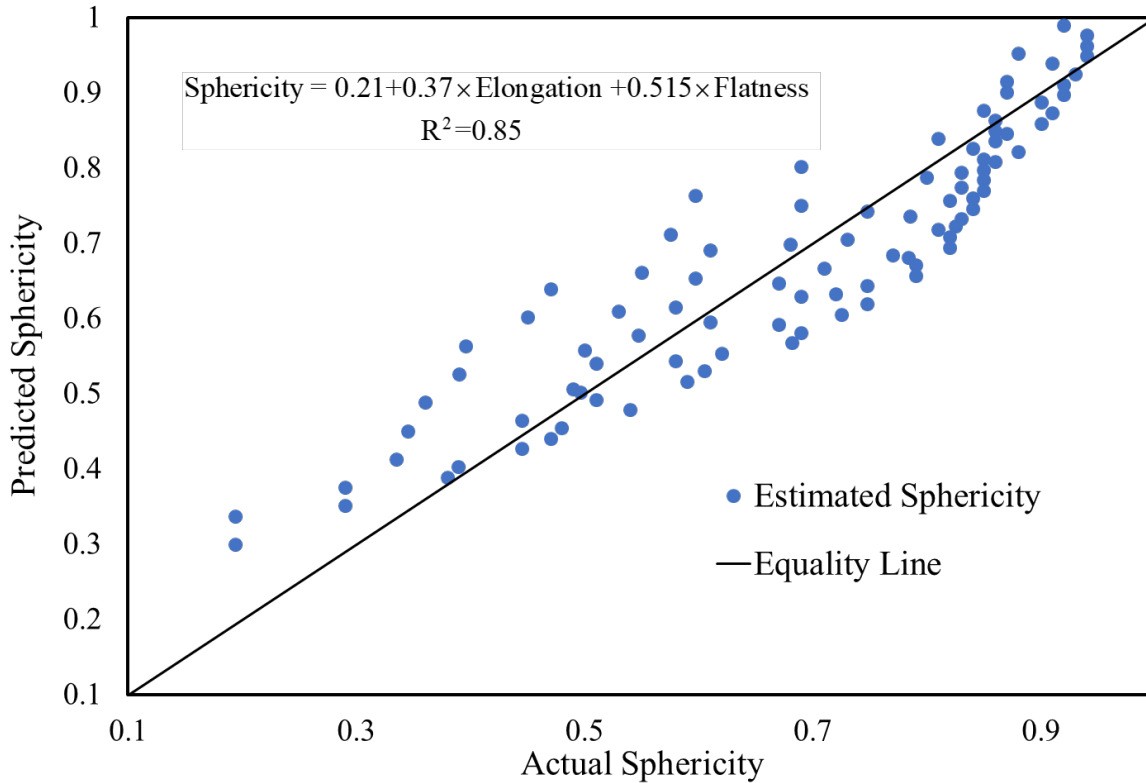


Figure 5.15 Correlation between Flatness and Elongation and Sphericity.

Table 5.5 Regression Equations and Corresponding Statistical Parameters for Initial Density.

Initial Density (%)= $\sqrt[3]{(54436+60765 \times \text{Flatness}+78588 \times (\text{Elongation}))}$					
Root MSE	3,955.78	R2	0.89	Adjusted R <sup>2</sup>	0.87
Variable	DF	Parameter Estimate	t Value	Pr >  t	
Intercept	1	18,145	16.51	<0.0001	
Flatness	1	20,255	16.13	<0.0001	
Elongation	1	26,196	19.72	<0.0001	
Initial Density (%)= $\sqrt[2.75]{19044+54725 \times (\text{Roundness})+13599 \times (\text{Sphericity})-2643 \times (\text{Regularity})}$					
Root MSE	0.942	R2	0.94	Adjusted R <sup>2</sup>	0.934
Variable	DF	Parameter Estimate	t Value	Pr >  t	
Intercept	1	6,925.7	21.18	<.0001	
Roundness	1	19,900	39.90	<.0001	
Sphericity	1	4,945.26	15.85	<.0001	
Regularity	1	-961.72	-7.43	<.0001	

Figures 5.17 and 5.18 are contour maps that illustrate the changes in initial density due to changes in flatness and elongation, and roundness and sphericity. The classification names on these figures are based on those proposed by Blott and Pye (2008) for flatness and elongation, Powers (1953) for roundness, and Riley (1941) for sphericity. In the case of flatness and elongation, flatness and elongation values greater than 0.6 (E1F1, E1F2, E2F2 and E2F1) result in high initial density, while flatness and elongation values less than 0.4 show the lowest value of initial density (see Figure 5.17). Additionally, increasing a mixture's average flatness and elongation from 0.2 (class E5F5) to 0.9 (class E1F1) results in a 27% initial mixture density increase. This implies that compared to cubic or spherical shaped particles, the particles with relatively equal dimensions in all directions, flat or elongated particles tend to reduce the packing density of a mixture. This is likely due to flat and elongated particles resisting reorientation into a denser packing condition because they lock with adjacent aggregate particles. This mechanism also creates bridged particles and results in inter-particle voids.



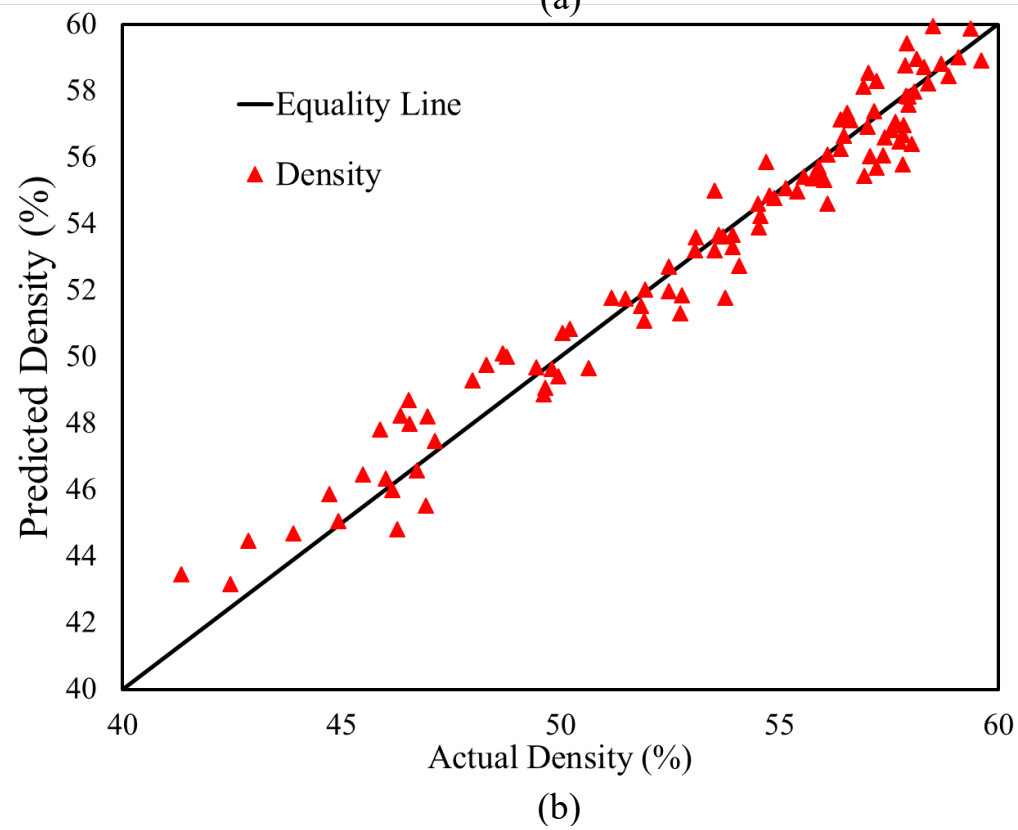
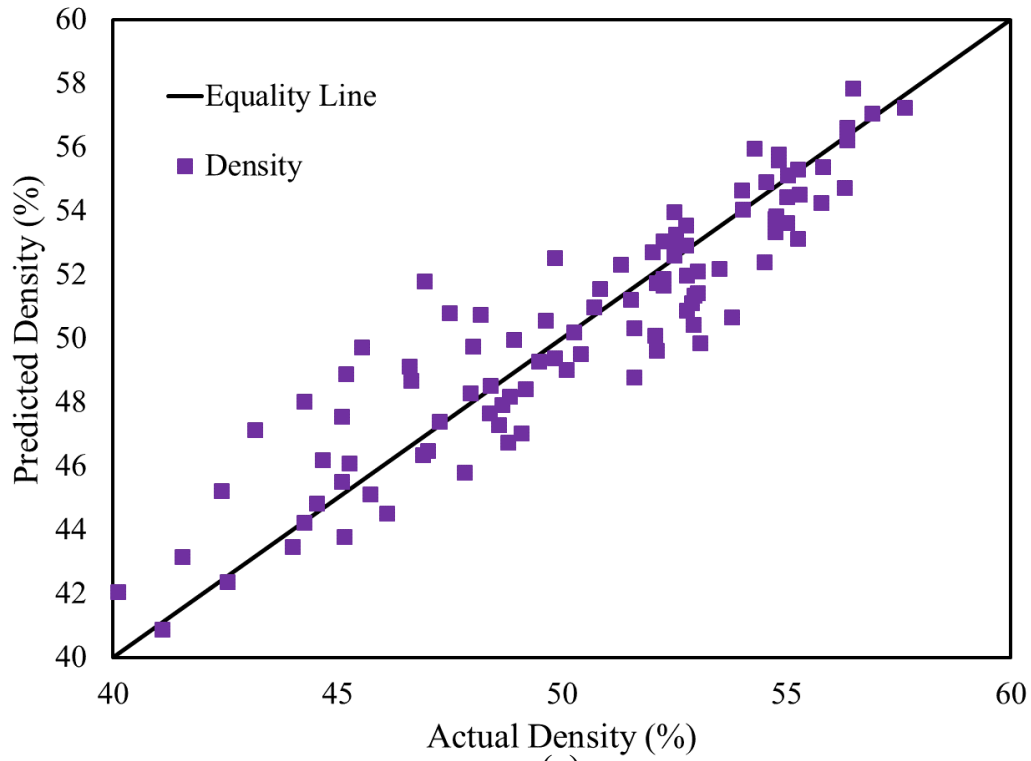


Figure 5.16 Predicted vs. Actual Initial Density Values: (a) Flatness, Elongation as Explanatory Variables, and (b) Roundness, Sphericity, and Regularity as Explanatory Variables.

For mixture with sphericity values less than 0.4 (class S5), changes in roundness have an insignificant effect on the initial mixture density (see Figure 5.18). However, high sphericity, values greater than 0.70 (class S1, S2, and S3), show high initial densities. Therefore, changes in sphericity have a significant effect on mixture packing density. In general, high sphericity and roundness (less angularity) particles tend to compact easily, as is experienced in asphalt mixture field compaction. Changes in roundness and sphericity from 0.1 (class R6S5) to 0.9 (class R1S1) can result in an approximate 30% improvement in initial mixture density. A previous study revealed that most crushed and natural sands have a roundness and sphericity of about  $R=0.2$  to  $0.3$  and  $S=0.7-0.8$  and  $R=0.3-0.9$  and  $S=0.5-0.9$ , respectively (Cho, 2004). For these ranges, Figure 5.18 suggests the maximum percent change in initial mixture density would be 5 and 18% for crushed and natural sands, respectively.

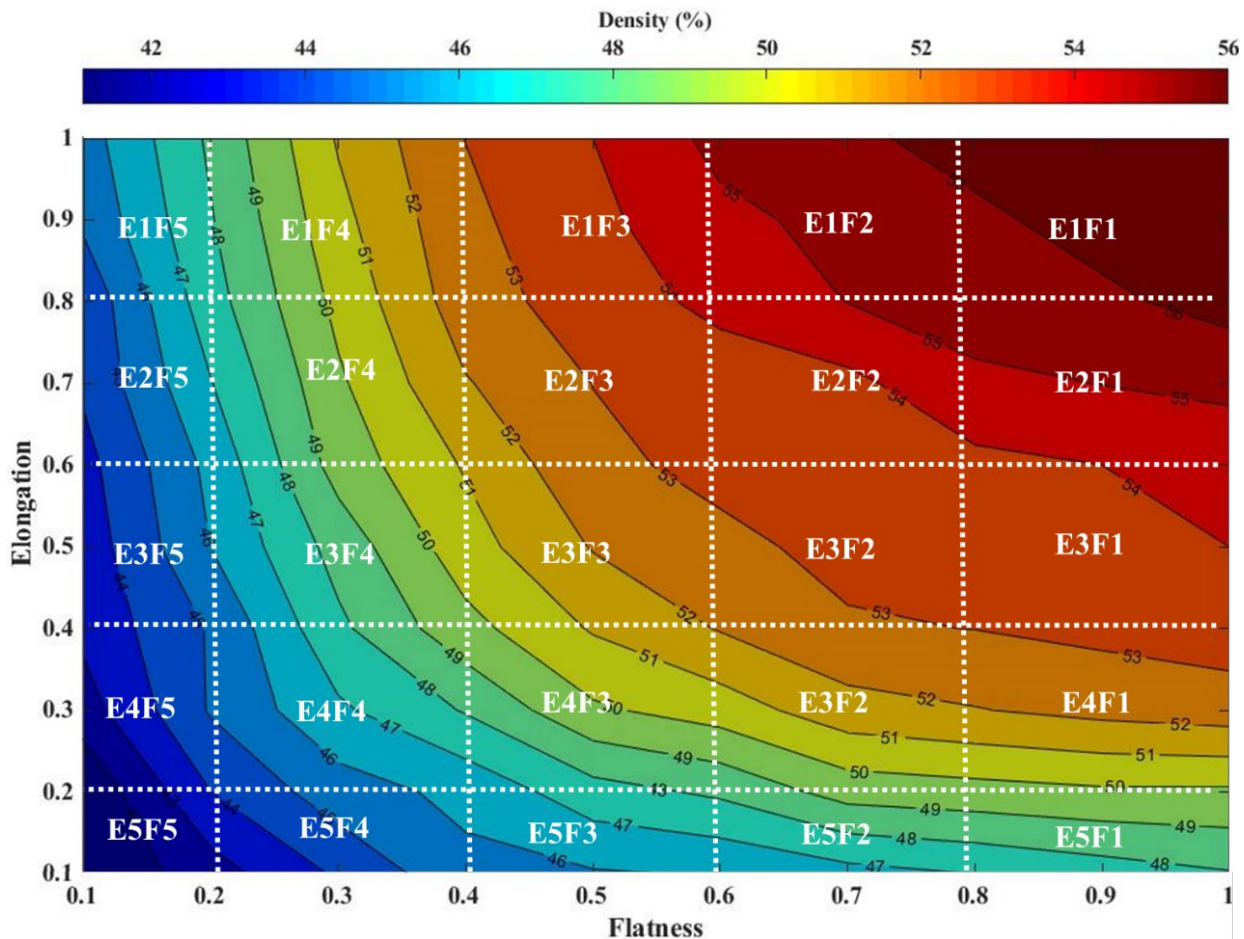


Figure 5.17 Changes in Initial Density due to Changes in Flatness and Elongation.

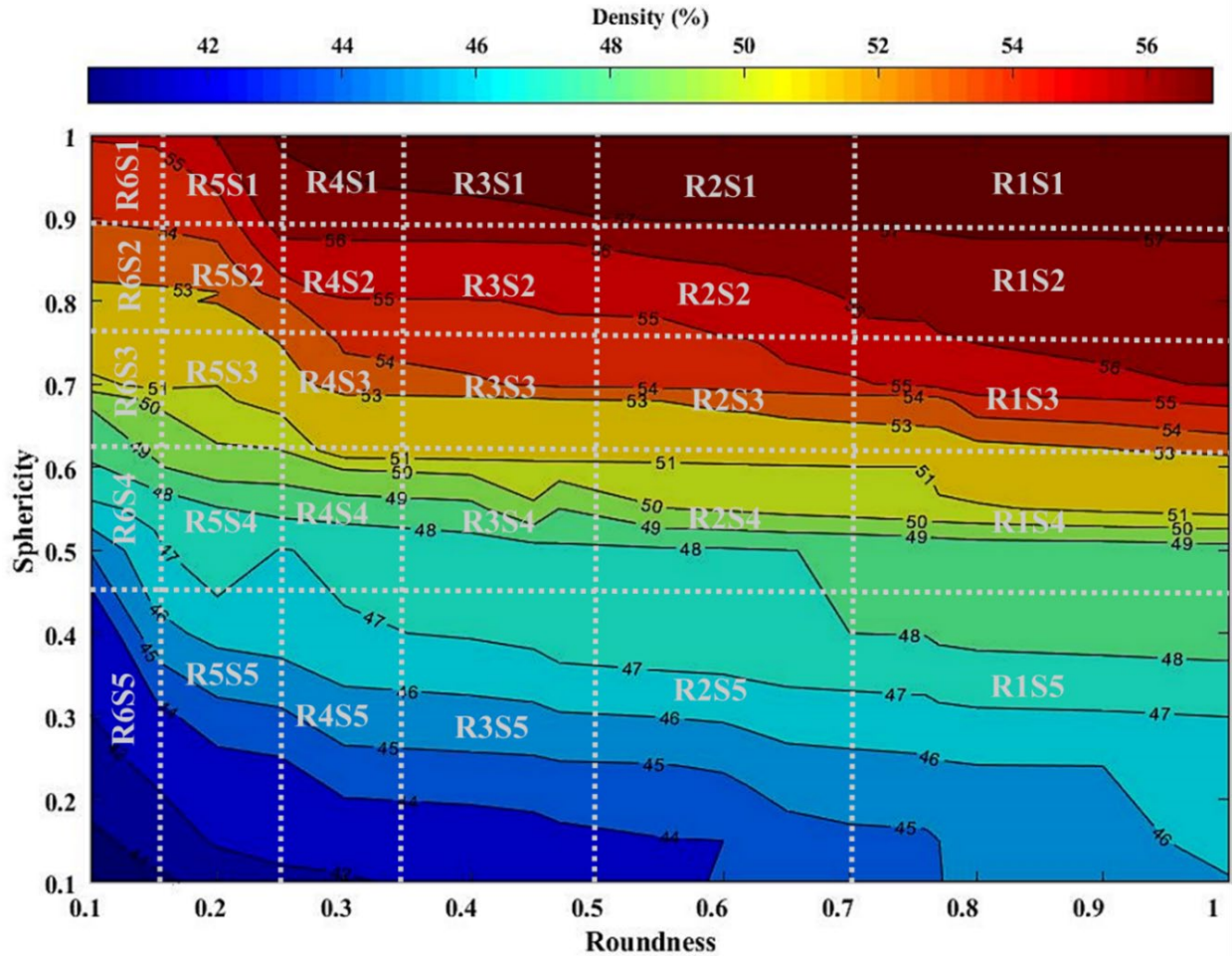


Figure 5.18 Changes in Initial Density due to Changes in Roundness and Sphericity.

When compaction slope is the dependent variable, analysis reveals that roundness and regularity are the only particle shape descriptors that are statistically significant, as shown in Table 7. The results indicate that particles with high roundness and regularity indices tend to have a lower compaction slope. In combination with the roundness effect on initial density, it can be concluded that although increasing roundness results in higher initial density, the rate of change in density becomes smaller with increasingly larger roundness values. As mentioned previously, a higher compaction slope means higher shear modulus or lower shear strains in asphalt mixtures. Therefore, lower roundness values (higher angularity) can result in improved asphalt mixture permanent characteristics while increasing the necessary compaction effort to reach a desirable density due to lower initial mixture density.

Table 5.6 Regression Equation and Corresponding ANOVA for Compaction Slope.

Compaction Slope= 2.699-1.575×Roundness-0.059×Regularity					
Root MSE	3955.78	R2	0.74	Adjusted R <sup>2</sup>	0.724
Variable	DF	Parameter Estimate	t Value	Pr >  t	
Intercept	1	2.699	31.56	<0.0001	
Roundness	1	-1.575	-7.85	<0.0001	
Regularity	1	-0.059	4.78	<0.02	

In most of asphalt mixture design methods, the maximum percentage of flat and elongated particles in an asphalt mixture is typically a design parameter and specified. In the asphalt industry, one of the most popular definitions for defining flat and elongated aggregate particles for use in asphalt mixtures is the flat and elongated (F&E) parameter. F&E is defined as the ratio of the smallest to largest dimensions of a particle. The minimum value of F&E varies from specification to specification, but it is typically 3:1, 4:1 or 5:1. For example, the Superpave mixture design method suggests the dimensional ratio 5:1 as the criterion to define the flat and elongated coarse particles and that coarse aggregates should not contain more than 10% F&E by total mixture aggregate mass. Additionally, using more than 10% 5:1 F&E particles can result in a significant asphalt mixture performance decrease due to aggregate breakage (Aho, 2001).

To further investigate the effect of F&E particles in an asphalt mixture, a set of simulations with four F&E ratios (2:1, 3:1, 4:1 and 5:1) and ten different F&E percentages (0, 5, 10, 15, 20, 30, 40, 50, 80 and 100) compared to particles with flatness and elongation equal to 0.88. The results in Figure 5.19 show that increasing the percentage of F&E particles in a mixture (more than 15%) results in larger changes to the initial mixture density as the dimensional ratio increases. Although the DEM method cannot account for particle fracture, the results suggest that increasing the percentage of F&E particles above approximately 15% may result in a significant decrease in initial density due to less optimum particle orientation. This finding consistent with practice.

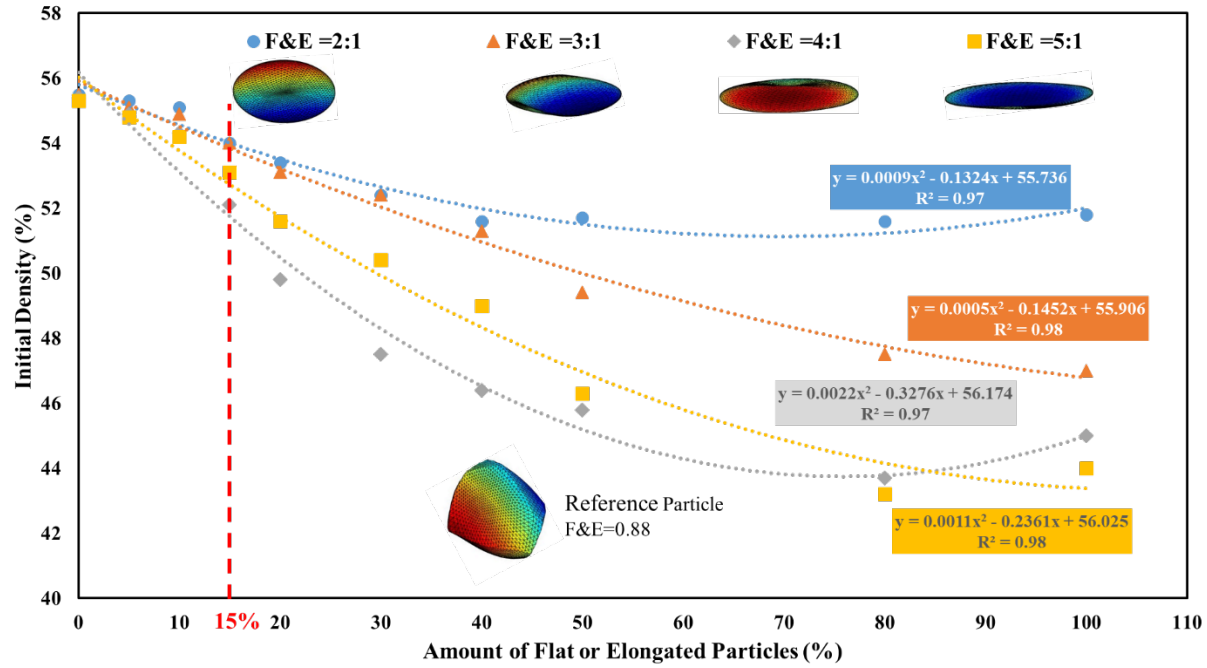


Figure 5.19 Effect of Flat and Elongated Particle Percentage on Initial Mixture Density.

## 5.2 Microscopic Packing Properties

The average coordination number (CN) of a particle packing system is a micro-structural parameter widely used to describe the bulk strength and structure of granular materials (Delaney and Cleary, 2010; Wu et al., 2017). CN is defined as the number of particles in contact with a considered particle. Figure 5.20 demonstrates the changes in the average of CN due to changes in flatness and elongation. The figure shows that flatness and elongation values greater than approximately 0.75 (E1F1, E1F2 and E2F1) produce lower CN values ( $3.6 \pm 0.37$ ), while flatness and elongation values less than 0.75 result in an approximately constant CN value ( $4.04 \pm 0.05$ ). Comparison between Figures 5.17 and 5.20 indicates that a high packing density does not necessarily mean high CN in a packing system. Previous attempts to define a relationship between CN and the packing density of mixtures containing ellipsoidal (Delaney and Cleary, 2010; Zhou et al., 2011) and cubical particles (Wu et al., 2017) with different aspect ratios (a ratio between the largest and smallest particle dimensions) have indicated the same conclusion, a high packing density does not necessarily have a high CN.



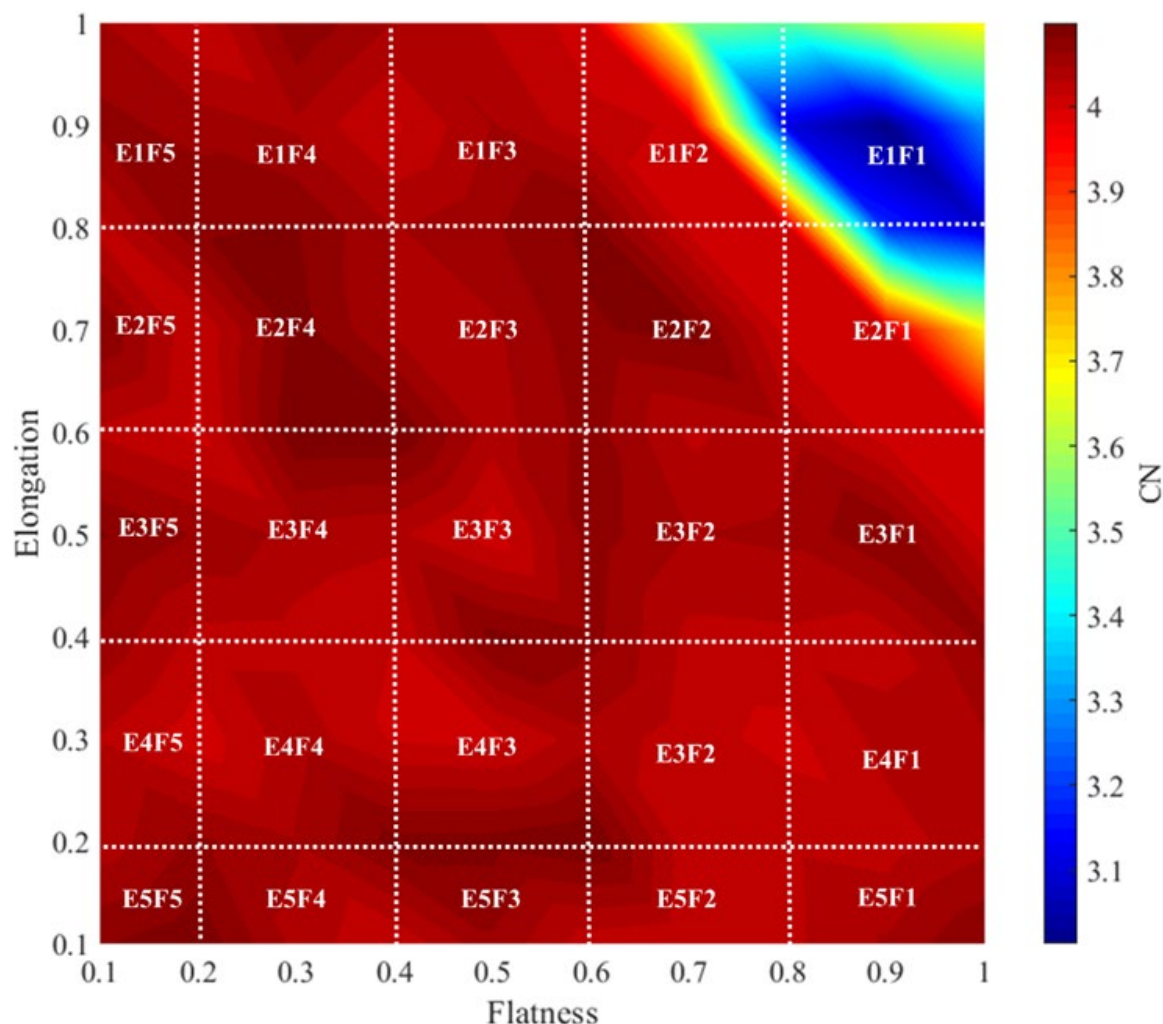


Figure 5.20 Changes in Average Coordination Number due to Changes in Flatness and Elongation.

The analyses to determine the relationship between sphericity and the average CN of packing mixtures show the same conclusion (Figure 5.21). Sphericities greater than 0.7 results in a significant reduction in CN values, while for sphericities less than 0.7, an approximately constant CN is observed. As mentioned earlier, there is a high correlation between flatness and elongation and sphericity, and so the trend of CN with sphericity is expected. Figure 5.22 shows the frequency distribution of average CN values for three mixtures with different flatness (F), elongation (E) and sphericity (S). It can be seen that distribution for all three can be described by Gaussian distributions; as flatness, elongation, or sphericity decrease, the distribution moves to the right, corresponding to the increase of average CN. However, the peaks of distribution curves do not show any specific trend.

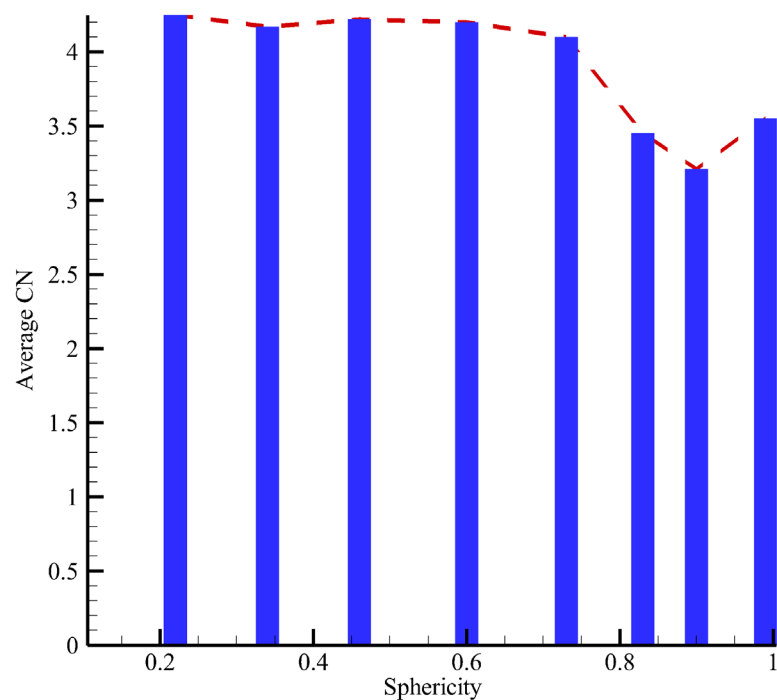


Figure 5.21 Changes in Average Coordination Number due to Changes in sphericity.

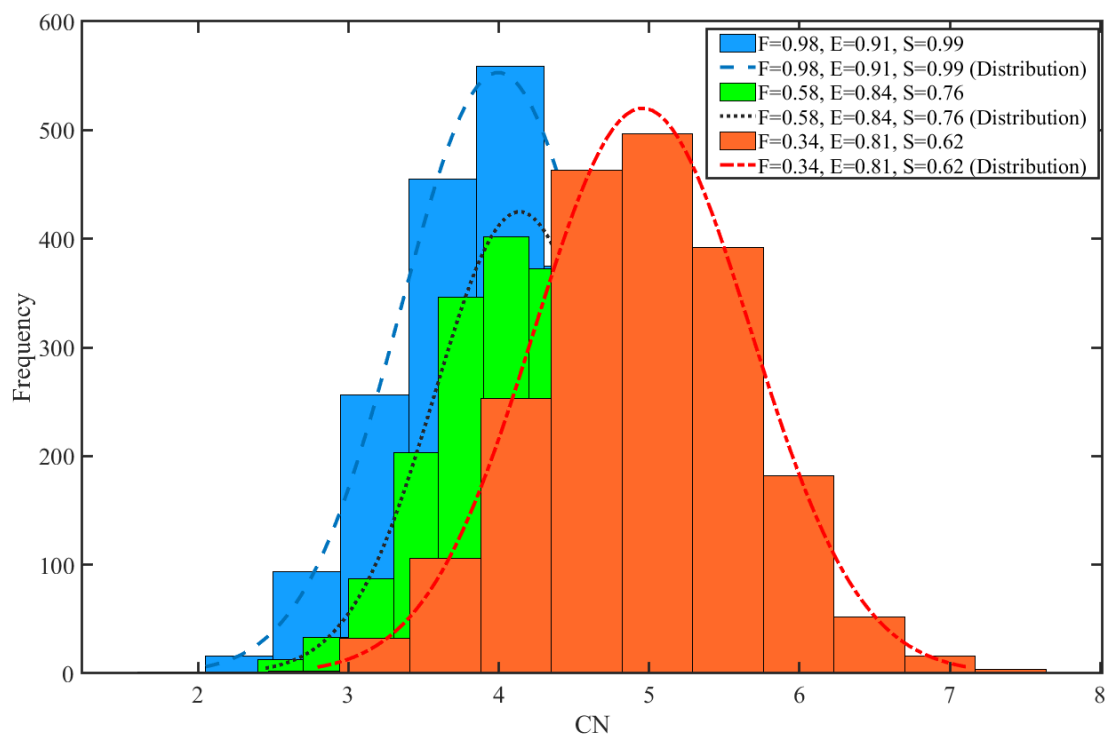


Figure 5.22 Coordination Number Distributions for Three Mixtures with Different Shape Parameters.

It has been reported that distribution of internal contact forces is an influential factor affecting stress localization and fracture behavior of bonded granular mixtures, such as asphalt mixtures (Guises et al., 2009; Dondi et al., 2012a and b). In this study, the total force (summation of normal and shear forces) of particles was used to determine the distribution of contact forces. Since normalization allows a comparison between different simulation results having different numbers of total contact forces, the total force of each particle was normalized using the following equations:

$$F_{\text{norm-i}} = \frac{F_{ti}}{\bar{F}_t} \quad (5.14a)$$

$$F_{ti} = \left| \vec{F}_{ni} + \vec{F}_{si} \right| \quad (5.14b)$$

where  $F_{ni}$ ,  $F_{si}$  and  $F_{ti}$  are normal, shear, and magnitude of the total forces of particle  $i$ , respectively.  $F_{\text{norm-i}}$  is the normalized total force of particle  $i$  and  $\bar{F}_t$  is the average contact force of the packing system. Marketos and Bolton (2007) and Dondi et al. (2012a) also proved that the probability distribution function (PDF) of the normalized force ( $F_{\text{norm}}$ ) for a packed granular system can be explained by the following exponential equation:

$$\text{PDF}(F_{\text{norm}}) = (F_{\text{norm}} + P_1)^{P_2} \times \exp(P_3 \times F_{\text{norm}} + P_4) \quad (5.15)$$

where,  $P_1$ ,  $P_2$ ,  $P_3$ , and  $P_4$  are the fitting curve parameters.

Figure 5.23 shows the distribution of the normalized contact forces and the corresponding PDF curves for four packing systems constructed from particles with different flatness, elongation and sphericity values. The figure shows an exponential decrease of forces larger than the average force ( $F_{\text{norm}}=1$ ) for all packing systems regardless of the variation in flatness, elongation, and sphericity. Additionally, for the very high contact forces ( $F_{\text{norm}} > 3$ ) the exponential tail of the PDF curves appears to be same for all packing systems. The distribution of the very high contact forces is independent of the particle shape. However, for high contact forces ( $1 < F_{\text{norm}} < 3$ ), no particular trend is detected. For low contact forces ( $F_{\text{norm}} < 1$ ), it appears the distribution of contact force depends on the flatness, elongation and sphericity of particles. As the flatness, elongation, and sphericity decrease, the variation in the frequency of low contact forces increases.



Given the CN results, it appears that although decreasing flatness, elongation or sphericity can result in increasing contact between particles (higher CN), this higher CN mainly affects the total number of low contact forces and does not have a notable effect on high or very high contact force distribution. The values of fitting parameters ( $P_1$ ,  $P_2$ ,  $P_3$ , and  $P_4$ ) for the four packing systems with different shape parameters as shown in Table 5.7. From this table, it can be seen there is no specific correlation between the fitting parameters of PDF curves and shape parameters.

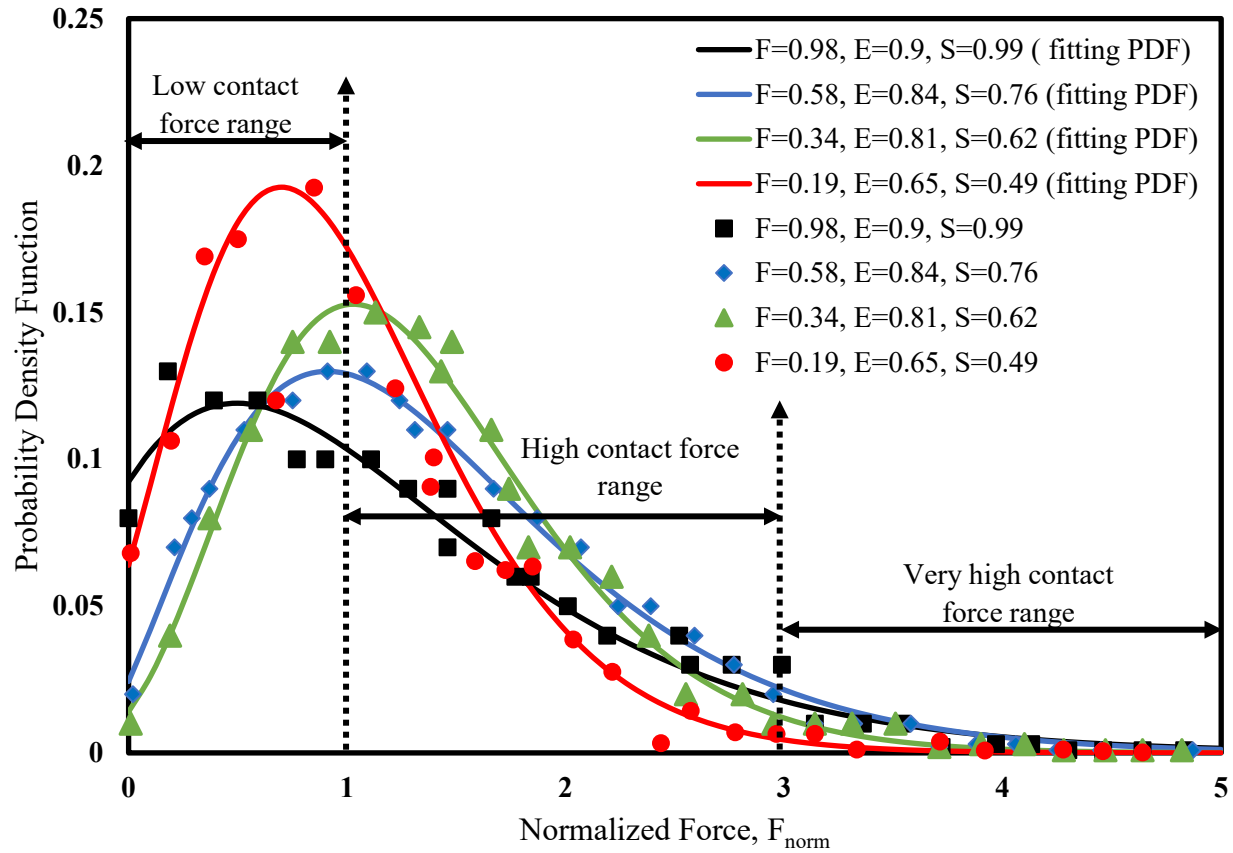


Figure 5.23 Probability Density Function of Normalized Contact Force for Mixtures with Different Shape Parameters.

Table 5.7 Fitting Parameters of PDF Distribution for some Mixtures.

Shape Parameters	P1	P2	P3	P4	R2
F=0.98, E=0.9, S=0.99	0.6783	5.486	-3.982	-0.6187	0.98
F=0.58, E=0.84, S=0.76	0.5291	5.698	-3.659	-0.6414	0.95
F=0.34, E=0.81, S=0.62	0.2733	2.405	-2.032	-0.5965	0.98
F=0.19, E=0.65, S=0.49	0.6315	1.816	-1.611	-1.5470	0.99

## 6.6 Summary

In this chapter, the effect of coarse aggregate shape properties on the compactability of asphalt mixtures was investigated using five shape descriptors, i.e., flatness, elongation, sphericity, roundness and regularity. To create mixtures with controllable shape descriptors, a method based on discrete random fields theory and spherical harmonics was implemented and a DEM framework was used to simulate the SGC compaction of the virtual asphalt mixtures. The fine aggregates and asphalt binder were assumed to be an asphalt mastic and its effect on compaction of coarse aggregates was considered using Burger's viscoelastic model. This study shows that particle shape can significantly affect the laboratory compactability parameters of asphalt mixtures. While some shape parameters such as elongation and flatness mainly affect the initial density, other parameters such as roundness and regularity primarily influence the compaction slope of asphalt mixtures. Additionally, the results proved that the shape parameters (flatness, elongation and sphericity) of particle mainly impact the average coordination number and frequency distribution of low contact forces in a packing system.

The findings presented in this chapter also suggest that having less rounded, flat and elongated particles reduce the energy requires to compact asphalt mixtures and consequently result in better compactability. Finally, the findings of this study put a workable mathematical theory to the compactability of asphalt mixtures based on aggregate properties. With such a theory in place it should be possible to predict asphalt mixture compactability numerically, rather than performing numerous asphalt mixture design trials, thus saving time and money.

## CHAPTER 7. SUMMARY AND CONCLUSIONS

Aggregate size distribution, or gradation, and aggregate shape characteristics are two important parameters in asphalt mixture design, compactability and performance due to their significant impact on the development of aggregate structure in asphalt mixtures. In this research, the objective was to use particle packing theories and discrete element methods (DEM) to better define the impact of aggregate morphological properties and particle size distribution on asphalt mixture aggregate structure and thereby asphalt mixture volumetric and compaction properties. The work had three main tasks.

The first task proposed an analytical approach for estimating changes in voids in the mineral aggregate (VMA) due to gradation variation and determining the relevant aggregate skeleton characteristics of asphalt mixtures using the linear-mixture packing model, an analytical packing model that considers the mechanisms of particle packing, filling and occupation. Application of the linear-mixture packing model to estimate the VMA of asphalt mixtures shows there is a high correlation between laboratory measured and model estimated values. Additionally, the model defines a new variable, the central particle size of asphalt mixtures that characterizes an asphalt mixture's aggregate skeleton. Finally, the proposed analytical model shows a significant potential to be used in the early stages of asphalt mixture design to determine the effect of aggregate gradation changes on VMA and to predict mixture rutting performance.

As the second task, a framework to define and understand the aggregate structure of asphalt mixtures was proposed. To develop this framework, an analytical model for binary mixtures was suggested. The model considers the effect of size ratio and air volume between the particles on the aggregate structure and packing density of binary mixtures. Based on this model, four aggregate structures, namely coarse pack (CP), coarse-dense pack (CDP), fine-dense pack (FDP) and fine pack (FP), were defined. The model was validated using a series of 3D discrete element simulations.

Furthermore, the simulation of multi-sized aggregate blends using two representative sizes for fine and coarse stockpiles was completed and the proposed analytical model applied to actual aggregate blends. In order to assess how well the model applies to asphalt mixtures, compaction parameters including compaction slope (CS), initial density ( $N_{ini}$ ), locking point and compaction energy index (CEI) were analyzed. The numerical simulations verify the proposed analytical model can satisfactorily determine the particle structure of binary and multi-sized asphalt mixture

gradations and can, therefore, be used to better design asphalt mixtures for improved field performance.

Additionally, the effect of aggregate gradation on asphalt mixture compactability was investigated using different combinations of coarse and fine aggregates and, four gradation zones of CP, CDP, FDP and FP. Two main compaction parameters, the compaction slope and initial density, and three gradation parameters, chosen to describe the representative size and uniformity of the gradation were compared. Statistical analyses indicate a significant correlation between the two compaction parameters as response variables and three gradation parameters as explanatory variables. These relationships were used to determine the optimum aggregate gradation with respect to asphalt mixture compactability and rutting performance. The models developed using the gradation parameters were used with two independent data sets, one from a laboratory experiment and one from a field project, to show the parameters can predict the compactability behavior of asphalt mixtures.

After gradation, the physical properties of aggregates are the most influential parameters for the development of the aggregate skeleton, compactability, and performance of asphalt mixtures. As a third task, the effect of coarse aggregate shape characteristics on the compactability of asphalt mixtures was virtually investigated using a discrete element method (DEM). The 3D particles were constructed using a method based on discrete random fields' theory and spherical harmonic and their size distribution in the container was controlled by applying a constrained Voronoi tessellation (CVT) method. The effect of fine aggregates and asphalt binder was considered by constitutive Burger's interaction model between coarse particles. Five aggregate shape descriptors including flatness, elongation, roundness, sphericity and regularity and, two Superpave gyratory compactor (SGC) parameters (initial density at  $N_{ini}$  and compaction slope) were selected for investigation and statistical analyses. Results reveal there is a statistically significant correlation between flatness, elongation, roundness, and sphericity as shape descriptors and initial compaction density. The analyses discovered that among all particle shape descriptors, only roundness and regularity had a statistically significant relation with compaction slope, and as the amount of roundness and regularity increase (low angularity), the compaction slope decreases. Additionally, the effect of flat and elongated (F&E) particles percentage in a mixture was investigated and the results indicated that increase of F&E particles in a mixture (more than 15%) results in a significant reduction in the initial density of the mixture especially for lower dimensional ratio.

In summary, the findings of this study use the workable analytical models to determine the impact of aggregate gradation and morphological properties on volumetric properties and the compactability of asphalt mixtures. With such models in place, it should be possible to predict asphalt mixture volumetric properties and compactability in the early stages of asphalt mixture design, rather than performing numerous asphalt mixture design trials, thus saving time and money.

The following recommendations are offered as future works:

- the proposed linear-mixture packing model could predict the effect of change in gradation on the aggregate structure of asphalt mixture by assuming constant asphalt binder. Therefore, improvement and modification of the proposed model to consider the effect of asphalt binder content and type is highly recommended as a future work.
- The proposed framework to understanding the role of aggregate structure on compactability of asphalt mixtures can be used to determine the impact of different aggregate structures on other performance criteria such as cracking and rutting of asphalt mixtures.
- The effect of coarse aggregate shape characteristics on the compactability of asphalt mixtures was virtually investigated. Therefore, an experimental work to verify the numerical results is to be necessary.

## REFERENCES

- AASHTO M 323, (2015). Standard specification for Superpave volumetric mix design. *American Association of State Highway and Transportation Officials*.
- Abbas, A., Masad, E., Papagiannakis, T., & Shenoy, A. (2005). Modelling asphalt mastic stiffness using discrete element analysis and micromechanics-based models. *International Journal of Pavement Engineering*, 6(2), 137–146.
- Aho, B., Vavrik, W., & Carpenter, S. (2001). Effect of flat and elongated coarse aggregate on field compaction of hot-mix asphalt. *Transportation Research Record: Journal of the Transportation Research Board*, (1761), 26-31.
- Alavi, M. Z., Pouranian, M. R., & Hajj, E. Y. (2014). Prediction of asphalt pavement temperature profile with finite control volume method. *Transportation Research Record*, 2456(1), 96-106.
- Alonso-Marroquín, F., Mühlhaus, H. B., & Herrmann, H. J. (2008). Micromechanical investigation of granular ratcheting using a discrete model of polygonal particles. *Particuology*, 6(6), 390-403.
- Andreasen, A., & Anderson, J. (1929). The relation of grading to interstitial voids in loosely granular products. *Kolloid-Z*, 49(2), 217-218.
- Anderson, R. M., Turner, P. A., Peterson, R. L., & Mallick, R. B. (2002). NCHRP Report 478: Relationship of Superpave Gyratory Compaction Properties to HMA Rutting Behavior. *TRB, National Research Council, Washington, DC*.
- Arasan, S., Yenera, E., Hattatoglu, F., Hınıslıoglu, S., & Akbuluta, S. (2011). Correlation between shape of aggregate and mechanical properties of asphalt concrete: Digital image processing approach. *Road Materials and Pavement Design*, 12(2), 239-262.
- Asphalt Institute. (1997). *Mix design methods for asphalt concrete and other hot-mix types* (No. 2). *Asphalt Institute*. Lexington, KY.
- Asphalt Institute. (2001). Superpave mix design. *Superpave series No. 2 (SP-2)*. *Asphalt Institute*. Lexington, KY.
- Asphalt Institute. (2015). *Asphalt mix design methods*. *Asphalt Institute*. Lexington, KY.
- Aste, T., Saadatfar, M., & Senden, T. J. (2005). Geometrical structure of disordered sphere packings. *Physical Review E*, 71(6), 061302.
- Aurenhammer, F. (1991). Voronoi diagrams—a survey of a fundamental geometric data structure. *ACM Computing Surveys (CSUR)*, 23(3), 345-405.

- Awed, A., Kassem, E., Masad, E., & Little, D. (2015). Method for predicting the laboratory compaction behavior of asphalt mixtures. *Journal of Materials in Civil Engineering*, 27(11), 04015016.
- Azéma, E., Radjai, F., Peyroux, R., & Saussine, G. (2007). Force transmission in a packing of pentagonal particles. *Physical Review E*, 76(1), 011301.
- Azéma, E., Radjai, F., & Saussine, G. (2009). Quasistatic rheology, force transmission and fabric properties of a packing of irregular polyhedral particles. *Mechanics of Materials*, 41(6), 729-741.
- Bahia, H. U., Friemel, T. P., Peterson, P. A., Russell, J. S., & Poehnel, B. (1998). Optimization of constructibility and resistance to traffic: a new design approach for HMA using the Superpave compactor. *Journal of the Association of Asphalt Paving Technologists*, 67.
- Bahuguna, S., Panoskaltsis, V. P., & Papoulia, K. D. (2006). Identification and modeling of permanent deformations of asphalt concrete. *Journal of engineering mechanics*, 132(3), 231-239.
- Baron, J., & Sauterey, R. (1995). Le béton hydraulique: Connaissance et pratique. Paris: Presses de l'école nationale des Ponts et chaussées. [In French].
- Barrett, P. J. (1980). The shape of rock particles, a critical review. *Sedimentology*, 27(3), 291-303.
- Benn, D. I., & Ballantyne, C. K. (1992). Pebble shape (and size!): Discussion. *Journal of Sedimentary Research*, 62(6).
- Benson, F. J. (1970). Effects of aggregate size, shape, and surface texture on the properties of bituminous mixtures—A literature survey. *Special report*, 109, 12-22.
- Bessa, I. S., Branco, V. T. C., Soares, J. B., & Neto, J. A. N. (2014). Aggregate shape properties and their influence on the behavior of hot-mix asphalt. *Journal of Materials in Civil Engineering*, 27(7), 04014212.
- Birgisson, B., & Ruth, B. E. (2001). Development of tentative guidelines for the selection of aggregate gradations for hot-mix asphalt. In *Aggregate Contribution to Hot Mix Asphalt (HMA) Performance*. ASTM International.
- Blott, S. J., & Pye, K. (2008). Particle shape: a review and new methods of characterization and classification. *Sedimentology*, 55(1), 31-63.
- Blumenfeld, R., Edwards, S. F., & Ball, R. C. (2005). Granular matter and the marginal rigidity state. *Journal of Physics: Condensed Matter*, 17(24), S2481.
- Brouwers, H. J. H. (2006). Particle-size distribution and packing fraction of geometric random packings. *Physical review E*, 74(3), 031309.
- Brown, E. R., Haddock, J. E., Mallick, R. B., & Lynn, T. A. (1997). Development of a mixture design procedure for stone matrix asphalt (SMA). *National Center for Asphalt Technology, Report*, (97-03).

- Brown, E. R., Kandhal, P. S., Roberts, F. L., Kim, Y. R., Lee, D.-Y., Kennedy, T. W., National Asphalt Pavement Association., ... National Center for Asphalt Technology (U.S.). (2009). *Hot mix asphalt materials, mixture design, and construction*. Lanham, Md: NAPA Research and Education Foundation.
- Button, J. W., Perdomo, D., & Lytton, R. L. (1990). Influence of aggregate on rutting in asphalt concrete pavements. *Transportation Research Record*, (1259).
- Cai, W., McDowell, G. R., & Airey, G. D. (2014). Discrete element visco-elastic modelling of a realistic graded asphalt mixture. *Soils and Foundations*, 54(1), 12-22.
- Chen, J. S., Shiah, M. S., and Chen, H. J. (2001). "Quantification of coarse aggregate shape and its effect on engineering properties of hot-mix asphalt mixtures." *Journal of Testing and Evaluation*, 29(6), 513-519.
- Chen, J. (2011). Discrete element method (DEM) analyses for hot-mix asphalt (HMA) mixture compaction [Ph. D. thesis]. *University of Tennessee, Knoxville, USA*.
- Chen, J., Huang, B., Shu, X., & Hu, C. (2014). DEM simulation of laboratory compaction of asphalt mixtures using an open source code. *Journal of Materials in Civil Engineering*, 27(3), 04014130.
- Cho, G. C., Dodds, J., & Santamarina, J. C. (2006). Particle shape effects on packing density, stiffness, and strength: natural and crushed sands. *Journal of geotechnical and geoenvironmental engineering*, 132(5), 591-602.
- Christensen, D. W. (2009). Draft final report to the National Cooperative Highway Research Program (NCHRP) on Project NCHRP 9-33: A mix design manual for hot mix asphalt. *Advanced Asphalt Technologies, LLC*. Sterling, VA.
- Cook, B. K., & Jensen, R. P. (2002). Discrete element methods: numerical modeling of discontinua. *American Society of Civil Engineers, Geo Institute*.
- Coree, B., & Hislop, W. P. (2000). *A laboratory investigation into the effects of aggregate-related factors of critical VMA in asphalt paving mixtures* (No. IDOT TR-415). Iowa State University. Center for Transportation Research and Education.
- Cundall, P. A., & Strack, O. D. (1979). A discrete numerical model for granular assemblies. *geotechnique*, 29(1), 47-65.
- Das, N. (2007). *Modeling three-dimensional shape of sand grains using discrete element method* (Doctoral dissertation, University of South Florida).
- Delage, K. P. (2000). The Effect of Fine Aggregate Angularity on Hot Mixture Asphalt Performance. *Master Degree Thesis, Department of Civil and Environmental Engineering, University of Wisconsin-Madison*.



- Delaney, G. W., & Cleary, P. W. (2010). The packing properties of superellipsoids. *EPL (Europhysics Letters)*, 89(3), 34002.
- De Larrard, F. (1999). Concrete Mixture Proportioning—A Scientific Approach. E & FN Spon. New York, NY.
- Dondi, G., Simone, A., Vignali, V., & Manganelli, G. (2012a). Discrete element modelling of influences of grain shape and angularity on performance of granular mixes for asphalts. *Procedia-Social and Behavioral Sciences*, 53, 399-409.
- Dondi, G., Simone, A., Vignali, V., & Manganelli, G. (2012b). Numerical and experimental study of granular mixes for asphalts. *Powder Technology*, 232, 31-40.
- Dukatz, E. L. (1989). Aggregate properties related to pavement performance. In *Proceedings of the association of asphalt paving technologists* (Vol. 58, pp. 492-501).
- Elliott, R. P., Ford Jr, M. C., Ghanim, M., & Tu, Y. F. (1991). Effect of aggregate gradation variation on asphalt concrete mix properties. *Transportation Research Record*, (1317).
- Fuller, W. B. and Thompson, S. E. (1907). The Laws of Proportioning Concrete. *Transactions of the American Society of Civil Engineers*, LIX, pp. 67-143.
- Furnas, C. C. (1931). Grading aggregates-I.-Mathematical relations for beds of broken solids of maximum density. *Industrial & Engineering Chemistry*, 23(9), 1052-1058.
- Galindo-Torres, S. A., & Pedroso, D. M. (2010). Molecular dynamics simulations of complex-shaped particles using Voronoi-based spheropolyhedra. *Physical Review E*, 81(6), 061303.
- Garboczi, E. J. (2002). Three-dimensional mathematical analysis of particle shape using X-ray tomography and spherical harmonics: Application to aggregates used in concrete. *Cement and concrete research*, 32(10), 1621-1638.
- Garboczi, E. J., Cheok, G. S., and Stone, W. C. (2006). "Using LADAR to characterize the 3-D shape of aggregates: Preliminary results." *Cement and Concrete Research*, 36(6), 1072-1075.
- Gaudette, B. E., & Welke, R. A. (1977). Investigation of crushed aggregates for bituminous mixtures. *Michigan Department of State Highways and Transportation Report No. TB-58*.
- Goltermann, P., Johansen, V., & Palbøl, L. (1997). Packing of aggregates: an alternative tool to determine the optimal aggregate mix. *Materials Journal*, 94(5), 435-443.
- Goode, J. F., & Lufsey, L. A. (1965). Voids, permeability, film thickness vs. asphalt hardening. In *Proceedings, AAPT* (Vol. 34).
- Guarin, A., Roque, R., Kim, S., & Sirin, O. (2013). Disruption factor of asphalt mixtures. *International Journal of Pavement Engineering*, 14(5), 472-485.
- Guisés, R., Xiang, J., Latham, J. P., & Munjiza, A. (2009). Granular packing: numerical simulation and the characterisation of the effect of particle shape. *Granular Matter*, 11(5), 281-292.

- Haddock, J., Pan, C., Feng, A., & White, T. D. (1999). Effect of gradation on asphalt mixture performance. *Transportation research record*, 1681(1), 59-68.
- He, H. (2010). Computational modelling of particle packing in concrete [Ph. D. thesis]. *Delft University of Technology, Ipskamp Drukkers, Delft, The Netherlands*.
- Herrmann, H. J., & Luding, S. (1998). Modeling granular media on the computer. *Continuum Mechanics and Thermodynamics*, 10(4), 189-231.
- Huang, Y. H. (2012). Pavement analysis and design. *Pearson/Prentice Hall*, Upper Saddle River, NJ.
- Isola, R. (2008). *Packing of granular materials* (Doctoral dissertation, University of Nottingham).
- Jiang, M. J., Yu, H. S., & Harris, D. (2005). A novel discrete model for granular material incorporating rolling resistance. *Computers and Geotechnics*, 32(5), 340-357.
- Kassem, E., Scullion, T., Masad, E., & Chowdhury, A. (2012). Comprehensive evaluation of compaction of asphalt pavements and a practical approach for density predictions. *Transportation Research Record: Journal of the Transportation Research Board*, (2268), 98-107.
- Katagiri, J., Matsushima, T., & Yamada, Y. (2010). Simple shear simulation of 3D irregularly-shaped particles by image-based DEM. *Granular Matter*, 12(5), 491-497.
- Kennedy, T. W., Huber, G. A., Harrigan, E. T., Cominsky, R. J., Hughes, C. S., Von Quintus, H., & Moulthrop, J. S. (1994). *Superior performing asphalt pavements (Superpave): The product of the SHRP asphalt research program* (No. SHRP-A-410). Washington, DC, USA: Strategic Highway Research Program, National Research Council.
- Ketterhagen, W. R., am Ende, M. T., & Hancock, B. C. (2009). Process modeling in the pharmaceutical industry using the discrete element method. *Journal of pharmaceutical sciences*, 98(2), 442-470.
- Kozicki, J., & Donzé, F. V. (2009). Yade-open dem: an open-source software using a discrete element method to simulate granular material. *Engineering Computations*, 26(7), 786-805.
- Kruyt, N. P., & Rothenburg, L. (2006). Shear strength, dilatancy, energy and dissipation in quasi-static deformation of granular materials. *Journal of Statistical Mechanics: Theory and Experiment*, 2006(07), P07021.
- Lee, D. L. (1970). Packing of Spheres and its Effect on the Viscosity of Suspension. *J. Paint Technol.*, 42, 579-584.
- Leitzelement, M., Lo, C. S., & Dodds, J. (1985). Porosity and permeability of ternary mixtures of particles. *Powder Technology*, 41(2), 159-164.
- Leiva, F. (2007). *Relationships between laboratory measured characteristics of HMA and field compactability* (Doctoral dissertation Auburn University).

- Leiva, F., & West, R. (2008). Analysis of hot-mix asphalt lab compactability using lab compaction parameters and mix characteristics. *Transportation Research Record: Journal of the Transportation Research Board*, (2057), 89-98.
- Lira, B., Jelagin, D., & Birgisson, B. (2013). Gradation-based framework for asphalt mixture. *Materials and structures*, 46(8), 1401-1414.
- Lottman, R. R. and Goetz, W. H., (1956). "Effect of Crushed Gravel Fine Aggregate on the Strength of Asphaltic Surfacing Mixtures." *National Sand and Gravel Association Circular*. No. 63.
- Ma, T., Zhang, D., Zhang, Y., Wang, S., & Huang, X. (2018). Simulation of wheel tracking test for asphalt mixture using discrete element modelling. *Road Materials and Pavement Design*, 19(2), 367-384.
- Map, S. O., & Kohonen, T. (1990). Self-organizing map. *Proceedings of the IEEE*, 78, 1464-1480.
- Marketos, G., & Bolton, M. D. (2007). Quantifying the extent of crushing in granular materials: a probability-based predictive method. *Journal of the Mechanics and Physics of Solids*, 55(10), 2142-2156.
- Masad, E., Al-Rousan, T., Button, J., Little, D., & Tutumluer, E. (2007). NCHRP Report 555: Test Methods for Characterizing Aggregate Shape, Texture, and Angularity. *Transportation Research Board of the National Academies, Washington, DC*.
- Matsushima, T., Katagiri, J., Uesugi, K., Tsuchiyama, A., & Nakano, T. (2009). 3D shape characterization and image-based DEM simulation of the lunar soil simulant FJS-1. *Journal of Aerospace Engineering*, 22(1), 15-23.
- McDowell, G., Li, H., & Lowndes, I. (2011). The importance of particle shape in discrete-element modelling of particle flow in a chute. *Géotechnique Letters*, 1(3), 59-64.
- McGennis, R. B., Anderson, R. M., Kennedy, T. W., & Solaimanian, M. (1995). Background of SUPERPAVE asphalt mixture design and analysis. *Asphalt Institute*. Lexington, KY.
- McLeod, N. W. (1959). Void requirements for dense-graded bituminous paving mixtures. *American Society for Testing and Materials (ASTM) Special Technical Publication, SPT 252*, Philadelphia.
- Meegoda, J. N., & Chang, K. G. (1995). A Fundamental Study on the Discontinuities and Heterogeneities of Asphalt Concrete. In *Engineering Mechanics* (pp. 465-468). ASCE.
- Minh, N. H., & Cheng, Y. P. (2013). A DEM investigation of the effect of particle-size distribution on one-dimensional compression. *Géotechnique*, 63(1), 44.
- Moavenzadeh, Fred, & Goetz, William Harner. (1963). Aggregate Degradation in Bituminous Mixtures: Technical Paper. *JTRP Technical Reports*, Purdue University.
- Mohammad, L. N., & Al-Shamsi, K. H. A. L. I. D. (2007). A look at the Bailey method and locking point concept in Superpave mixture design. *Transportation Research Board Circular E-*

*C124: Practical Approaches to Hot-Mix Asphalt Mix Design and Production Quality Control Testing*, 12-32.

- Mollon, G., & Zhao, J. (2012). Fourier–Voronoi-based generation of realistic samples for discrete modelling of granular materials. *Granular matter*, 14(5), 621-638.
- Mollon, G., & Zhao, J. (2014). 3D generation of realistic granular samples based on random fields theory and Fourier shape descriptors. *Computer Methods in Applied Mechanics and Engineering*, 279, 46-65.
- Montoya, M., Pouranian, M. R., & Haddock, J. (2018). Increasing Asphalt Pavement Density Through Mixture Design: A Field Project. In *Asphalt Paving Technology: Association of Asphalt Paving Technologists-Proceedings of the Technical Sessions*.
- Mostofinejad, D., & Reisi, M. (2012). A new DEM-based method to predict packing density of coarse aggregates considering their grading and shapes. *Construction and Building Materials*, 35, 414-420.
- Muras, A. J. (2010). *Prediction of asphalt mixture compactability from mixture, asphalt, and aggregate properties* (Doctoral dissertation, Texas A & M University).
- NCAT (National Center for Asphalt Technology). (2011). Using lab data to predict the field compactability. *Hot Mix Asphalt Technology*, 16(1), 57–58.
- Neter, J., Kutner, M. H., Nachtsheim, C. J., & Wasserman, W. (1996). *Applied linear statistical models* (Vol. 4, p. 318). Chicago: Irwin.
- Nijboer, L. (1948). *Plasticity as a factor in the design of dense bituminous road carpets*. Elsevier Pub.
- Ng, T. T. (2009). Particle shape effect on macro-and micro-behaviors of monodisperse ellipsoids. *International journal for numerical and analytical methods in geomechanics*, 33(4), 511-527.
- Olard, F., & Perraton, D. (2010). On the optimization of the aggregate packing characteristics for the design of high-performance asphalt concretes. *Road Materials and Pavement Design*, 11(sup1), 145-169.
- Orford, J. D., & Whalley, W. B. (1983). The use of the fractal dimension to quantify the morphology of irregular-shaped particles. *Sedimentology*, 30(5), 655-668.
- Ouadfel, H., & Rothenburg, L. (2001). Stress–force–fabric relationship for assemblies of ellipsoids. *Mechanics of materials*, 33(4), 201-221.
- Pan, T., & Tutumluer, E. (2006). Evaluation of visual based aggregate shape classifications using the University of Illinois Aggregate Image Analyzer (UIAIA). In *Pavement Mechanics and Performance* (pp. 203-211).

- Pan, T., Tutumluer, E., & Carpenter, S. H. (2006). Effect of coarse aggregate morphology on permanent deformation behavior of hot mix asphalt. *Journal of transportation engineering*, 132(7), 580-589.
- Pettijohn, F. J. (1975). *Sedimentary rocks* (Vol. 3). New York: Harper & Row.
- Pine, W. J. (2016). The Bailey method: Achieving volumetrics and HMA compactability, Asphalt Institute, Lexington, KY.
- Pouranian, M. R., & Haddock, J. E. (2018). Determination of voids in the mineral aggregate and aggregate skeleton characteristics of asphalt mixtures using a linear-mixture packing model. *Construction and Building Materials*, 188, 292-304.
- Pouranian, M. R., Imaninasab, R., & Shishehbor, M. (2018). The effect of temperature and stress level on the rutting performance of modified stone matrix asphalt. *Road Materials and Pavement Design*, 1-13.
- Pouranian, M. R., & Shishehbor, M. (2019). Sustainability assessment of green asphalt mixtures: a review. *Environments*, 6(6), 73.
- Pouranian, M. R., & Haddock, J. E. (2019). A new framework for understanding aggregate structure in asphalt mixtures. *International Journal of Pavement Engineering*, 1-17.
- Pouranian, M. R., Rahbar-Rastegar, R., & Haddock, J. E. (2019, September). Development of a Soybean-Based Rejuvenator for Asphalt Mixtures Containing High Reclaimed Asphalt Pavement Content. In *International Symposium on Asphalt Pavement & Environment* (pp. 264-273). Springer, Cham.
- Pournin, L., Weber, M., Tsukahara, M., Ferrez, J. A., Ramaioli, M., & Liebling, T. M. (2005). Three-dimensional distinct element simulation of spherocylinder crystallization. *Granular Matter*, 7(2-3), 119-126.
- Powers, M. C. (1953). A new roundness scale for sedimentary particles. *Journal of Sedimentary Research*, 23(2), 117-119.
- Prowell, B. D., Zhang, J., & Brown, E. R. (2005). *Aggregate properties and the performance of superpave-designed hot mix asphalt* (Vol. 539). Transportation Research Board, Washington, DC, USA.
- Riley, N. A. (1941). Projection sphericity. *Journal of Sedimentary Research*, 11(2), 94-95.
- Roberts, F. L., Kandhal, P. S., Brown, E. R., Lee, D. Y., & Kennedy, T. W. (1991). Hot mix asphalt materials, mixture design and construction. *National Asphalt Pavement Association Research and Education Foundation*, Lanham, MD, United States.
- Roberts, F. L., Mohammad, L. N., & Wang, L. B. (2002). History of hot mix asphalt mixture design in the United States. *Journal of Materials in Civil Engineering*, 14(4), 279-293.

- Roque, R., Birgisson, B., Kim, S. and Guarin, A. (2006). Development of mix design guidelines for improved performance of asphalt mixtures. *Florida Department of Transportation*, Final Report, UF Project no. 49104554032-12.
- Russell, R. D., & Taylor, R. E. (1937). Roundness and shape of Mississippi River sands. *The Journal of Geology*, 45(3), 225-267.
- Salot, C., Gotteland, P., & Villard, P. (2009). Influence of relative density on granular materials behavior: DEM simulations of triaxial tests. *Granular matter*, 11(4), 221-236.
- Shen, S., & Yu, H. (2011). Characterize packing of aggregate particles for paving materials: Particle size impact. *Construction and Building Materials*, 25(3), 1362-1368.
- Shishehbor, M., Dri, F. L., Moon, R. J., & Zavattieri, P. D. (2018). A continuum-based structural modeling approach for cellulose nanocrystals (CNCs). *Journal of the Mechanics and Physics of Solids*, 111, 308-332.
- Shishehbor, M., & Zavattieri, P. D. (2019). Effects of interface properties on the mechanical properties of bio-inspired cellulose nanocrystal (CNC)-based materials. *Journal of the Mechanics and Physics of Solids*, 124, 871-896.
- Sneed, E. D., & Folk, R. L. (1958). Pebbles in the lower Colorado River, Texas a study in particle morphogenesis. *The Journal of Geology*, 66(2), 114-150.
- Standish, N., & Borger, D. E. (1979). The porosity of particulate mixtures. *Powder Technology*, 22(1), 121-125.
- Standish, N., & Yu, A. B. (1987). Porosity calculations of ternary mixtures of particles. *Powder Technology*, 49(3), 249-253.
- Stovall, T., De Larrard, F., & Buil, M. (1986). Linear packing density model of grain mixtures. *Powder technology*, 48(1), 1-12.
- Suzuki, M., & Oshima, T. (1983). Estimation of the co-ordination number in a multi-component mixture of spheres. *Powder technology*, 35(2), 159-166.
- Taghavi, R. (2011). Automatic clump generation based on mid-surface. In *Proceedings, 2nd International FLAC/DEM Symposium, Melbourne* (pp. 791-797).
- Thornton, C., Yin, K. K., & Adams, M. J. (1996). Numerical simulation of the impact fracture and fragmentation of agglomerates. *Journal of Physics D: Applied Physics*, 29(2), 424.
- Tutumluer, E., Pan, T., & Carpenter, S. H. (2005). *Investigation of aggregate shape effects on hot mix performance using an image analysis approach*. Federal Highway Administration, Washington, DC.
- Ueda, T., Matsushima, T., & Yamada, Y. (2011). Effect of particle size ratio and volume fraction on shear strength of binary granular mixture. *Granular Matter*, 13(6), 731-742.

- Van Hulle, M. M. (2012). Self-organizing maps. In *Handbook of Natural Computing* (pp. 585-622). Springer Berlin Heidelberg.
- Vavrik, W., & Carpenter, S. (1998). Calculating air voids at specified number of gyrations in Superpave gyratory compactor. *Transportation Research Record: Journal of the Transportation Research Board*, (1630), 117-125.
- Vavrik, W. R. (2000). *Asphalt mixture design concepts to develop aggregate interlock* (Doctoral dissertation, University of Illinois at Urbana-Champaign).
- Vavrik, W. R., Pine, W. J., Huber, G., Carpenter, S. H., & Bailey, R. (2001). The bailey method of gradation evaluation: the influence of aggregate gradation and packing characteristics on voids in the mineral aggregate (with discussion). *Journal of the Association of Asphalt Paving Technologists*, 70.
- Vavrik, W. R., Huber, G., Pine, W. J., & Carpenter, S. H. (2002). Bailey method for gradation selection in HMA mixture design. *Transportation Research Circular No. E-C044. Transportation Research Board*.
- Wadell, H. (1932). Volume, shape, and roundness of rock particles. *The Journal of Geology*, 40(5), 443-451.
- Wang, L., Park, J.-Y., and Fu, Y. (2007a). "Representation of real particles for DEM simulation using X-ray tomography." *Construction and Building Materials*, 21(2), 338-346.
- Wang, L., Park, J. Y., and Fu, Y. (2007b). "Representation of real particles for DEM simulation using X-ray tomography." *Construction and Building Materials*, 21(2), 338-346.
- Wang, L., Sun, W., Lally, E. M., Wang, A., Druta, C.; and Tutumluer, E. (2012). "NCHRP Report 724: Application of LADAR in the Analysis of Aggregate Characteristics". *Transportation Research Board National Research*, Washington DC.
- Westman, A. E. R. (1936). The packing of particles: empirical equations for intermediate diameter ratios. *Journal of the American Ceramic Society*, 19(1-12), 127-129.
- Widuliński, Ł., Kozicki, J., & Tejchman, J. (2009). Numerical simulations of triaxial test with sand using DEM. *Archives of Hydro-Engineering and Environmental Mechanics*, 56(3-4), 149-172.
- Wu, Y., An, X., & Yu, A. B. (2017). DEM simulation of cubical particle packing under mechanical vibration. *Powder technology*, 314, 89-101.
- Yu, A. B., & Standish, N. (1991). Estimation of the porosity of particle mixtures by a linear-mixture packing model. *Industrial & engineering chemistry research*, 30(6), 1372-1385.
- Zaniewski, J. P., & Srinivasan, G. (2004). Evaluation of indirect tensile strength to identify asphalt concrete rutting potential. *Asphalt Technology Program, Department of Civil and Environmental Engineering, West Virginia University, Performed in Cooperation with the US Department of Transportation-Federal Highway Administration*.

- Zhao, Y., Xu, T., Huang, X., & Li, Z. (2012). Gradation design of the aggregate skeleton in asphalt mixture. *Journal of Testing and Evaluation*, 40(7), 1071-1076.
- Zhou, Z. Y., Zou, R. P., Pinson, D., & Yu, A. B. (2011). Dynamic simulation of the packing of ellipsoidal particles. *Industrial & Engineering Chemistry Research*, 50(16), 9787-9798.
- Zhou, C., Zhang, M., Li, Y., Lu, J., & Chen, J. (2017). Influence of particle shape on aggregate mixture's performance: DEM results. *Road Materials and Pavement Design*, 1-15.
- Zhu, H. P., Zhou, Z. Y., Yang, R. Y., & Yu, A. B. (2007). Discrete particle simulation of particulate systems: theoretical developments. *Chemical Engineering Science*, 62(13), 3378-3396.
- Zingg, T. (1935). Beitrag zur Schotteranalyse. *Schweiz. Mineral. Petrog. Mitt.*, 15, 39-140.